Casimir screening of the QGEM-protocol

Coming one step closer in exploring the quantumness of gravity

Thomas W. van de Kamp

A bachelors thesis presented for the Bachelor degree program of Physics

University of Groningen
First Supervisor: Prof. Dr. A. Mazumdar
Second Supervisor: Prof. Dr. D. Roest
July 2020

Casimir screening of the QGEM-protocol

Coming one step closer in exploring the quantumness of gravity

Thomas W. van de Kamp

Abstract

The **Q**uantum **G**ravity induced **E**ntanglement of **M**asses (**QGEM**)-protocol is an experiment whose goal is to test the quantum nature of gravity by bringing two, mesoscopic, test masses both in a spatial superposition and letting them entangle through their gravitational interaction. Measuring the entanglement implies that the communicator responsible for the entanglement, which is gravity, is of a quantum nature. One of the problems of the current setup of the **QGEM**-protocol is that this communicator, depending on the separation of the masses, can also be of electromagnetic nature, since the Casimir-Polder force can entangle the test masses. This restricts the length scale in which the gravitational force is dominant, limiting the mass and superposition size needed to measure the entanglement induced by the gravitational interaction. Therefore, in this thesis, a slight modification to this setup is proposed: the insertion of a thin perfectly conducting plate in between the test masses which effectively screens the Casimir-Polder potential, but introduces a Casimir force between the plate and the test masses. With this modified setup, one can measure entanglement for masses and superposition sizes of one order magnitude lower than suggested in the original proposal, from 10^{-14} to 10^{-15} kg and 200 to 23μm respectively. Consequently, this also reduces the need to use a highly advanced magnetic field gradient of 10^6 Tm^{-1}, to create the superposition, to a laboratory allowed magnetic field gradient of 10^4 Tm^{-1}. This brings needed parameters for the Stern-Gerlach interferometry closer towards a currently allowed parameter space. The new modified setup is also able to better probe theorized Ultra-Violet deviations from the known $1/r$ potential of gravity as one can measure the entanglement with shorter separations between test masses. The decoherence on the test masses was modeled according to "which-path" information loss through absorption/scattering and/or emission of environmental particles/photons, which is an unavoidable source of decoherence in the **QGEM**-protocol.

Contents

1 Introduction

Gravity is the most famous but yet least understood force in our universe, as gravity, as understood up till now, is still incompatible with quantum physics. Tying gravity to quantum physics is, therefore, if proven, one of the most important discoveries in physics as quantum gravity can provide explanations for various problems in physics such as the big bang singularity [1] and the cosmological constant problem. However, the theory of quantum gravity involves most of the time the quantization of space-time, which up to now is understood to be a classical configuration [2]. There is still no evidence that proves that quantum gravity even exists at all, however, recently Bose & Mazumdar et al [1] proposed an experiment that can conclude if gravity has a quantum mechanical origin or not. Therefore this experiment could give a solution to one of the most challenging and famous problems of physics: is quantum mechanics compatible with general relativity? A similar proposal of this experiment was presented by Marletto and Vedral [3] on the same day. The similar experiments, which will be referred to as the **Q**uantum **G**ravity induced **E**ntanglement of **M**asses (**QGEM**)-protocol, relies on entangling two neutral mesoscopic test masses, both in a spatial superposition, through their gravitational interaction [1]. Such an entanglement can only occur if gravity is a quantum entity as it would otherwise violate the Local Operation and Classical Communication (LOCC) theorem [1, 4, 5]. Therefore, measuring the entanglement provides evidence that gravity has a quantum nature [1] and should be mediated by a quantum mediator such as the theorized virtual Graviton [5]. The **QGEM**-protocol, see Sec.(6), is for its time an advanced experiment relying on futuristic technologies. One of which is the need of a high spatial superposition size, $\sim 200\mu$m, for relatively high masses, $\sim 10^{-14}$ kg, which needs a high magnetic field gradient of 10^6 Tm^{-1} to create the spatial superposition to produce a significant entanglement to overcome the main source of decoherence: collisional decoherence of the environment [6, 7]. The main reason for this limitation is that with the current **QGEM**-protocol the gravitational force is not the only force which can entangle the test masses, as the so-called Casimir force [8, 9, 10] can also entangle them. This will limit the separation between the closest states of the test masses from below, as will be shown in Sec.(7), limiting the degree of entanglement. To overcome this limitation a modification of the **QGEM**-protocol will be introduced, see Sec.(8), which consists of the insertion of a perfectly conducting plate between the test masses. This plate will act as a Faraday cage, which screens the electromagnetic interaction between the test masses, thus overcoming the separation limit as the Casimir-Polder potential is unable to entangle the test masses. Consequently, this allows, in principle, for smaller seperations between the test masses. This will, as shown in Sec.(10), allow for smaller masses $\sim 10^{-15}$ kg as well as lower superposition sizes of $\sim 23\mu$m, which are attainable through a laboratory allowed magnetic field gradient of 10^4 Tm^{-1} [1]. Although the mass and the superposition size are still too large to create a superposition with the current technology of Stern-Gerlach (SG) interferometers [11, 12, 13], it brings theory and experiment closer together making the **QGEM**-protocol one day closer to being realized.

In Sec.(2) up to Sec.(5), of this thesis, a theoretical background will be given on underlying aspects of the **QGEM**-protocol such as: the superposition principle, entanglement, decoherence, and the Casimir force. In Sec.(6) and Sec.(7) the current **QGEM**-protocol and its limitation will in more detail be discussed. Here, one of the most crucial terms called the "effective entanglement phase" (Φ_{eff}) will be introduced, which is related to the degree of entanglement pointed out earlier. The modified setup of the **QGEM**-protocol, consisting of the Casimir-screening with the conducting plate will be introduced, and explained, in Sec.(8), followed by the discussion in Sec.(9) about the entanglement entropy, which is the actual indication of the degree of entanglement. In this section a suitable entanglement witness ($\mathcal{W}$) for measuring the entanglement of the **QGEM**-protocol will also be discussed.

In Sec.(10) the comparison between both the current setup and the newly introduced modified setup with the Casimir screening of the **QGEM**-protocol will be made. Here, it will be concluded that the modified setup allows for masses with smaller superposition sizes and lower magnetic field gradients as mentioned briefly before. It will also be shown that if one falls back to the high magnetic field gradient of 10^6 Tm^{-1}, one is with the modified setup more robust against decoherence of the environment. Consequently, this reduces the expectation value of the witness to $\langle W \rangle \sim -0.5$, which is almost double the value of the current setup, which is $\langle W \rangle \sim -0.26$, and thus fewer measurements are needed to conclude if gravity has a quantum nature. The build-up of this section is as follows:

1.) In Sec.(10.1) the maximization of the effective entanglement phase for a given mass will be performed to achieve the largest entanglement for a given mass for the largest magnetic field gradient of 10^6 Tm^{-1}. The results for this are displayed as the minimum mass needed in achieving a required entanglement phase. These "required" phases are taken one order apart and are given by: $\Phi_{\mathrm{eff}} \sim 1$,$\Phi_{\mathrm{eff}} \sim 0.1$ and $\Phi_{\mathrm{eff}} \sim 0.01$ rad.
2.) In Sec.(10.2) the same procedure will be followed for the modified setup, for the same magnetic field gradient, to see how this already affects the possibilities if one allows for this relatively high magnetic field gradient.
3.) In Sec.(10.3) the same procedure will be done for both setups, but for the lower magnetic field gradients of 10^5 Tm^{-1} and 10^4 Tm^{-1}. Here, one will see that the current **QGEM**-protocol is incapable of generating the required entanglement phases, whereas the modified setup can still generate all the phases for a magnetic field gradient of 10^5 Tm^{-1} and up to the requirement of $\Phi_{\mathrm{eff}} \sim 0.01$ rad for a magnetic field gradient of 10^4 Tm^{-1}.
4.) In Sec.(10.4) the mass possibilities for both setups will be compared for all magnetic field gradient, which will give the reader already an indication of the huge improvements that this modified setup can provide.
5.) In Sec.(10.5) an expression for the decoherence of both setups in terms of "which-path" information loss due to interactions with the environmental gas/photons and emission of photons [1, 6, 7] will be derived in terms of the parameters of the experiment as well as environmental controllable parameters (temperature and number density of the environmental gas). In this section, it will also be shown how the change of the size/mass of the test masses will alter the decoherence of the superposition for certain parameters.
6.) Finally, in Sec.(10.6), the results of Sec.(10.1) up to Sec.(10.5) will be combined to show for which parameters of the environment and the experiment the **QGEM**-protocol can measure possible entanglement induced by quantum gravity.

In Sec.(11) it will be argued how the modified setup, with the smaller separation between test masses, has a significant advantage to probe deviation from the Newtonian gravitational potential, which also arises from linearized quantum gravity (see Sec.(6.4)) [5, 14, 15]. Here it will also be shown how the strength of the deviation from the Newtonian potential will impact the detectability of the entanglement of the modified setup with the reduced parameter space. In Sec.(12) it will be shown how the highly hypothetical decoherence of the collapse models [6, 7, 16] will negatively influence the **QGEM**-protocol. This analysis is based on the theoretical results obtained in Ref.[6] on the decoherence of different collapse models on a spatially separated superposition of a microscopic object. Finally, in Sec.(13), some extra considerations that have to be taken into account with the modified setup will be discussed. Including for which parameters the plate will not get vibrationally excited, such that it does not act as an extra "which-path" information source of the system and, therefore, does not decrease the coherence of the test masses. The perfect conductor assumption and the extra challenge in bringing back the superposition will also be discussed in this section.

2 Superposition Principle

To understand and improve the current **QGEM**-protocol, first, a light should be thrown on the theoretical aspects underlying this promising project. One of these theoretical aspects is the superposition principle [7]. This states that if multiple states satisfy the Schrödinger equation (SE) for a specific system ($\mathcal{S}$) then the linear combination of them also satisfies the SE [7, 17]:

$$|\Psi\rangle = \sum c_n \, |\Psi_n\rangle \tag{1}$$

Here, $|\rangle$ denotes a state and $|\Psi\rangle$ is the total state of the system consisting of all the individual states $|\Psi_n\rangle$ of the system. All these individual states can under a (complex) basis transformations made such that they are orthogonal to each other, having that, in such a case, the inner product of two individual states becomes:

$$\langle \Psi_m | \Psi_n \rangle = \delta^{mn} \tag{2}$$

The (complex) constant c_n indicates how likely it is to "find" the system in the state $|\Psi_n\rangle$ upon observation, which for superpositions can be time and position dependent[1], with a probability of $|c_n|^2$. Here, the sum of

[1]This time and position dependence is exactly how interference patterns from superpositions can be observed [7, 18].

all individual probabilities should, of course, add up to 1 for the system to have a sensible probability [17]:

$$\sum |c_n|^2 = 1 \tag{3}$$

The important thing to remember from the quantum nature of the superposition principle, which will be important later on, is that the system can be simultaneously in all the individual states ($|\Psi_n\rangle$) instead of just being in one of them like for mixed states[2] [7]. This means that when you perturb the system, with for example a magnetic field, you will affect all the states in the superposition.

An example of a superposition that will be important for the **QGEM**-protocol is the superposition of a system where the only degree of freedom of the different states is its spin. This spin can be spin up ($\uparrow$) or spin down ($\downarrow$) with equal probability (and sign), such that the superposition is given by:

$$|\Psi\rangle = \frac{1}{\sqrt{2}} \left(|\uparrow\rangle + |\downarrow\rangle\right) \tag{4}$$

The factor of $1/\sqrt{2}$ makes sure that that $|\Psi\rangle$ is normalized.

3 Entanglement

The individual states ($|\Psi_n\rangle$) of a system $\mathcal{S}$ span the Hilbert space ($\mathcal{H}$) of that system [19]. If one has two different systems ($\mathcal{S}_1$& $\mathcal{S}_2$), than in the combined Hilbert space of those systems ($\mathcal{H}$=$\mathcal{H}_1 \otimes \mathcal{H}_2$) one can have that the total state of the combined system ($\mathcal{S}$) can be written either as a tensor product of the two states of both systems, or not [19]. If one has the former then the state of the combined system can be expressed as:

$$|\Psi\rangle = |\Psi\rangle_1 \otimes |\Psi\rangle_2 = \sum\sum c_n c_m \, |\Psi_n\rangle_1 \, |\Psi_m\rangle_2 \tag{5}$$

From this we see that a particular state $|\Psi_m\rangle$ in $\mathcal{S}_2$ couples to all individual states $|\Psi_n\rangle$ of $\mathcal{S}_1$ in a similar manner, hence the states are separable [19]. This implies that a measurement on $\mathcal{S}_2$ gives no information about the conditions of $\mathcal{S}_1$ [7], having that the total system $\mathcal{S}$ can just be described by $\mathcal{S}_1$ and $\mathcal{S}_2$ separably. However, when the states of $\mathcal{S}$ upon coupling of $\mathcal{S}_1$ and $\mathcal{S}_2$ cannot be written as a tensor product, like in Eq.(5), we have that the systems are entangled [7, 19], implying that both systems are no longer separable [19]. This non-separability implies that a measurement on $\mathcal{S}_2$ directly influences the result of a measurement on $\mathcal{S}_1$. The degree of entanglement of pure states, or in other words the degree in which a measurement on $\mathcal{S}_2$ influences that of $\mathcal{S}_1$, can be expressed by the von Neumann entropy[3] [7, 19]. If two systems are maximally entangled than one can get the most information out of $\mathcal{S}_1$ by measurements on $\mathcal{S}_2$, this corresponds to the von Neumann entropy by a value of $\log_2(d)$, with d the dimension of the Hilbert space[4] [19]. When S_{VN} equals zero the states are not entangled, they are separable, and the system is in the form of Eq.(5). The von Neumann entropy with regards to the **QGEM**-protocol will in more detail be discussed in Sec.(9) as more concepts underlying this protocol need to be addressed first.

Entanglement can occur in different ways, in the famous Einstein-Podolsky-Rosen (EPR) paradox entanglement occurs due to conservation laws after the decay of a particle [17]. In this "paradox" the decay of a neutral pion into a positron and an electron is considered:

$$\pi^0 \rightarrow e^- + e^+ \tag{6}$$

As the pion does not carry a spin ($S = 0$) one has by conservation of angular momentum that the electron and positron should have an opposite spin and the combined system has to be in the singlet configuration

[2] Mixed states are already in one of the pure states $|\Psi_n\rangle$ before measurements are taken [7].

[3] One can also express the degree of entanglement utilizing the state negativity [19]. However, in this thesis, only the von Neumann entropy (S_{VN}) will be considered for the degree of entanglement.

[4] It should be noted that this entropy is determined for one system only so, for example, concerning $\mathcal{S}_1$. This entropy comes from the effect the other system, $\mathcal{S}_2$, has on the reduced density matrix of $\mathcal{S}_1$. The concept of this "reduced density matrix" will be explained in the next section.

as they have $S = 0$ after the decay [17]. This means that the state for the spin degree of freedom, for the combined electron-positron system, after decay looks like [17]:

$$|\Psi\rangle = \frac{1}{\sqrt{2}} \left(|\uparrow\rangle_- |\downarrow\rangle_+ - |\downarrow\rangle_- |\uparrow\rangle_+ \right) \tag{7}$$

Here, the subscript (-) is understood to correspond to the electron and the subscript (+) to the positron. We can see that Eq.(7) is not of the form of Eq.(5) as not all the state combinations are included, therefore, the electron and the positron are entangled. The other thing to note is that the system is also maximally entangled as a measurement on the spin of the positron would automatically tell you what the spin of the electron should be, as one can see from Eq.(7)[5]. For example, if the positron is measured to be "spin-up" the electron should, as one can infer from Eq.(7), instantaneously collapse to the "spin-down" state to not violate conservation of angular momentum [17], therefore, a subsequent measurement on the electron would reveal that it has "spin-down". This instantaneous collapse into the "spin-down" state is independent on the distance between the electron and positron. One might, therefore, think that this violates causality, however, one has to remember that if one wants to compare the measurements, one has to transmit the outcomes to one another with normal, subluminal, methods as one cannot make copies of the system, due to the no-cloning theorem [17]. Therefore, causality is not violated.

Entanglement can also occur under the time evolution of interactions of different states of a superposition with those of another superposition, like in the **QGEM**-protocol. The time evolution of entanglement of the **QGEM**-protocol is induced by the gravitational force, and the interfering electromagnetic force (in the form of the Casimir-Polder potential), of 2 spatially separated mass superpositions, as will be discussed in Sec.(6). Another consequence of entanglement is that a single superposition can easily entangle with states of the environment, such as scattered air molecules, which will lead to decoherence of the superposition [6, 7, 18] as will be discussed in the next section.

One of the principles underlying entanglement is that Local Operations and Classical Communication (LOCC) cannot entangle systems which are initially separable [1, 4, 5]. This means that if we have two systems, A and B, both being influenced by their local operations, e.g. measurements by experimentalists, scattering with the environment or altercation by external fields, then these systems cannot become entangled if the communication between them happens through a classical channel. An example of this is that if we have say two quantum coins: Alice's coin (system A) and Bob's coin (system B), with the coin having two sides, head or tails. Then, if both Alice's and Bob's coin are flipped countless times there is no way that a coin flip of Alice's coin can influence the outcome of Bob's coin or vice versa if the communication between them is through a classical channel and thus no entanglement can occur. The implication, as we will see in Sec.(6.4), is that entanglement of both test masses of the **QGEM**-protocol cannot occur through a classical gravitational potential as this is a classical communicator. Suggesting that a measured entanglement of the two test masses should be of quantum nature and thus provides possible evidence for the quantum nature of their communicator: gravity.

4 Decoherence

4.1 General formalism

In reality, holding a superposition, as created in the **QGEM**-protocol, is very difficult due to decoherence effects. Decoherence is the loss of information of a system due to the entanglement of the system with the environment [7]. To understand the mathematical formulations around decoherence and how it ties to the **QGEM**-protocol, I have to introduce some theoretical formulations underlying the decoherence such as the density matrix of a system, which is defined as [7, 19]:

$$\rho = |\Psi\rangle \langle\Psi| \tag{8}$$

[5]That the system is maximally entangled can, also, be shown mathematically using the von Neumann entropy (S_{VN}), as one can show that the reduced density matrix, a concept to be introduced in the next section, of the electron/positron is proportional to the identity matrix. This implies that $S_{VN} = 1 = \log_2(2) = \log_2(d)$ and, thus, a maximum entanglement is present. How the reduced density is related to the von Neuman entropy is in more detail explained in Sec.(9).

For a two-component superposition, as indicated by Eq.(1), one will have that the reduced density matrix becomes:

$$\rho = \begin{pmatrix} |c_1|^2 & c_1 c_2^* \\ c_2 c_1^* & |c_2|^2 \end{pmatrix} \tag{9}$$

It should be stressed that this form of the density matrix depends on the basis of interest [7]. If we would, for example, have the basis of the superposition in the orthonormal basis, one would have that the off-diagonal terms in Eq.(9) are zero. On the other hand, if one would have expressed the superposition in a different basis than the off-diagonal terms are not necessarily zero [7].

If the superposition of the system is now "inserted" into an environment we have that each component of the system can interact differently with the states of the environment, having that the environment contains information of the system[6] [7]. Hence, as described in Sec.(3), this will result in entanglement of our n-component super-positioned system with the environment given by [7, 18]:

$$|\Psi\rangle = \sum c_n |\psi_n\rangle |E_n\rangle \tag{10}$$

In general it is impossible to know how this entanglement looks like due to the difficulty in expressing how $|E_n\rangle$ will unfold. However, luckily for us, one is only interested in the desired system ($\mathcal{S}$) composed of $|\psi_n\rangle$. One can extract the information of this desired system by means of the reduced density matrix [7, 18]:

$$\rho_{\mathcal{S}} = Tr_E(\rho_{SE}) = \sum \langle \phi_k | \rho_{SE} | \phi_k \rangle \tag{11}$$

Here, $\mathrm{Tr}_E(\rho_{SE})$ implies that the trace of the density matrix of our combined system-environment system with respect to the orthonormal basis in the environment system should be taken ("tracing out the degrees of freedoms of the environment"), which are the $|\phi_k\rangle$ states [7]. This results in the last expression of Eq.(11). If one uses Eq.(10) for ρ_{SE} than one would get using a similar approach as equation 2.49 in [7] that the reduced density matrix of the system will be:

$$\rho_{\mathcal{S}} = \sum_{nm=1}^{N} c_n c_m^* |\psi_n\rangle \langle \psi_m| \langle E_m | E_n \rangle \tag{12}$$

A similar expression can be found (without the explicit notation of the summation sign) in section 3.3.2 of Ref.[19]. By implementing the superposition of the spins as introduced by Eq.(4) in Sec.(2), where one should note that c_n=1/2 for both n=1,2, the reduced density matrix of the system reduces to:

$$\rho_{\mathcal{S}} = \frac{1}{2}(|\uparrow\rangle \langle\downarrow| + |\downarrow\rangle \langle\downarrow| + |\uparrow\rangle \langle\downarrow| \langle E2|E1\rangle + |\downarrow\rangle \langle\uparrow| \langle E2|E1\rangle) = 1/2 \begin{pmatrix} 1 & \langle E2|E1\rangle \\ \langle E2|E1\rangle & 1 \end{pmatrix} \tag{13}$$

From this expression, one can observe that the off-diagonal elements, the coherence terms, are completely dependent on the overlap of the two environmental states. If the two environmental states are completely distinguishable ($\langle E2|E1\rangle$=0) one has that the off-diagonal terms are zero and we will lose all coherence of the system [18], meaning a complete decoherence of the system. This is because the off-diagonal terms will be zero no matter the basis transformation on the system, implying that we will never measure the superposition of the system by employing only measurements on the system itself [18] due to the complete entanglement with the environment. The only way the retrieve this information is by doing measurements on the combined $\mathcal{S}E$ system, however, the states of the environment are usually inaccessible, making it impossible [18] to measure. On the other hand, if the two environmental states are completely indistinguishable then the overlap of the states is just unity, implying that $\rho_{\mathcal{S}}$ is the same as it would be if there was no environment present, having no external decoherence effects acting the system.

The relation of this overlap of the two resulting environmental states $|E_1\rangle$ & $|E_2\rangle$ and the decoherence of system $\mathcal{S}$ can formally be understand by the term "which-path" information, "which-state" information

[6] This is formally known as "which-path" information [7], which will in more detail be discussed at the end of this subsection and for the example of the scattering model of Sec.(4.2).

[7] or "which-way" information [18]. This expresses that the resulting environmental states carry certain information of the system after interaction with the system, resulting in the entanglement with the system. If the environmental states carry the same information than in no way will a measurement on the environment tell you anything about the system itself, having no decoherence of the system. However, in the other extreme case of no overlap of these states, we saw a complete decoherence of the system. This can with the "which-path" information be understood by the fact that $|E_1\rangle$ & $|E_2\rangle$ carry complete, but opposite, information of the system, implying that if one were to measure the environment to be in $|E_1\rangle$ than the system would collapse to $|\Psi_1\rangle$ in our case [18]. In between these extreme cases, the states of the environment carry partial-information of the system and this would reduce the coherence of the system to a certain degree [18].

4.2 Scattering model

In the **QGEM**-protocol, with the spatial superposition of a mesoscopic test mass, the main source of decoherence comes from the leaking of "which-path" information upon the scattering of environmental particles/photons[7]. One can see why this will lead to decoherence with the following reasoning: The state of the scattered particle depends on the energy and the position of the scattering center, however as the superimposed states of the test mass are spatially separated , one has that the positional state of the scattered particle will depend on which state of the test mass we are dealing with. Therefore, the scattered particle carries away "which-path" as the final state will give information about the particular states of the superposition. For a single scattered particle this leakage will not be significant [7] but as the number of scattered particles increases the leakage will grow and grow, eventually leading to full decoherence of the superposition. As this leakage depends on the scattering rate, one can intuitively guess that the decoherence of the system is time-dependent. In this section a derivation on this time dependence will be provided which is known as the scattering model [7]. This derivation follows the key points and assumptions made of the derivation given in Ref.[7], therefore, for a more detailed analysis of this derivation of the scattering model I refer the reader to Ref.[7].

In the scattering model we have that the two massive, superimposed states, of system are described by their position states, $|\mathbf{x}\rangle$, and are hit by the environmental particles, which can be molecules or photons, which can be described by their initial state $|\chi_i\rangle$ before interaction. The first assumption made is that the environment and system are initially uncorrelated [7], implying that their density matrices can be written as a tensor product at time t=0. The second assumption made is that the combined system-environment system is invariant under space translations [7], which is valid for an isotropic environment. The third assumption made is that the object of the system is much more massive than the environmental particles [7]. Therefore, it can safely be assumed that there is no recoil on the object of the system, hence $|\mathbf{x}\rangle$ is not affected by the scattering and stays intact. Combining the above assumptions, one will arrive as derived in Ref.[7] that the product of superimposed state with the scattered particle becomes:

$$|\mathbf{x}\rangle|\chi_i\rangle \rightarrow |\mathbf{x}\rangle|\chi(\mathbf{x})\rangle\,; \quad |\chi(\mathbf{x})\rangle = e^{-i\mathbf{q}\cdot\mathbf{x}/\hbar}\hat{S}_0 e^{i\mathbf{q}\cdot\mathbf{x}/\hbar}|\chi_i\rangle \tag{14}$$

Here, $\mathbf{q}$ is the momentum of the scattered environmental particle and $\hat{S}_0$ is the scattering operator acting on the scattering center (the systems object) located at the center, such that $e^{-i\mathbf{q}\cdot\mathbf{x}/\hbar}\hat{S}_0 e^{i\mathbf{q}\cdot\mathbf{x}/\hbar} = \hat{S}_{\mathbf{x}}$ is called the translated scattering operator. If one would do the same procedure for the other superimposed state with position state $|\mathbf{x}'\rangle$ one would logically arrive that the final state of the scattered particle is given by $|\chi(\mathbf{x}')\rangle$. Then, by using Eq.(14) together with the first assumption and Eq.(12) with c_n=1, one will as shown in Ref.[7] have that the evolution of the reduced density matrix of the system is given by:

$$\rho_{\mathcal{S}}(\mathbf{x},\mathbf{x}',0) \rightarrow \rho_{\mathcal{S}}(\mathbf{x},\mathbf{x}',0)\,\langle\chi(\mathbf{x}')|\chi(\mathbf{x})\rangle \tag{15}$$

From this equation, we note that the diagonal terms do not evolve in time as they correspond to the same superimposed state ($\mathbf{x}$'=$\mathbf{x}$), and the off-diagonal terms depend on the overlap of the final environmental

[7]There will also be a contribution of leaking of "which-path" information of the systems by absorption of the environmental photons and emission of photons from the test masses itself [6]. The leaking of "which-path" information of these sources will also be implemented in Sec.(10.5).

states ($\langle\chi(\mathbf{x}')|\chi(\mathbf{x})\rangle$), which is consistent with the arguments of Sec.(4.1).

The next step includes the calculation of $\langle\chi(\mathbf{x}')|\chi(\mathbf{x})\rangle$, using Eq.(15) one will get that $\langle\chi(\mathbf{x}')|\chi(\mathbf{x})\rangle = \langle\chi_i|\hat{S_{\mathbf{x}'}}^{\dagger}\hat{S}_{\mathbf{x}}|\chi_i\rangle$, which is just the expectation value of $\hat{S_{\mathbf{x}'}}^{\dagger}\hat{S}_{\mathbf{x}}$. This can also be calculated with the tracing rule in the environmental system [7], because $\langle O\rangle = \mathrm{Tr}_E(\rho_E O)$. Therefore, we get that $\langle\chi(\mathbf{x}')|\chi(\mathbf{x})\rangle$ is given by:

$$\langle\chi(\mathbf{x}')|\chi(\mathbf{x})\rangle = Tr_E(\rho_E(0)\hat{S_{\mathbf{x}'}}^{\dagger}\hat{S}_{\mathbf{x}}) \tag{16}$$

From here on, the assumption is made that the environmental particles are confined in a box like volume [7], which fixes the allowed momentum states in the volume, where we call this "momentum-set" $\mathbf{Q}_V$. Using the normalized momentum states in this box ($|\tilde{\mathbf{q}}\rangle = (\frac{(2\pi\hbar)^3}{V})^{1/2}|\mathbf{q}\rangle$), one will have that the density matrix of the environment at $t=0$ can be expressed as [7]:

$$\rho_E(0) = \frac{(2\pi\hbar)^3}{V}\sum_{\mathbf{q}\,\in\,\mathbf{Q}_V}\mu(\mathbf{q})\,|\tilde{\mathbf{q}}\rangle\,\langle\tilde{\mathbf{q}}|\ , \tag{17}$$

Here, V is the volume of the box, and $\mu(\mathbf{q})$ is the momentum space operator given by [20]:

$$\mu(\mathbf{q}) = (\frac{1}{2\pi m k_B T})^{3/2} e^{-\mathbf{q}^2/(2mk_bT)} \tag{18}$$

Then, one can substitute Eq.(17) in Eq.(16), where one can also use that $\hat{S_0}$ can be expressed as $\hat{S_0} = \hat{I} + i\hat{T}$, where $\hat{T}$ is the T-matrix that is diagonal in the orthonormal basis of the momentum $\{|\tilde{\mathbf{q}}\rangle\}$ [7]. Doing so, one will have that the overlap function becomes:

$$\langle\chi(\mathbf{x}')|\chi(\mathbf{x})\rangle = 1 - \int d\mathbf{q}\,\mu(\mathbf{q})\frac{(2\pi\hbar)^3}{V}\int d\mathbf{q}'(1 - e^{i(\mathbf{q}\text{-}\mathbf{q}')\cdot(\mathbf{x}\text{-}\mathbf{x}')/\hbar})|\,\langle\mathbf{q}|\hat{T}|\mathbf{q}'\rangle\,|^2 \tag{19}$$

The intermediate steps and expressions used in arriving to this result can be found in section 3.2 of Ref.[7].

By substituting this expression in Eq.(15) the reduced density matrix reduces to:

$$\rho_S(\mathbf{x},\mathbf{x}',0) \to \rho_S(\mathbf{x},\mathbf{x}',0) \times \left(1 - \int d\mathbf{q}\,\mu(\mathbf{q})\frac{(2\pi\hbar)^3}{V}\int d\mathbf{q}'(1 - e^{i(\mathbf{q}\text{-}\mathbf{q}')\cdot(\mathbf{x}\text{-}\mathbf{x}')/\hbar})|\,\langle\mathbf{q}|\hat{T}|\mathbf{q}'\rangle\,|^2\right) \tag{20}$$

The next step includes calculating the transition probability of the environmental particle to go from momentum $\mathbf{q} \to \mathbf{q}'$ upon scattering ($|\,\langle\mathbf{q}|\hat{T}|\mathbf{q}'\rangle\,|^2$). This calcultation can be done by noting that $|\,\langle\mathbf{q}|\hat{T}|\mathbf{q}'\rangle\,|^2 = \frac{1}{(2\pi m\hbar)^2}\delta^2(E-E')|f(\mathbf{q},\mathbf{q}')|^2$ [7]. Here, $|f(\mathbf{q},\mathbf{q}')|^2$ is the differential cross-section of the scattering process. The delta function can be evaluated using its Fourier integral representation:

$$\delta(E-E') = \frac{1}{2\pi\hbar}\lim_{T'\to\infty}\int_{-T'/2}^{T'/2} e^{i(E-E')t/\hbar}dt \tag{21}$$

Substituting that in the expression of the transition probability and taking a time T to be sufficiently larger than the scattering time such that $\lim_{T'\to\infty} = T$ one will arrive at:

$$\delta^2(E-E) = \delta(E-E')\frac{1}{2\pi\hbar}\lim_{T'\to\infty}\int_{-T'/2}^{T'/2} e^{i(E-E')t/\hbar}dt = \delta(E-E')\frac{T}{2\pi\hbar} \tag{22}$$

T is also assumed to be smaller than the decoherence time, this is valid because it takes a lot of collisions for the system to decohere [7]. Then, after taking the limit of the integral, and by using $E^{(\prime)} = \frac{|q^{(\prime)}|}{2m}$m, one will (as shown in Ref.[7]) have that $|\,\langle\mathbf{q}|\hat{T}|\mathbf{q}'\rangle\,|^2$ becomes:

$$|\,\langle\mathbf{q}|\hat{T}|\mathbf{q}'\rangle\,|^2 = \frac{mT}{(2\pi\hbar)^3}\frac{\delta(|\mathbf{q}|-|\mathbf{q}'|)}{|\mathbf{q}|}|f(\mathbf{q},\mathbf{q}')|^2) \tag{23}$$

This equation tells us that, due to presence of the delta-function, we have that upon integration the magnitudes of the momentum are equal before and after the collision [7], which allows us to write $\mathrm{d}\mathbf{q}'=|\mathbf{q}|^2\mathrm{d}n'$ & $\mathbf{q}^{(\prime)}=|\mathbf{q}^{(\prime)}|n^{(\prime)}$, where $\mathrm{d}n'$ is a solid angle in momentum space. Substituting these expressions together with Eq.(23) in Eq.(20) gives us as shown in Ref.[7]:

$$\rho_{\mathcal{S}}(\mathbf{x},\mathbf{x}',0) \to \rho_{\mathcal{S}}(\mathbf{x},\mathbf{x}',0) \times \left(1 - T\int d\mathbf{q}\,\mu(\mathbf{q})\frac{|\mathbf{q}|}{mV}\int dn'(1-e^{iq(\mathbf{n\text{-}n'})\cdot(\mathbf{x\text{-}x'})/\hbar})|f(q\mathbf{n},q\mathbf{n}')|^2\right) \tag{24}$$

Next, we can set $\frac{|\mathbf{q}|}{m} = v(q)$ in the above expression, with $v(q)$ denoting the velocity of the particle of a certain momentum q[8]. The obtained expression is valid for a single scattering event, however, we are interested in multiple scattering events (where we call this number N). Therefore, one can simply multiple the obtained expression by N and make our final assumption: the incoming particles/photons have an isotropic distribution, this implies that one can write [7]

$$\mathrm{d}\mathbf{q}\,\mu(\mathbf{q}) = \frac{N}{4\pi V}\mathrm{d}|\mathbf{q}|\,\varrho(q)\mathrm{d}n\,, \tag{25}$$

having that Eq.(24) becomes:

$$\rho_{\mathcal{S}}(\mathbf{x},\mathbf{x}',0) \to \rho_{\mathcal{S}}(\mathbf{x},\mathbf{x}',0) \times (1 - T\ \mathrm{F}(\mathbf{x}-\mathbf{x}'))$$

$$\text{With } \mathrm{F}(\mathbf{x}\text{-}\mathbf{x}') \text{ given by: } \int \mathrm{d}q\varrho(q)v(q)\int\frac{\mathrm{d}n\mathrm{d}n'}{4\pi}(1-e^{iq(\mathbf{n\text{-}n'})\cdot(\mathbf{x\text{-}x'})/\hbar})|f(q\mathbf{n},q\mathbf{n}')|^2 \tag{26}$$

Here, $\mathrm{F}(\mathbf{x}\text{-}\mathbf{x}')$ is what we call the decoherence factor. This equation gives the general description of the evolution of the off-diagonal terms of the reduced density matrix [7] and thus gives a description of the decoherence of our superposition.

4.3 Short- and long-wavelength limit

Eq.(26) is still a very general equation that describes the collisional decoherence. Therefore, to get analytical results, one can distinguish between two limiting cases, namely the short- and long-wavelength limit [7]. The short-wavelength limit relies on the assumption that the wavelengths (λ) of the environmental particles/photons are much smaller than the superposition size ($|\mathbf{x}-\mathbf{x}'| = \Delta x$), whereas for the long-wavelength it is the other way around. For the derivation of both limiting cases, I will again follow the main points of the derivation of Ref.[7].

- As mentioned earlier in the short wavelength limit we have that

$$\lambda << |\mathbf{x}-\mathbf{x}'| = \Delta x\,, \tag{27}$$

  implying that $q\Delta x/\hbar = \frac{2\pi\Delta x}{\lambda} >> 1$. Consequently, the contribution of the exponent in the integral w.r.t to the factor of 1 of $\mathrm{F}(\mathbf{x}\text{-}\mathbf{x}')$ can be neglected as it oscillates very rapidly [7]. Therefore, one will arrive at the following approximation for the decoherence factor:

$$F(\mathbf{x}-\mathbf{x}') = \int \mathrm{d}q\varrho(q)v(q)\int\frac{\mathrm{d}n\mathrm{d}n'}{4\pi}|f(q\mathbf{n},q\mathbf{n}')|^2 \tag{28}$$

  As defined earlier, $|f(q\mathbf{n},q\mathbf{n}')|^2$ is the differential cross-section, therefore, integrating over the solid angle $\mathrm{d}\mathbf{n}'$ will give us the cross section of momentum q in the $\mathbf{n}$ direction. Hence, performing the integral over $\mathrm{d}\mathbf{n}/4\pi$ will average over all the momentum q and we will get the total cross-section for

[8] After substitution of $\frac{|\mathbf{q}|}{m} = v(q)$ the expression for these particles will be the same if one deduced the same expressions for photons, because than the previously used energy would have been E=$|\mathbf{q}|$c instead of $E^{(\prime)} = \frac{|q^{(\prime)}|}{2m}$. One should also note that for photons one has $v(q) = c$.

momentum q: $\int \frac{\mathrm{d}n\mathrm{d}n'}{4\pi}|f(q\mathbf{n}, q\mathbf{n}')|^2 = \sigma_{tot}(q)$ [7]. Next, we realise that $\varrho(q)v(q)\sigma_{tot}(q)$ is nothing else than the scattering rate for an incoming environmental particle/photon with momentum q ($\Gamma(q)$) [7], hence, one arrives at the following description for the decoherence factor for the short wavelength limit [7]:

$$F(\mathbf{x}-\mathbf{x}') = \int \mathrm{d}q\,\Gamma(q) = \Gamma_{\mathrm{tot}} \tag{29}$$

Here, Γ_{tot} is the total scattering rate of the environmental particles.

- For the long wavelength limit one has that

$$\lambda >> |\mathbf{x}-\mathbf{x}'| = \Delta x\,, \tag{30}$$

hence the term in the exponent in Eq.(26) is now much smaller than 1. Therefore one can Taylor expand the exponent to the first relevant term. This firt relevant term is the quadratic term of the expansion, because the "1" cancels with the 1 already present in F(**x**-**x**'), and the linear term results in the integral to be zero. This is because the linear term is odd in (**n**-**n**′), while $|f(q\mathbf{n}, q\mathbf{n}')|^2$ is even in (**n**-**n**′) [7]. With the first relevant term the expression for F(**x**-**x**') will reduce to:

$$F(\mathbf{x}-\mathbf{x}') = \int \mathrm{d}q\varrho(q)v(q)q^2 \int \frac{\mathrm{d}n\mathrm{d}n'}{8\pi\hbar}[(\mathbf{x}-\mathbf{x}')\cdot(\mathbf{n}-\mathbf{n}')]^2|f(q\mathbf{n}, q\mathbf{n}')|^2 \tag{31}$$

The next step in the derivation includes making the assumption that the scattering cross-section is isotropic, i.e. only depends on the momentum and the scattering angle (Θ) [7]. With this assumption one will as argued in [7] arrive at:

$$F(\mathbf{x}-\mathbf{x}') = (\mathbf{x}-\mathbf{x}')^2 \int \mathrm{d}q\varrho(q)v(q)q^2 \int \frac{\mathrm{d}\cos\Theta 2\pi}{3\hbar^2}(1-\cos\Theta)|f(q,\cos(\Theta)|^2 \tag{32}$$

The intermediate steps in arriving at the above equation can also be found in Ref.[7]. Defining the second integral as the effective cross section ($\hbar^{-2}\sigma_{\mathrm{eff}}(q)$), and after that defining $\int \mathrm{d}q\varrho(q)v(q)q^2\hbar^{-2}\sigma_{\mathrm{eff}}(q) = \Lambda$, with Λ as the scattering constant, one will get that the resulting decoherence factor F(**x**-**x**') for the long wavelength limit results in [7]:

$$F(\mathbf{x}-\mathbf{x}') = \Lambda(\mathbf{x}-\mathbf{x}')^2 \tag{33}$$

Combining the expression for the long- wavelength limit, Eq.(33), with the equation for the short- wavelength limit, Eq.(29), in the equation of the decoherence factor, Eq.(26), and making the assumption that we are dealing with N different types of short-wavelength particles/photons and M long wavelength particles/photons one will have that Eq.(26) becomes:

$$\rho_{\mathcal{S}}(\mathbf{x},\mathbf{x}',T) = \rho_{\mathcal{S}}(\mathbf{x},\mathbf{x}',0) \times (1 - T(\sum_i^N \Gamma_{\mathbf{tot},i} + \sum_j^M \Lambda_j(\mathbf{x}-\mathbf{x}')^2) \tag{34}$$

Then the final assumption is made: the change in the reduced density matrix due to collisional decoherence is the most significant contribution in the change of the reduced density matrix, such that its time evolution is dominantly determined by Eq.(34)[9]. With this assumption, one will have that the time evolution of the reduced density matrix can be written as:

$$\frac{\rho_{\mathcal{S}}(\mathbf{x},\mathbf{x}',T) - \rho_{\mathcal{S}}(\mathbf{x},\mathbf{x}',0)}{T} = -\rho_{\mathcal{S}}(\mathbf{x},\mathbf{x}',0)(\sum_i^N \Gamma_{\mathbf{tot},i} + \sum_j^M \Lambda_j(\mathbf{x}-\mathbf{x}')^2) \tag{35}$$

[9] One has to note again that there is also a significant decoherence contribution form absorption and emission of photons, but they can be modelled in a similar fashion [6], and will just be an addition to the summation over Λ_j as we will see in Sec.(10.5) and App.(B.2).

The term on the right is nothing else then the differential limit of the reduced density matrix with respect to T. So by taking this differential limit and rewriting the time variable as t, as normally done for time, one obtains:

$$\frac{\partial \rho_{\mathcal{S}}(\mathbf{x}, \mathbf{x}', t)}{\partial t} = -\rho_{\mathcal{S}}(\mathbf{x}, \mathbf{x}', t)(\sum_{i}^{N} \Gamma_{\mathbf{tot},i} + \sum_{j}^{M} \Lambda_j (\mathbf{x} - \mathbf{x}')^2) \tag{36}$$

This is just a first order differential equation. By noting that $\sum_i^N \Gamma_{\mathbf{tot},i} + \sum_j^M \Lambda_j (\mathbf{x} - \mathbf{x}')^2$ is for a constant superposition size, in a constant isotropic medium, time independent, we obtain:

$$\rho_{\mathcal{S}}(\mathbf{x}, \mathbf{x}', t) = \rho_{\mathcal{S}}(\mathbf{x}, \mathbf{x}', 0) e^{-\gamma t} \quad ; \quad \gamma = \sum_{i}^{N} \Gamma_{\mathbf{tot},i} + \sum_{j}^{M} \Lambda_j (\mathbf{x} - \mathbf{x}')^2 \tag{37}$$

This equation describes the time evolution of the off-diagonal terms of the reduced density matrix of the system in terms of the decoherence rate (γ) assuming that this is the only "source" that influences the reduced density matrix. From this equation we also make the observation that as time evolves, the off-diagonal terms are reduced exponentially, meaning that decoherence of the system is exponential in time. The strength of the decoherence is determined by the decoherence rate, which in turns depends on the scattering rates & constants of the environmental particles/photons, and the size of the superposition.

We will also see that, during some steps of the **QGEM**-protocol, the superposition size (**x**-**x**') is depended on time, in that limit Eq.(36) will reduce to:

$$\rho_{\mathcal{S}}(\mathbf{x}, \mathbf{x}', t) = \rho_{\mathcal{S}}(\mathbf{x}, \mathbf{x}', 0) \exp\left\{ - \left(\sum_{i}^{N} \Gamma_{\mathbf{tot},i} t + \sum_{j}^{M} \Lambda_j \int (\mathbf{x}(t) - \mathbf{x}'(t))^2 \mathrm{d}t \right) \right\} \tag{38}$$

In the rest of the thesis, the term in the exponent will be written down as:

$$\int \gamma_k \mathrm{d}t = \sum_k \gamma_k \Delta t = \left(\sum_{i}^{N} \Gamma_{\mathbf{tot},i} t + \sum_{j}^{M} \Lambda_j \int (\mathbf{x}(t) - \mathbf{x}'(t))^2 \mathrm{d}t \right) \tag{39}$$

4.4 Master equations

In the previous subsection it was assumed that to get from Eq.(34) to Eq.(37) there were no other factors that give a time-dependent contribution to the time evolution of the reduced density matrix of the system. However, besides the external decoherence, we also have the contribution of the self Hamiltonian of the system on the evolution of $\rho_{\mathcal{S}}$, which can be altered by the environment and will be denoted by $H_{\mathcal{S}'}$. To see that this Hamiltonian changes the reduced density matrix we make use of the Schrödinger equation and follow the derivation of Ref.[21]. Neglecting the decoherence for the moment we have:

$$\frac{\partial \rho_{\mathcal{S}}}{\partial t} = \frac{\partial}{\partial t} (|\psi\rangle \langle\psi|) \tag{40}$$

Here, use has been made of the definition of Eq.(8). By expending the differential expression on the right and by using the definition of the Schrödinger equation as indicated by equation 1.25 in Ref.[21], we obtain:

$$\frac{\partial \rho_{\mathcal{S}}}{\partial t} = -\frac{i}{\hbar}(H_{\mathcal{S}'} \rho_{\mathcal{S}} - \rho_{\mathcal{S}} H_{\mathcal{S}'}) = -\frac{i}{\hbar}[H_{\mathcal{S}'}, \rho_{\mathcal{S}}] \tag{41}$$

This term will for time-independent Hamiltonians not lead to decoherence in the long time limit, but will give an oscillation of the off-diagonal terms in terms of the energy terms of the states [21], or in the case of the free hamiltonian will lead to a growing coherence length of the system [7]. Therefore, such unitary Hamiltonians are not the worrying part for the evolution of the density matrix in terms of decoherence.

Combining Eq.(41) with a general decoherence term, $\mathcal{D}$, will give a general description of the time evolution of the off-diagonal terms of the reduced density matrix of a system, which is called a master equation [7]. The general form of the master equation is therefore

$$\frac{\mathrm{d}\rho_{\mathcal{S}}}{\mathrm{d}t} = -\frac{i}{\hbar}[H_{\mathcal{S}'}, \rho_{\mathcal{S}}] + \mathcal{D}[\rho_{\mathcal{S}}]\,, \tag{42}$$

where all terms are understood to be operators. One can get to more simplified master equations by making some additional assumptions on the system. Some examples of these simplified master equations are the Born-Markov master equation or the Lindblad form, which can be found in chapter 4 of [7]. However, in this thesis, we focus our interest only on the worrying term of the evolution of $\rho_{\mathcal{S}}$, which is the decoherence term $\mathcal{D}[\rho_{\mathcal{S}}]$. For the scattering of environmental particles on a superposition, this term can as derived earlier be represented by the right term of Eq.(36)[10].

5 Casimir Effect

Another important aspect related to the **QGEM**-protocol is the Casimir Effect. From quantum field theory we now that fields, like the electric field, possess the so-called vacuum energy with an infinite constant energy [22]. This will in our daily life not cause any problems as we are measuring energy differences. However, when one imposes boundary conditions on the field one will get a difference in the vacuum energy in between those boundaries, as there is a restriction the allowed eletromagnetic wave modes in between the boundarie. This causes a force to exhibit between those boundaries [10] as the pressure of the fluctation of the vacuum from the outside of the boundaries is different from that of in between the two boundaries. It is good to note that this force is a manifestation of quantum field theory and would with a classical treatment not be present. Consequently, this force is a quantum communicator and can entangle two systems.

For the electromagnetic (EM) field such boundary conditions arise when one puts two dielectric/conducting materials very close to each other as this fixes the allowed electromagnetic wave modes in between and outside of the two materials [10] and this fixes, therefore, the allowed fluctuations of the EM-field in the different regions. This phenomenon was first studied by H. Casimir who showed that the insertion of two perfect conducting plates very close to each other led to an attractive force between these plates [10], this is why we call this phenomenon the "Casimir effect".

Logically different boundary conditions will give rise to different forms of the Casimir force. Besides the geometrical shapes of the objects, the type of material (dielectric, conductor, perfect conductor) will also affect the boundary conditions as the type of material affects the transmission of electromagnetic waves. This transparency of the material plays an important part in the boundary conditions as lower transparent materials lower the amount of distinguishable electromagnetic wave modes outside and inside the boundaries, lowering the Casimir force [9].

In this thesis, we are interested in the Casimir force caused by two types of boundary conditions:
1.) The Casimir force caused by two dielectric spheres, as in the **QGEM**-protocol two diamond test masses approach each-other up to around 200 μm [1], which will restrict the experiment as we will see in Sec.(7). The test masses can be assumed to be spherical [1] and because diamond is a dielectric we get the boundary conditions for two dielectric spheres.
2.) The Casimir force between a dielectric sphere and a conductive plate. In Sec.(8), the modified setup for the **QGEM**-protocol will be proposed in which the test mass are very close to a conductive plate, in the order of 10μm. This causes a force to exhibit between the dielectric test mass and the conductive plate, which will also cause a restriction on the experiment. Therefore, the manifestation of this Casimir force should also be modeled.

[10] It should be noted that writing the decoherence term this way is also what comes forward for the decoherence term for scattering events if the master equation would be written in the Lindblad form [7].

For the case of the dielectric spheres, the mesoscopic test masses of the **QGEM**-protocol will be modeled as large neutral atoms, which is also what is done in the original paper [1]. The resulting Casimir force of two neutral atoms was calculated by Casimir and Polder [8] and as we are dealing with relatively large separations with respect to the size of the objects, $R \sim 100n\text{m}{-}1\mu\text{m}$, we can apply the large distance limit giving the potential energy between the two test masses of [8]:

$$V_{CP} = -\frac{23\hbar c}{4\pi}\frac{\alpha(A)\alpha(B)}{x^7} = -\frac{23\hbar c}{4\pi}\frac{\alpha^2(A)}{x^7} \tag{43}$$

Here, x is the separation of the two test masses and $\alpha(A)$ & $\alpha(B)$ are the static polarizabilities of both test masses. In the last line use has been that we are dealing with identical test masses such that their static polarizabilities are equal.

Using that the test masses are only made out of diamond, are again spherical, and are in a high vacuum environment [1] the static polarizibility can as in Ref.[23] be modelled to be:

$$\alpha(A) = R^3\frac{\epsilon - 1}{\epsilon + 2} \tag{44}$$

Here, R is the radius of the test mass and ϵ is the dielectric constant of the test mass. Substituting this expression in Eq.(43) gives the Casimir-Polder potential between the diamond test masses of [1] to be:

$$V_{CP} = -\frac{23\hbar c}{4\pi}\frac{R^6}{x^7}\left(\frac{\epsilon - 1}{\epsilon + 2}\right)^2 \tag{45}$$

The Casimir force between a dielectric sphere and a conducting plate was derived in Ref.[24]. However, for complete screening of electromagnetic waves by the conducting plate the assumption will be made that the plate is a perfect conductor (reflective for all electromagnetic waves). The validity of this assumption will be discussed in Sec.(13.2). In the perfect conducting limit the Casimir force between the plate and the dielectric test mass is also given in Ref.[24] and is given by:

$$F_{\text{casimir}} = -\frac{1}{4\pi x^4}\int_0^\infty \mathrm{d}\omega\, \alpha_1(\omega)[3\sin(2\omega x) - 6\omega x\cos(2\omega x) - 6\omega^2 x^2\sin(2\omega x) + 4x^3\omega^3\cos(2\omega x)]\,, \tag{46}$$

here, x is again a separation, but now between sphere and plate, $\alpha_1(\omega)$ is the real part of the polarizability of the sphere and ω is the frequency of the electromagnetic waves in the medium in between the sphere and the plate. The polarizability of the sphere is again the static polarizibility of Eq.(44), but now with a frequency dependence on the dielectric constant[11] [24]:

$$\alpha = R^3\frac{\epsilon(\omega) - 1}{\epsilon(\omega) + 2} \tag{47}$$

6 QGEM-protocol

As mentioned before, the **QGEM**-protocol aims to prove the existence of the quantum nature of gravity through the entanglement of spatially separated superpositions of two mesoscopic test masses utilising the difference in gravitational interactions [1]. To provide evidence for this quantum nature of gravity, the current setup of the experiment consists of three steps which will thoroughly be explained in this section. These steps are also displayed in Fig.(1) with the relevant parameters.

[11] In Sec.(8) this static polarizibility will again reduce to the one of Eq.(44) as α of the test mass can be assumed to be frequency independent for diamond.

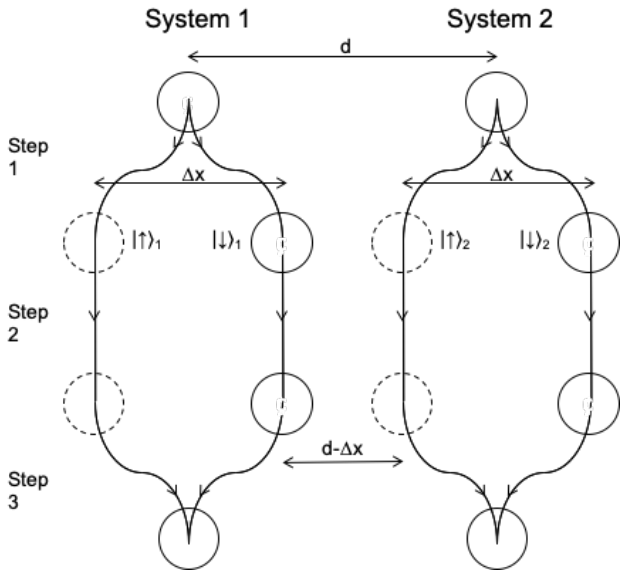

Figure 1: Setup of the current proposition of the **QGEM**-protocol. First, two superpositions are created by spin coupling to the NV-point of diamond. The states of the superposition will be spatially separated by a Stern-Gerlach interferometer (step 1). After this, both superpositions will become entangled by mutual gravitational interaction during a free fall (step 2), this entanglement can only occur if gravity has a quantum nature. The last step (step 3) consists of bringing the superpositions back by "reversing" the magnetic field of the Stern-Gerlach interferometer of step 1, followed by a measurement of the entanglement with a suitable entanglement witness $\mathcal{W}$. It is good to realize that the indicated distances and paths traveled in each step are not drawn on a scale.

6.1 Step 1

Step 1 consists of creating a superposition of the test mass of significant size [1]. To create the superposition spin coupling to the Nitrogen-Vacancy(NV)-point defect of the diamond test mass is used[12]. This makes the initial center of mass of the test mass "split up" into two spin-dependent superimposed states: the left localized state $|L,\uparrow\rangle$ and the right localized state $|R,\uparrow\rangle$[13] [1]. For further analysis, the shorthand notation of $|\uparrow\rangle$ for the left and $|\downarrow\rangle$ for the right localized state will be used. Although, usually, one would use spin-up and spin-down states which have a magnitude of S=$\hbar/2$, we are in this context dealing with S=$\hbar$ [11], meaning that $|\uparrow\rangle$ refers to a state with m_s=$\hbar$ & $|\downarrow\rangle$ refers to a state with m_s=-$\hbar$. The superposition that with this coupling mechanism is created is of the same form as in Eq.(4).

Now that a spin-dependent superposition is created the separation of these states can be increased utilizing a Stern-Gerlach matter-wave interferometer [1, 11]. The Stern-Gerlach interferometer makes use of the Stern-Gerlach effect, where objects with opposite spin are accelerated in the opposite direction when imposed in an inhomogeneous magnetic field [17]. By only caring about the motion in the horizontal direction ($\hat{x}$) of Fig.(1)[14] one has the Hamiltonian of one of the states given by:

$$H = \frac{\hat{p}_x^2}{2m} - \mu_s B\hat{x} \tag{48}$$

Here, μ_s is the magnetic moment of the spin, p_x the momentum of the state, mass m, in the x-direction and B

[12]For this it is assumed that there are no other point or surface defects present on the test masses itself and that the NV-point is in the center [11] of the test masses.

[13]We call the two spatially localized states left and right localized because the "left" state will be accelerated to the left and the "right" state to the right of Fig.(1) as we will see further on in this subsection. It is also good to note that this superposition is simultaneously created for both test masses.

[14]We also have, due to the free fall, gravitational potential energy in the vertical direction. However, this is not of importance for the superposition size created.

the magnetic field strength, which we assume to be only directed in the x-direction. This is the Hamiltonian which is taken into consideration in the original proposal of the **QGEM**-protocol [1, 11]. However, what was not realized and what was pointed out in Ref.[25] is that the test mass itself, made out of diamond, becomes magnetized when subjected to the magnetic field of the interferometer. This introduces an extra term in the Hamiltonian independent on the spin but is dependent on the bulk material of the test mass. Assuming the test mass to be spherical and only made out of diamond, as done before, we have that the total Hamiltonian, of one of the states, is represented in the horizontal direction by [25]:

$$H = \frac{\hat{p}_x^2}{2m} - \mu_s B\hat{x} - \frac{\chi_V}{2\mu_0(1+\chi_V)} B^2\hat{x} \tag{49}$$

Here χ_V is the volume magnetic susceptibility of the diamond test mass, which is $\chi_V \sim -2.2 \cdot 10^{-5}$ and V is the volume of the test mass. As shown in Ref.[25], the introduction of this magnetization term, let us call this the diamagnetic-energy term, will lead to an oscillatory motion[15] of the states around an equilibrium position, which depends if the state is spin-up or spin-down. This will restrict the maximum achievable superposition size, independent of the strength of the magnetic field gradient. For the given period of step 1 of the experiment of 500 ms [1], this will give a maximum superposition size of $\sim$ 10 nm for the mass of 10^{-14} kg. This is 5 orders of magnitude lower than what is needed for the original **QGEM**-protocol. Therefore, one needs to work around this new term in the Hamiltonian to make the experiment achievable. To do this, one needs to observe that diamond is a diamagnetic material, as χ_V is negative, therefore, the induced magnetic field inside the diamond is opposite to the external magnetic field. That is why the diamond test mass is attracted to the low magnetic field region and thus works against the gradient in the SG-interferometer. Paramagnetic and ferromagnetic materials, on the other hand, have a positive magnetic susceptibility and, therefore, align their induced magnetic field gradient towards the direction of the external magnetic field. Hence, such materials are attracted towards the high magnetic field region and work along the magnetic field gradient. Therefore, by coating the diamagnetic diamond core by a paramagnetic/ferromagnetic shell it is possible to cancel the induced diamagnetic energy of the core with that of the paramagnetic/ferromagnetic shell. This implies that one can cancel, or reduce significantly, the diamagnetic energy term in Eq.(49). The best suitable material for the coating and the most suitable way of coating, one layer or an extra diamond layer on top to keep the surface properties of diamond, are beyond the scope of this thesis, but in theory, it is, as argued, possible to make the diamagnetic energy contribution in the creation of the superposition size negligible and retrieve the Hamiltonian of Eq.(48).

A detailed description of how the superposition is reached with the SG-interferometer, with the Hamiltonian of Eq.(48), can be found in Ref.[11]. I will only go into the use-full points made to get the corresponding formula for the superposition size (Δx) in terms of the variable parameters: the magnetic field gradient and the mass of the test mass. For this derivation, I will first focus on the "traveled" distance of one of the superimposed states, for example, $|L,\uparrow\rangle$.

As described in Refs.[1, 11], we are dealing with a homogeneous magnetic field gradient ($\partial_x B$), thus, one can infer from the Hamiltonian of Eq.(48) that the acceleration in the horizontal direction of Fig.(1) is given by:

$$a = a_{\text{mag}} = \ddot{x} = \frac{\mu_s \cdot \partial_x B}{m} = \frac{g\mu_B}{m\hbar} S_x \partial_x B \tag{50}$$

Here, μ_B is the Bohr magnetic moment , g the Lande g factor and S_x is either spin up ($\hbar$) or spin down (-$\hbar$). From Eq.(50), one can observe that the acceleration is constant. Therefore, if the state is accelerated by a time of $\frac{\tau}{2}$ (with τ=500 ms as proposed in the original paper [1]) one will have that the travelled distance (Δx_1) will just be:

$$\Delta x_1 = \frac{a(\tau/2)^2}{2} \tag{51}$$

[15]This oscillatory motion is true as a magnetic field source with $B = 0$ at the center of the superposition is taken. If one wold have taken a mangetic field that has no zero point in the considered gradient region, we would not achieve an oscillatory motion but a translational one. Still the argument of the reduction of this diamangetic term is still relevant for such a magnetic source as this would also dimish this translational motion.

As mentioned in the **QGEM**-protocol (Ref.[1]) a spin flip happens at $t = \tau/2$, meaning that the acceleration will be directed in the opposite direction, leading to a deceleration of the state. This deceleration has also a period of t=$\tau/2$, leading to a further travelled distance of Δx_2 given by:

$$\Delta x_2 = -\frac{a(\tau/2)^2}{2} + a(\tau/2)^2 = \frac{a(\tau/2)^2}{2} \tag{52}$$

Combining the distance travelled by both the acceleration and deceleration period will give the total travelled distance of a single state $\Delta x_3 = \Delta x_1 + \Delta x_2$:

$$\Delta x_3 = \frac{a(\tau/2)^2}{2} + \frac{a(\tau/2)^2}{2} = a(\tau/2)^2 = \frac{g\mu_B}{m\hbar} S_x \partial_x B(\tau/2)^2 \tag{53}$$

It is important to know that up to now only the "travelled" distance of a single state has been treated. Both the spin up and spin down state have the same magnitude of $|S_x| = \hbar$, but are orientated in different directions. Therefore, they are accelerated in different directions and they both will have travelled a distance Δx_3 in opposite direction, giving a separation between the two states of:

$$\Delta x = 2\Delta x_3 = 2\frac{g\mu_B}{m\hbar} S_x \partial_x B(\tau/2)^2 = \frac{g\mu_B \partial_x B}{2m} \tau^2 \tag{54}$$

This expression matches the one given in the original paper [1]. It is also important to note that because the acceleration and deceleration period have the same time period, we get that the states are stationary with respect to the horizontal axis of Fig.(1) at the end of step 1.

6.2 Step 2

In this step the spin is coupled to its nuclear counterpart to make the states unaffected by the magnetic field [1]. However, one can also turn of the magnetic field inside the interferometer to accomplish the same goal. This implies that there is only a free fall towards the gravitational center of the earth (the vertical direction in Fig.(1)) for the two systems for a given time (t_{int}) which was originally proposed to be 2.5 s [1]. It is also good to note that the superposition created in step 1 is done for both test masses in adjacent Stern-Gernlach interferometers, which are initially a distance d apart. So we will get a situation with the indicated distances as shown in step 2 of Fig.(1).

In the **QGEM**-protocol it is assumed that we only have an entanglement in this step of the experiment[16] such that we initially have in step 2 of the experiment that the combined state of both test masses is given by [1]:

$$|\Psi(t=0)\rangle = \frac{1}{2}(|\uparrow\rangle_1 + |\downarrow\rangle_1)(|\uparrow\rangle_2 + |\downarrow\rangle_2) \tag{55}$$

The subscript 1 or 2 indicates with which interferometer/system, or in other words which test mass, we are dealing with. It is also good to observe that this equation is just of the form as written down in Eq.(5), having that the two systems are not entangled (yet). The entanglement comes from the difference in phase evolution of the interaction of the different states given by $\mathrm{e}^{iE_i t_{\text{int}}/\hbar}$, where E_i indicates the energy of the different combination of the states of Eq.(55), and $\hbar$ is the reduced plancks constant. Because the combination of states all have a different energy evolution we get that their phases ($E_i t_{\text{int}}/\hbar$) are different. This implies that in general Eq.(55) cannot be written as a tensor product anymore, but is given by:

$$|\Psi(t)\rangle = \frac{1}{2}[e^{iE_1 t/\hbar}|\uparrow\rangle_1|\downarrow\rangle_2 + e^{iE_2 t/\hbar}|\uparrow\rangle_1|\uparrow\rangle_2 + e^{iE_3 t/\hbar}|\downarrow\rangle_1|\downarrow\rangle_2 + e^{iE_4 t/\hbar}|\downarrow\rangle_1|\uparrow\rangle_2] \tag{56}$$

The goal of the experiment is that these phases are purely generated by the gravitational force. However, with the distances used to make the phase evolution measurable there is also a contribution of the Casimir-Polder interaction [1]. In order to have the phase evolution to depend mainly on the gravitational force I

[16] In Sec.(10.6) the evolution of the entanglement phase during step 1 and step 3 will, also, be included for a more realistic picture.

demand in this thesis that the graviational induced potential (V_G) is one order of magnitude larger than the Casimir-Polder potential (V_{CP}), just as what is originally proposed in Ref.[1] and will give better results than smaller ratios [26]. With this requirement it is also fairly reasonable to assume that the entanglement phases are generated by the gravitational force, as the induced phases will have the same order of magnitude difference. By assuming that the gravitational acceleration of the different states towards each-other is negligible, which is pretty accurate as we will see later on, one has that the horizontal distances between the states as indicated in Fig.(1) remain constant. Consequently, we get, with the distances indicated in Fig.(1), that Eq.(56) becomes at a time t=t_{int}:

$$|\Psi(t_{int})\rangle = \frac{1}{2}[e^{i\frac{Gm^2}{\hbar(d+\Delta x)}t_{int}}|\uparrow\rangle_1|\downarrow\rangle_2 + e^{i\frac{Gm^2}{\hbar d}t_{int}}|\uparrow\rangle_1|\uparrow\rangle_2 + e^{i\frac{Gm^2}{\hbar d}t_{int}}|\downarrow\rangle_1|\downarrow\rangle_2 + e^{i\frac{Gm^2}{\hbar(d-\Delta x)}t_{int}}|\downarrow\rangle_1|\uparrow\rangle_2] \tag{57}$$

Where I used that the energy between the states (E_i) is the Newtonian gravitational potential between two spheres[17] which is given by:

$$V_G = -\frac{Gm^2}{x} \tag{58}$$

With G the gravitational constant, m the mass of the test mass (assumed to have identical test masses), and x is again the separation between two states. By renaming $\frac{Gm^2}{\hbar d}t_{\text{int}} = \phi$, $\phi_{\uparrow\downarrow} = \frac{Gm^2}{\hbar(d+\Delta x)}t_{\text{int}}$,$\phi_{\downarrow\uparrow} = \frac{Gm^2}{\hbar(d-\Delta x)}t_{\text{int}}$, $\Delta\phi_{\uparrow\downarrow} = \phi_{\uparrow\downarrow} - \phi$, and $\Delta\phi_{\downarrow\uparrow} = \phi_{\downarrow\uparrow} - \phi$, one gets that Eq.(57) can be written as:

$$|\Psi(t_{int})\rangle = \frac{1}{2}e^{i\phi}[|\uparrow\rangle_1\{|\uparrow\rangle_2 + e^{i\Delta\phi_{\uparrow\downarrow}}|\downarrow\rangle_2\} + |\downarrow\rangle_1\{e^{i\Delta\phi_{\downarrow\uparrow}}|\uparrow\rangle_2 + |\downarrow\rangle_2\}] \tag{59}$$

This is exactly the same expression as the one given in Ref.[1]. We can also pull out the exponent of the second term in the equation to read:

$$|\Psi(t_{int})\rangle = \frac{1}{2}e^{i\phi}[|\uparrow\rangle_1\{|\uparrow\rangle_2 + e^{i\Delta\phi_{\uparrow\downarrow}}|\downarrow\rangle_2\} + e^{i\Delta\phi_{\downarrow\uparrow}}|\downarrow\rangle_1\{|\uparrow\rangle_2 + e^{-i\Delta\phi_{\downarrow\uparrow}}|\downarrow\rangle_2\}] \tag{60}$$

From this we see that when the phase in the exponent of the last term represents the exact same phase as the one of the first term ($\Delta\phi_{\uparrow\downarrow}$ represents the same phase as $-\Delta\phi_{\downarrow\uparrow}$) we have that $\{|\uparrow\rangle_2 + e^{i\Delta\phi_{\uparrow\downarrow}}|\downarrow\rangle_2\}$ is the same as $\{|\uparrow\rangle_2 + e^{-i\Delta\phi_{\downarrow\uparrow}}|\downarrow\rangle_2\}$, meaning that Eq.(60) can be factorized as:

$$|\Psi(t)\rangle = \frac{1}{2}(|\uparrow\rangle_1 + e^{i\Delta\phi_{\downarrow\uparrow}}|\downarrow\rangle_1)(|\uparrow\rangle_2 + e^{i\Delta\phi_{\uparrow\downarrow}}|\downarrow\rangle_2) \tag{61}$$

One can observe from this expression that it is in the form of Eq.(5), hence we have no entanglement. However, when $\Delta\phi_{\uparrow\downarrow}$ does not represent the same phase as $-\Delta\phi_{\downarrow\uparrow}$, we have that Eq.(60) cannot be factorized as in Eq.(61), hence it is not of the form of Eq.(5), implying that the two systems are entangled.

Saying that $\Delta\phi_{\uparrow\downarrow}$ represents the same phase as $-\Delta\phi_{\downarrow\uparrow}$ is the same as saying:

$$-\Delta\phi_{\downarrow\uparrow} = 2n\pi + \Delta\phi_{\uparrow\downarrow} \;\rightarrow\; \Delta\phi_{\uparrow\downarrow} + \Delta\phi_{\downarrow\uparrow} = 2n\pi\,; \quad \text{n is an integer} \tag{62}$$

This is the same as the requirement mentioned in Ref.[1]. Here it should be mentioned that the entanglement is maximum when $\Delta\phi_{\uparrow\downarrow} + \Delta\phi_{\downarrow\uparrow} = \pi$ as we will see in Sec.(9). Therefore, Eq.(63) below can be thought of representing how much the systems are entanglement, which is also what comes forward in Sec.(9) and this quantity will be called "the effective entanglement phase" throughout this thesis and has the exact form of:

$$\Phi_{\text{eff}} = \Delta\phi_{\uparrow\downarrow} + \Delta\phi_{\downarrow\uparrow} = \phi_{\uparrow\downarrow} + \phi_{\downarrow\uparrow} - 2\phi = \frac{Gm^2}{\hbar}t_{\text{int}}\left(\frac{1}{d-\Delta x} + \frac{1}{d+\Delta x} - 2\frac{1}{d}\right) \tag{63}$$

[17] This is as indicated in Ref.[1] and based on the results of Ref.[15] valid for the distance and non-relativistic regime we are dealing with. However, this is a classical approach, but as discussed in Sec.(3) we need a quantum potential for the systems to get entangled. This potential will be discussed in Sec.(6.4) and will give rise to the the same potential in the linearized gravity regime in the non-relativistic limit of the experiment.

6.3 Step 3

The last step of the experiment consists of proving that the entanglement of the two systems, as established in step 2 of the experiment, is indeed present. The first part of this step of the **QGEM**-protocol consists of bringing back the created superpositions. This is done first by "switching" the magnetic field back on by coupling the spin back from the nuclear part to the electronic state, or by simply turning the field back on. As mentioned before, the acceleration of the states towards each other is negligibly small in step 2 of the experiment, meaning that we can safely assume that the separation between the individual states and the size of the superposition remained constant during the free fall. Therefore, to bring the superposition back we can apply the same mechanism and time for both the acceleration and deceleration period ($\tau/2$) of step 1, but now in the inward direction. This makes that the superposition is brought back after a time of τ and is stationary [1] at the end.

After the superposition is brought back, one can measure the possible entanglement created in step 2 by measuring the spin of both test masses in different bases and look for the correlation between them. This is possible as we saw in Sec.(3) that entanglement of systems means that outcome of separate measurements on both systems are correlated to one another and, therefore, the spins (which is our degree of freedom) of both systems should be correlated if the systems are entangled. Certain combinations of measurements on the spin basis give rise to the so-called entanglement witness ($\mathcal{W}$) [1, 19, 26]. The expectation value of this witness can distinguish if the two systems are separable (no correlation between the measurements), or entangled (correlation between the measurements). The most suitable operator for this witness will in more detail be discussed in Sec.(9).

As mentioned in Sec.(3), if one finds that $\langle \mathcal{W} \rangle$ is, after statistical analysis, such that it would conclude that the two systems are entangled we have as argued by the LOCC theorem of Sec.(3) that gravity and its communicator (the Graviton) are of a quantum nature as will in more detail be explained in the next subsection. Therefore, this measurement determines the fate of gravity, is it classical or quantum?

6.4 Quantum potential

During the **QGEM**-protocol all external fields that are acting on, and being experienced by, both test masses[18] can only make local operations on both systems [1]. Therefore, the entanglement of both systems as represented by Eq.(59), with the phase of Eq.(63), cannot be created by a classical communicator, which is in our case the Newtonian gravitational potential.

A classical potential is the construction of a potential that causes the interaction of two bodies without any mediating field and causes the so-called "action at a distance" [27], which is in violation with special relativity. In this picture, a particle acts as the source of the potential in which other particles scatter and a perturbation of this potential is instantaneously felt by the scattering particle (action at a distance). This is precisely what happens with Newton's gravity and is, therefore, the classical potential that cannot entangle the systems. A quantum interaction, on the other hand, is no longer an action at a distance but is mediated by a so-called "virtual" particle between the involved particles [27]. To see this, one has to look at the transition matrix arising from quantum mechanics which lies in the center of quantum field theory. This transition matrix relates the final state (f) and initial state (i) of interacting particles through the potential and looks, in a second order expansion, like:

$$T_{fi} = \langle f|V|i\rangle + \sum_{j\neq i} \frac{\langle f|V|j\rangle \langle j|V|i\rangle}{E_i - E_j} + ... \tag{64}$$

Here, j denotes the intermediate state present in the time after the initial state and before the final state. The first term in this equation is exactly how one would represent a scattering through a fixed potential and represents the classical scenario [27]. The second term is the "scattering via an intermediate state j" [27],

[18] These external fields can come for example from the interaction with the environment causing the decoherence or gravitational fields of the apparatus, or interactions with the conducting plate, which will be introduced in the next section.

having that the force is no longer an action at a distance but is mediated by an exchange particle from the intermediate states [5, 27]. To be more precise, the force carrier is a superposition of all the possible mediators arising from all possible intermediate states j. Therefore, the mediator is a mathematical construct of quantum nature [27] and, thus, we have that the communication between the particles is not classical any more. If one has, for example, the interaction $a + b \to c + d$, then one can have that the virtual particle is "released" from state a as well as being released from state b [27]. Denoting these two mediators by X and $\tilde{X}'$ respectively, one has the two intermediate states $j = c + b + X$ and $\tilde{j}' = d + a + \tilde{X}$ [27] respectively. From Eq.(64), one can see that both these time-ordered intermediate steps should be taken into account in the interaction and the combination of these two events is the actual picture, giving rise to the superposition of X and X'. Graphically this results in the famous Feynman diagram, a key subject of quantum field theory [27]. The combination of the matrix elements of the intermediate states is what we call the Feynman propagator [27] and represents the physics of the virtual particle. From this propagator, one can infer that the virtual exchange particle doesn't obey the Einstein energy-momentum relation [27], such particles are called "off-shell", giving another indication that this communicator is not a classical entity [5]. For all known forces, except the gravitational force, the existence of these virtual particles and thus the quantum nature has been confirmed. The hypothetical virtual particle of gravity is what we call the Graviton and, as it is in a superposition and it is off-shell, it is not limited by the LOCC principle as it is a quantum communicator. Therefore, it can entangle the test masses of the **QGEM**-protocol and measuring this entanglement would besides proving the quantum nature of gravity also confirm the existence of the Graviton.

Now that we know that we need a quantum gravitational field to entangle the test masses, one might ask the question whether the potential arising from the mediation of the Graviton would give the same $1/r$ dependence as the classical Newtonian potential, as this potential is used in arriving at the entanglement phase of Eq.(63). The potential can be calculated by integrating over all spatial momentum states of the Feynmann propagator from one vertex to the other [5]. As the masses are non-relativistic we have that the vertexes are just given by the 00 component of the energy-momentum tensor so that we get for the two masses [5]:

$$T_1^{00}(-k) = m\delta_0^0\delta_0^0\delta^{(3)}(r) = m\delta^{(3)}(r) \quad T_2^{00}(k) = m\delta_\mu^0\delta_\nu^0\delta^{(3)}(0) = m\delta^{(3)}(0) \tag{65}$$

Here, δ_μ^ν just represents the unit matrix in Einstein notation, k the four-momentum vector, and the particles are assumed to be separated a distance $r = x$ apart. The gravitational interaction between the two vertices can, as argued before, be represented by the Feynman diagram, which for this interaction looks in first-order like depicted in Fig.(2):

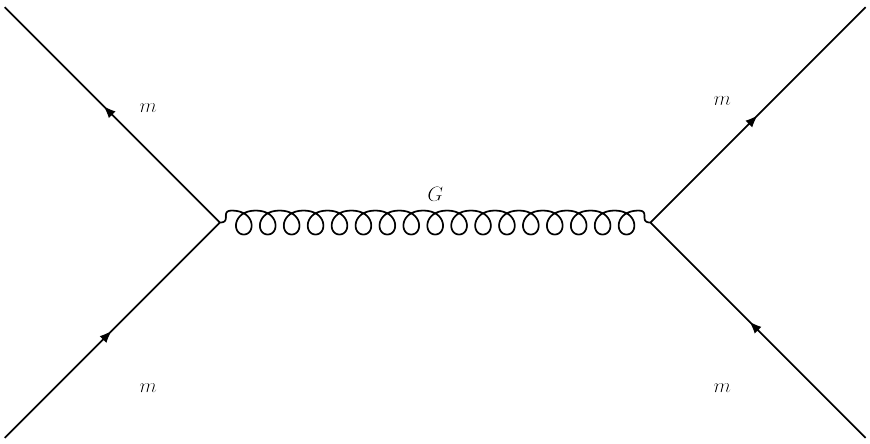

Figure 2: First order Feynman diagram of the Graviton exchange (G) between two states of the test masses. The test masses are identical in mass and the initial and final state of a single test mass are identical (both represented by "m"). The initial and final state of a single test masses are, as can be seen from the diagram, joint by the vertices where the Graviton originates from. The horizontal axis is understood to be the space axis and the vertical axis is the time axis. The manifestation of the graviton is possible due to the Heisenberg uncertainty principle.

For the linearized weak gravity regime which we are working in, we have that the Feynman propagator of the Graviton of Fig.(2) can be expressed as [5]:

$$\Pi_{\mu\nu\rho\sigma}(k) = \left(\frac{\mathcal{P}^2_{\mu\nu\rho\sigma}}{k^2} - \frac{\mathcal{P}^0_{s,\mu\nu\rho\sigma}}{2k^2} \right) \tag{66}$$

Here, $\mathcal{P}^2$ is the spin-2 projector of the Graviton, and $\mathcal{P}^0_s$ its corresponding spin-0 component. As derived in Ref.[28] one has the following property of the combination of energy-momentum tensor and the Feynman propagator of the Graviton of Eq.(66):

$$T^{\mu\nu}(-k)\Pi_{\mu\nu\rho\sigma}(k)T^{\rho\sigma}(k) = T^{\mu\nu}(-k)\frac{1}{2k^2}(\eta_{\mu\rho}\eta_{\nu\sigma} + \eta_{\nu\rho}\eta_{\mu\sigma} - \eta_{\mu\nu}\eta\rho\sigma)T^{\rho\sigma}(k) \tag{67}$$

Therefore, the propagation of the Graviton reduces in our case to:

$$T^{00}(-k)\Pi_{000}(k)T^{00}(k) = \frac{m^2}{2k^2} \tag{68}$$

Then, by performing the integration over the spatial momenta of this propagation, using the relevant coupling strength of the gravitational field, one will as shown in Ref.[5] arrive at:

$$V_G = -\frac{Gm^2}{x} \tag{69}$$

This is exactly the same potential as one would expect classically, meaning that the entanglement of Eq.(63) would have the same expression for this quantum gravity theory. The only difference is that the entanglement is now possible as we have the Graviton as the quantum mediator. This potential still has the $1/r$ singularity and exploration of how the **QGEM**-protocol can be used to test theories that account for this singularity, and how these theories will affect the results, will be explained in Sec.(11).

7 Limitation of the QGEM-protocol

As mentioned before, we require that the magnitude of the gravitational potential is one order of magnitude larger than that of the Casimir-Polder potential. The superimposed states that we are dealing with are spheres with the gravitational potential given by Eq.(69). As explained in Sec.(5), the Casimir-Polder potential for two dielectric spheres can be expressed by Eq.(45). With these expressions one can compute the ratio of the two potentials to be:

$$\frac{V_{CP}}{V_G} = \frac{1}{x^6}\frac{23\hbar c R^6}{4\pi G m^2}\left(\frac{\epsilon - 1}{\epsilon + 2}\right)^2 \tag{70}$$

From this equation, one can observe that the potential ratio is proportional to $x^{-1/6}$. Therefore, the requirement that the gravitational potential should be one order of magnitude larger than the Casimir-Polder potential breaks down first at the smallest separation, which is the separation between the states $|\downarrow\rangle_1$ and $|\uparrow\rangle_2$ of Fig.(1). This implies that this particular separation is the worrying aspect of the experiment. The separation between these states is (d-Δx), making that the potential ratio of Eq.(70) of the interactions of these states becomes:

$$\frac{V_{CP}}{V_G} = \frac{1}{(d - \Delta x)^6}\frac{23\hbar c R^6}{4\pi G m^2}\left(\frac{\epsilon - 1}{\epsilon + 2}\right)^2 \tag{71}$$

Assuming the diamond spheres to have a homogeneous mass distribution, meaning that $R = \frac{3m}{4\pi\rho}$, with ρ the density of diamond, we get that the potential ratio reduces to:

$$\frac{V_{CP}}{V_G} = \frac{1}{(d - \Delta x)^6}\frac{23\hbar c}{4\pi G}\left(\frac{3}{4\pi\rho}\frac{\epsilon - 1}{\epsilon + 2}\right)^2 = \frac{A}{(d - \Delta x)^6}\,, \tag{72}$$

Where $A = \frac{23\hbar c}{4\pi G}\left(\frac{3}{4\pi\rho}\frac{\epsilon-1}{\epsilon+2}\right)^2$. From this equation we observe that the potential ratio is not dependent on the mass of the spheres, meaning that our only variable is the separation distance (d-Δx). This insinuates that with the required potential ratio of $\frac{V_{CP}}{V_G} = 1/10$ the separation of the nearest states of the experiment is bounded from below by a constant:

$$(d - \Delta x) \geq (10A)^{\frac{1}{6}} \tag{73}$$

This limited lower bound of the separation gives a limitation on what is possible for the experiment as we will see in Sec.(10). This lower bound ($(10A)^{1/6}$) is with the appropriate constants equal to $\sim 157\mu$m. For the experiment to run as smoothly as possible, one wants to maximize the entanglement and, thus, the entanglement phase for a given mass. Or to phrase it more appropriate for the rest of the analysis: If one requires a certain entanglement phase for detection, e.g. 1 rad, what is the minimum mass that attains such a phase?[19]

From Eq.(63) one can observe that by fixing the separation of the closest states of the two systems by the lower bound of Eq.(73), we have that lowering the mass has two consequences:
1.) Lowering the mass will lower the common factor of $\frac{Gm^2}{\hbar}$ for all terms in Eq.(63), lowering the effective phase.
2.) Lowering the mass will increase Δx as can be seen from Eq.(54). Therefore, for a fixed distance $(d-\Delta x)$ we have that d should be larger, making the third term, which is larger than the second term, in Eq.(63) less dominant, thus, increasing the effective phase.
In general the effect of point 2.) is less significant than that of 1.), for the reason that in general $d-\Delta x >> d$, making the effect of an increased d not significant. Consequently, lowering the mass will result in a decrease in the phase, having that for a given phase requirement, e.g. $\Phi_{\text{eff}} \sim 1$ rad, there is a limitation on what is possible for the minimum mass of the diamond sphere, giving an upper-bound for the decoherence. This limits for what experimental parameters the entanglement is measurable, as we will see in Sec.(10). The actual expressions for the maximum entanglement phase and the minimum mass for a given phase requirement will be derived in Sec.(10.1) and are fully dependent on the limitation of the lower bound of Eq.(73).

With the lowest separation of the states we have as argued in this section that the gravitational force is the dominant force. With this closest separation of the states, we will have a gravitational acceleration of one of the states of:

$$a_g = \frac{Gm}{(d-\Delta x)^2} = \frac{Gm}{(10A)^{1/3}} \tag{74}$$

We will see, in Sec.(10), that a mass range of 10^{-16}-10^{-14} kg will be considered. This corresponds to a gravitational acceleration of at most $\sim 10^{-17}$ m/s^2, which leads to a truly negligible traveled distance during the free fall, which has a duration in the order of seconds.

8 Modified setup, perfect conducting plate

To overcome the limitation on the separation of the closest states $(d - \Delta x)$ of the current setup of the **QGEM**-protocol, as explained in the previous section, a modification of step 2 of the experiment is presented in Fig.(3). In this case, a conducting plate is put in the middle of the c.o.m. of both test masses. This plate is compared to the size of the test mass of an infinite extent in the vertical plane of Fig.(3). The conducting plate is assumed to be a perfect conductor, this makes that the electromagnetic waves cannot travel from one side of the plate to the other side, as a perfect conductor is completely reflective of all electromagnetic waves [24]. Therefore, by insertion of the plate in the system, we have that the Casimir-Polder potential between the states $|\downarrow\rangle_1$ and $|\uparrow\rangle_2$ is no longer present. This can also be seen by the fact that the plate will act as a *faraday cage* between system 1 and system 2. As we know from a farady cage, if you are

[19] This is because (as we will see later on in the analysis) a smaller mass will, in general, give smaller decoherence rates. However, in some cases, the decoherence rate might even by larger for smaller masses (large magnetic field gradient and lower phase requirements). But we will also see that the expression that maximizes the entanglement phase for this setup is the same for all masses, Eq.(100). Therefore, this reformulation does not change the outcome and one will always find the maximum phase for a given mass.

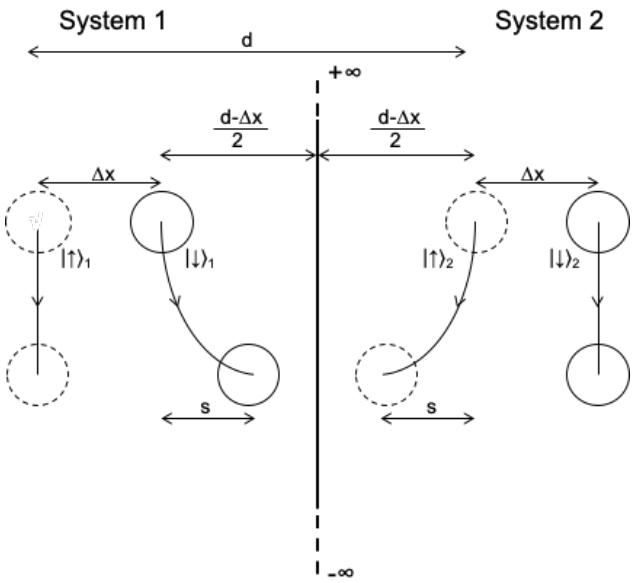

Figure 3: Modified setup for the **QGEM**-protocol which only changes step 2 of the experiment. There is a thin perfectly conducting plate, of assumingly infinite vertical extend, inserted midway between the two interferometers. This will destroy the Casimir force directly between the nearest states but will generate a significant Casimir force between the plate and the nearest states, which will accelerate the nearest states towards the plate. This will give a horizontal distance change of s at the end of step 2. The plate will for further analysis be assumed to be clamped at both ends along the "infinite" axis and will free-fall with the test masses. The length of the plate in consideration will be assumed to be $L = 1$mm together with a thickness of $W = 1\mu$m. The plate is also assumed to be a square plate with the length into the paper equal in magnitude to L. The length of 1mm will make sure that the infinite plate assumption is valid as the size of the test masses is at least 4 orders of magnitude lower.

inside the cage, you cannot feel the electromagnetic interaction of the outside. Here it is exactly the same, system 2 cannot electromagnetically interact with system 1 and vice versa. Therefore, vacuum fluctuations between system 1 and 2 cannot be present, and the only difference in vacuum fluctuations that will cause the Casimir force on system 1, is the one induced by the plate and the system, and not with system 2. This also means that vacuum fluctuations induced by the boundary conditions on the side of system 2 (by plate and states), are unable to cause a difference on the Casimir force on the states of system 1. Consequently, the Casimir force of system 1 is not influenced by the boundary conditions of system 2 and vice versa, such that we lose the Casimi-Polder force between the systems. The "loss" of this Casimir-Polder force means that one does not have to worry about the Casimir-Polder force entangling both systems, having that only the gravitational force can entangle the two systems[20]. Therefore, the **QGEM**-protocol is no longer limited by the separation of the closest states of Eq.(73) anymore, implying that in principle we can go to much lower masses for the same effective phase.

Although at first glance this idea seems favorable with respect to the current setup there will, however, be other limitations on the closest separation. With the insertion of the conducting plate, there will now be, as mentioned briefly before, a Casimir force present between the nearest state ($|\downarrow\rangle_1$ or $|\uparrow\rangle_2$) and the plate, as there can still be electromagnetic waves present in these regions. The corresponding Casimir force between the dielectric sphere and the perfect conductor, as derived in Ref.[24], is given by Eq.(46) in Sec(5).

In the rest of the analysis of Ref.[24] it is assumed that the dielectric constant is given by the drude model, which is valid for metals, however, we are dealing with diamond which is a dielectric. Luckily for us, the

[20] Assuming that there is not a fifth unknown force present which we are not aware of.

dielectric constant of diamond has a negligible small imaginary part [29], so the real part of the dielectric constant also gives the real part of Eq.(47). Furthermore, the dielectric constant of diamond is barely dependent on the frequency of the electromagnetic waves [30, 31]. Therefore, we can safely make the assumption that the dielectric constant of diamond is constant with respect to frequency, making that Eq.(46) can be written as:

$$F_{\text{casimir}} = -\frac{R^3}{4\pi x^4}\left(\frac{\epsilon-1}{\epsilon+2}\right)\int_0^\infty \mathrm{d}\omega[3\sin(2\omega x) - 6\omega x\cos(2\omega x) - 6\omega^2x^2\sin(2\omega x) + 4x^3\omega^3\cos(2\omega x)] \tag{75}$$

The integral can be evaluated by multiplying it with a frequency dependent exponent ($e^{-b\omega}$) and taking the limit b$\to$ 0 giving:

$$\lim_{b\to 0}\int_0^\infty \mathrm{d}\omega\, e^{-b\omega}[3\sin(2\omega x) - 6\omega x\cos(2\omega x) - 6\omega^2x^2\sin(2\omega x) + 4x^3\omega^3\cos(2\omega x)] = \frac{6}{x} \tag{76}$$

Substituting that in Eq.(75) gives us the expression for the Casimir force between the plate and the nearest state of one of the test masses:

$$F_{\text{casimir}} = -\frac{3\hbar c}{2\pi}\left(\frac{\epsilon-1}{\epsilon+2}\right)\frac{R^3}{x^5} \tag{77}$$

Here it should be noted that I inserted back in $\hbar c$ as Ref.[24] used natural units. As $\epsilon = 5.7 > 1$, one has that the Casimir force is attractive, suggesting that for sufficiently close separations the states will significantly be accelerated towards the plate, resulting in a change of the horizontal distance, denoted by s in Fig.(3), during the free fall period of the experiment.

We will see that, with this modified setup, the shortest separation of the states of both masses ($d-\Delta x$) is in the order of $\sim 10\mu$m, for such a separation the gravitational induced acceleration between the test masses is for the mass range in consideration (10^{-16}-10^{-14} kg) at most 10^{-15} m/s^2. This is for our free-fall time in the order of seconds again a negligible effect. However, with the inserted plate in this suggested modification of the experiment we also have to deal with the gravitational interaction of the thin plate with the states. As we assume a plate of infinite extent with respect to the states in the vertical direction as well as the direction in the paper of Fig.(3), one will have by imposing the appropriate Gaussian surface that with Gauss Law the gravitational interaction is given by [32]:

$$g = 2\pi G\sigma \;\to g = 2\pi G\rho_p W \tag{78}$$

Here, σ and ρ_p are respectively the surface and volume mass density of the plate, and W is the thickness of the conducting slab, which we assume to be 10^{-6} m, as, for example, copper plates are already in production by American Elements with this thickness [33]. With such a thickness and a density of 8.96 g/cm^3 [33], the gravitational acceleration is in the order of 10^{-11} m/s^2. This implies that with the interaction time which is in the order of seconds [1] there will be a horizontal distance change in the order of 10^{-11} m, which is truly negligible compared to the sizes of the test masses[21]. There is also a Casimir force present between the outer states of Fig.(3) and the plate since the test masses are made out of diamond, which is a dielectric, making it possible for electromagnetic waves to propagate through the inner states. As will be justified in Sec.(10.2) and Sec.(10.3), the acceleration on these outer states caused by the Casimir force with the plate can also be neglected in all cases except one and will, therefore, be included for this exception.

Therefore, for the most cases (which are also the cases taken into account for further analysis after Sec.(10.4)), the only significant acceleration is the one caused by the Casimir force with the inner states, which causes the acceleration sketched in Fig.(3) to be only caused by this force. From Eq.(77) we observe that when such a state/sphere approaches the edge of the plate ($x \to 0$) the force and thus the acceleration of the sphere will go to infinity. This suggests that there exists a separation of the states with respect to the plate for which the magnitude of the acceleration of the Casimir force (a_{Casimir}) is greater than that of the constant acceleration of the magnetic field (a_{magnetic}), which is indicated by Eq.(54). This causes a problem

[21] We will see in Sec.(10) that the sizes of relevant masses are in the order of 10^{-7} m and thus 4 orders of magnitude larger than the gravitationally induced distance change.

for the experiment because if one were to switch back on the magnetic field when the separation of the inner states with respect to the plate is such that $a_{\text{Casimir}} > a_{\text{magnetic}}$, then the states will keep on accelerating towards the plate, instead of being accelerated in the opposite position. Therefore, the superposition cannot be brought back in step 3 of the experiment for such a separation, having that the entanglement cannot be measured. Hence, we have that this setup will also give rise to a lower bound on the separation of $d - \Delta x$ as one cannot go the separations in which $a_{\text{Casimir}} > a_{\text{magnetic}}$.

This limitation will give the following restriction on the setup: We demand that the separation $(d - \Delta x)/2$ of the states $|\downarrow\rangle_1$ and $|\uparrow\rangle_2$ with respect to the plate is at the beginning of the free fall such that at the end of the free fall this separation, $(d - \Delta x)/2 - s$ as indicated in Fig.(3), is in agreement with the following requirement:

$$\frac{a_{\text{Casimir}}}{a_{\text{magnetic}}} < \frac{1}{10} \tag{79}$$

If the magnetic field is switched back on at the end of the free-fall there would still be a residual velocity in the direction of the plate. Therefore, the factor of 1/10 is chosen instead of 1 to not get a situation where the Casimir force becomes dominant over the magnetic force. That the magnetic force is one order of magnitude higher also makes sure that it will not take the $|\downarrow\rangle_1$ and $|\uparrow\rangle_2$ states long to accelerate away from the plate to not get a situation in which the state would not be stationary at the end of step 3. More on this will be discussed in Sec.(13).

9 Entanglement Entropy & Witness

9.1 Reduced density matrix of the QGEM-protocol

To look at how exactly the measurements on the system are affected by the decoherence, we have to look at the reduced density matrix of the system. The entangled state of our combined system is for both setups given by Eq.(59). The only difference is that the phases in the exponents take different values for the same mass and interaction time. With this equation one has the reduced density matrix of the combined system will become:

$$\rho_{\mathcal{S}_1\mathcal{S}_2} = \rho = |\psi\rangle\langle\psi| = \frac{1}{4}\begin{pmatrix} 1 & e^{-i\Delta\phi_{\uparrow\downarrow}} & e^{-i\Delta\phi_{\downarrow\uparrow}} & 1 \\ e^{i\Delta\phi_{\uparrow\downarrow}} & 1 & e^{i(\Delta\phi_{\uparrow\downarrow}-\Delta\phi_{\uparrow\downarrow})} & e^{i\Delta\phi_{\uparrow\downarrow}} \\ e^{i\Delta\phi_{\downarrow\uparrow}} & e^{-i(\Delta\phi_{\uparrow\downarrow}-\Delta\phi_{\uparrow\downarrow})} & 1 & e^{i\Delta\phi_{\downarrow\uparrow}} \\ 1 & e^{-i\Delta\phi_{\uparrow\downarrow}} & e^{-i\Delta\phi_{\downarrow\uparrow}} & 1 \end{pmatrix} \tag{80}$$

Where $\mathcal{S}_i$ indicates the system of a single superposition of a test mass in a single interferometer. This expression is the ideal reduced density matrix when there are no decoherence effects taken into account. However, realistically one needs to include the decoherence of the system. In this thesis the decoherence term is modelled according to the scattering model (as explained in Sec.(4.2)), in which the off-diagonal terms decay exponentially as given by Eq.(37) and Eq.(38), meaning that the reduced density for both superpositions becomes[22]:

$$\rho_{\mathcal{S}_1} = \begin{pmatrix} 1 & e^{-\gamma t} \\ e^{-\gamma t} & 1 \end{pmatrix} \quad \rho_{\mathcal{S}_2} = \begin{pmatrix} 1 & e^{-\gamma t} \\ e^{-\gamma t} & 1 \end{pmatrix} \tag{81}$$

The collisioned particles/photons of one superposition will in general not lead to scattering and thus entanglement with the other superposition, so for the environmental degrees of freedom we can combine this two density matrices by a tensor product, giving:

$$\rho = \rho_{\mathcal{S}_1} \otimes \rho_{\mathcal{S}_2} = \begin{pmatrix} 1 & e^{-\gamma t} & e^{-\gamma t} & e^{-2\gamma t} \\ e^{-\gamma t} & 1 & e^{-2\gamma t} & e^{-\gamma t} \\ e^{-\gamma t} & e^{-2\gamma t} & 1 & e^{-\gamma t} \\ e^{-2\gamma t} & e^{-\gamma t} & e^{-\gamma t} & 1 \end{pmatrix} \tag{82}$$

[22]Note that in this equation I have not included the initial constants ρ_0 of the off diagonal terms, as these will come from Eq.(80), which are not relevant at this stage. Also note that I used the form in the exponent of Eq.(37) and not Eq.(38) for simplicity. The only thing that would have changed if one used Eq.(38) is that the terms in the exponent would be longer.

It is good to note that Eq.(82) is a combination of the reduced density matrices of the systems with respect to the environmental scattering, therefore the degrees of freedom of the environment are already traced out in this expression and is in agreement with Ref.[26]. On the other hand, Eq.(80) describes the density matrices of both systems without any inclusion of the environment. Therefore we can insert Eq.(82) in Eq.(80) as inclusion of the environmental effect after tracing this out. This suggests that the components of Eq.(80) should be multiplied with those of Eq.(82) as the components of Eq.(80) can be thought of as the $\rho_{\mathcal{S}}(\mathbf{x},\mathbf{x}',0)$ of Eq.(37). With this, one would arrive at the reduced density matrix of:

$$\rho = \frac{1}{4}\begin{pmatrix} 1 & e^{-i\Delta\phi_{\uparrow\downarrow}}e^{-\gamma t} & e^{-i\Delta\phi_{\downarrow\uparrow}}e^{-\gamma t} & e^{-2\gamma t} \\ e^{i\Delta\phi_{\uparrow\downarrow}}e^{-\gamma t} & 1 & (e^{i(\Delta\phi_{\uparrow\downarrow}-\Delta\phi_{\uparrow\downarrow})})e^{-2\gamma t} & e^{i\Delta\phi_{\uparrow\downarrow}}e^{-\gamma t} \\ e^{i\Delta\phi_{\downarrow\uparrow}}e^{-\gamma t} & (e^{-i(\Delta\phi_{\uparrow\downarrow}-\Delta\phi_{\uparrow\downarrow})})e^{-2\gamma t} & 1 & e^{i\Delta\phi_{\downarrow\uparrow}}e^{-\gamma t} \\ e^{-2\gamma t} & e^{-i\Delta\phi_{\uparrow\downarrow}}e^{-\gamma t} & e^{-i\Delta\phi_{\downarrow\uparrow}}e^{-\gamma t} & 1 \end{pmatrix} \tag{83}$$

By tracing out the degrees of freedom of system $\mathcal{S}_2$ by means of the direct method [19], one obtains the reduced density matrix of system $\mathcal{S}_1$[23]. This direct method is just taking the partial trace in each 2x2 matrix of the Eq.(83) as the matrix is in the right order of the state combinations, this will give us:

$$\rho_{\mathcal{S}_1} = \mathrm{Tr}(\rho_{\mathcal{S}_1\mathcal{S}_2}) = \frac{1}{4}\begin{pmatrix} \mathrm{Tr}\begin{pmatrix} 1 & e^{-i\Delta\phi_{\uparrow\downarrow}}e^{-\gamma t} \\ e^{i\Delta\phi_{\uparrow\downarrow}}e^{-\gamma t} & 1 \end{pmatrix} & \mathrm{Tr}\begin{pmatrix} e^{-i\Delta\phi_{\downarrow\uparrow}}e^{-\gamma t} & e^{-2\gamma t} \\ (e^{i(\Delta\phi_{\uparrow\downarrow}-\Delta\phi_{\uparrow\downarrow})})e^{-2\gamma t} & e^{i\Delta\phi_{\uparrow\downarrow}}e^{-\gamma t} \end{pmatrix} \\ \mathrm{Tr}\begin{pmatrix} e^{i\Delta\phi_{\downarrow\uparrow}}e^{-\gamma t} & (e^{-i(\Delta\phi_{\uparrow\downarrow}-\Delta\phi_{\uparrow\downarrow})})e^{-2\gamma t} \\ e^{-2\gamma t} & e^{-i\Delta\phi_{\uparrow\downarrow}}e^{-\gamma t} \end{pmatrix} & \mathrm{Tr}\begin{pmatrix} 1 & e^{i\Delta\phi_{\downarrow\uparrow}}e^{-\gamma t} \\ e^{-i\Delta\phi_{\downarrow\uparrow}}e^{-\gamma t} & 1 \end{pmatrix} \end{pmatrix} \tag{84}$$

This reduces then to the desired reduced density matrix of:

$$\rho_{\mathcal{S}_1} = \frac{1}{4}\begin{pmatrix} 2 & e^{-\gamma t}(e^{-i\Delta\phi_{\downarrow\uparrow}} + e^{i\Delta\phi_{\uparrow\downarrow}}) \\ e^{-\gamma t}(e^{i\Delta\phi_{\downarrow\uparrow}} + e^{-i\Delta\phi_{\uparrow\downarrow}}) & 2 \end{pmatrix} \tag{85}$$

As a validity check we see that if there would be no decoherence (γ=0), we would obtain the same result as the reduced density matrix given in appendix B of Ref.[5].

Eq.(85) could also have been obtained with a more formal method. The formal method is more applicable in more general entanglements as this is independent of picking the right order of the reduced density matrix as is the case for the direct method. For this formal method, we can implement the formal expression of the reduced density matrix of Eq.(12) with the total wave-function of the system of Eq.(59), which for argumentation sake I will rewrite as:

$$|\Psi\rangle = \frac{1}{2}e^{i\phi}\left[|\uparrow\rangle_1|\uparrow\rangle_2 + e^{i\Delta\phi_{\uparrow\downarrow}}|\uparrow\rangle_1|\downarrow\rangle_2 + |\downarrow\rangle_1 e^{i\Delta\phi_{\downarrow\uparrow}}|\uparrow\rangle_2 + |\downarrow\rangle_1|\downarrow\rangle_2\right] \tag{86}$$

Then we can implement Eq.(12) to obtain the reduced density matrix of $\mathcal{S}_1$. Here we note that, in order to get $\rho_{\mathcal{S}_1}$, the $|\psi_n\rangle$ states are the spin-up and -down states of $\mathcal{S}_1$ and the $|E_n\rangle$ states are the spin-up and -down states of $\mathcal{S}_2$. Also, in order to make the derivation less lengthy, we make the observation that the spin up and down states of the same system are orthogonal states, therefore, $\langle\uparrow|\downarrow\rangle_{22} = \langle\downarrow|\uparrow\rangle_{22} = 0$. Secondly, we also have that the states are normalized, such that $\langle\uparrow|\uparrow\rangle_{22} = \langle\downarrow|\downarrow\rangle_{22} = 1$. Then, by utilizing these observations, we can implement Eq.(12) with Eq.(86) to get the reduced density matrix of system $\mathcal{S}_1$:

$$\begin{aligned}
\rho_{\mathcal{S}_1} =& \frac{1}{4}\left(|\uparrow\rangle_1\langle\uparrow|_1 + |\uparrow\rangle_1\langle\uparrow|_1 + |\downarrow\rangle_1\langle\downarrow|_1 + |\downarrow\rangle_1\langle\downarrow|_1 + e^{-i\Delta\phi_{\downarrow\uparrow}}|\uparrow\rangle_1\langle\downarrow|_1 + e^{i\Delta\phi_{\uparrow\downarrow}}|\uparrow\rangle_1\langle\downarrow|_1 + {}^{i\Delta\phi_{\downarrow\uparrow}}|\downarrow\rangle_1\langle\uparrow|_1 + e^{-i\Delta\phi_{\uparrow\downarrow}}|\downarrow\rangle_1\langle\uparrow|_1\right) \\
=& \frac{1}{4}\left(2|\uparrow\rangle_1\langle\uparrow|_1 + 2|\downarrow\rangle_1\langle\downarrow|_1 + (e^{-i\Delta\phi_{\downarrow\uparrow}} + e^{i\Delta\phi_{\uparrow\downarrow}})|\uparrow\rangle_1\langle\downarrow|_1 + (e^{i\Delta\phi_{\downarrow\uparrow}} + e^{-i\Delta\phi_{\uparrow\downarrow}})|\downarrow\rangle_1\langle\uparrow|_1\right) \\
=& \frac{1}{4}\begin{pmatrix} 2 & e^{-i\Delta\phi_{\downarrow\uparrow}} + e^{i\Delta\phi_{\uparrow\downarrow}} \\ e^{i\Delta\phi_{\downarrow\uparrow}} + e^{-i\Delta\phi_{\uparrow\downarrow}} & 2 \end{pmatrix}
\end{aligned} \tag{87}$$

This is, after implementing Eq.(81) for the decoherence decay of the off-diagonal elements, the same expression as the reduced density matrix of Eq.(85), obtained by the direct tracing.

[23] It should be noted that the reduced density matrix of system $\mathcal{S}_2$ will be the same, as one would expect, because of the anti-symmetry of Eq.(83).

9.2 Von Neumann Entropy

To quantify the degree of entanglement between systems one can use, as explained in Sec.(3), the von Neumann Entropy. This is defined based on the Shannon entropy known from thermodynamics and is given by [19]:

$$S_{\text{VN}} = -\text{Tr}\left(\rho_{\mathcal{S}_i}\log_2(\rho_{\mathcal{S}_i})\right) , \tag{88}$$

where $\rho_{\mathcal{S}_i}$ is again the reduced density matrix of system $\mathcal{S}_i$. One can also express this in terms of the eigenvalues of the reduced density matrix (λ_i). This gives that the von Neumann entropy can be defined as [19]:

$$S_{\text{VN}} = -\sum_i \lambda_i \log_2(\lambda_i) \tag{89}$$

This entropy is bounded by $0 \leq S \leq \log_2(d)$ [19], with d the dimension of the reduced density matrix. As the dimension of the reduced density matrix in the case for the **QGEM**-protocol, with a two component superposition, is two, we have

$$0 \leq S_{\text{VN}} \leq 1 , \tag{90}$$

where zero entropy ($S = 0$) corresponds to the case that the systems are seperable and, thus, no entanglement has occurred. A maximum entropy of $S = 1$ corresponds to a maximum entanglement of the two systems [19].

For the reduced density matrix of a single superposition, as derived in Eq.(85), one can compute the eigenvalues with

$$\det\left(\rho_{\mathcal{S}_1} - \lambda I\right) = 0 , \tag{91}$$

which will give the two eigenvalues of:

$$\lambda_\pm = \frac{1}{2} \pm \frac{e^{-\gamma t}}{2}\left[\frac{1}{2}(1 + \cos(\Phi_{\text{eff}}))\right]^{1/2} \tag{92}$$

Here, Φ_{eff} is again the effective entanglement phase represented by Eq.(63). As a validity check, we see that these eigenvalues are the same as in Ref.[5] by neglecting the decoherence ($\gamma = 0$). With these eigenvalues one will get that the corresponding von Neumann entropy of the system, using Eq.(89), is given by:

$$S_{\text{VN}} = -(\lambda_- \log_2(\lambda_-) + (\lambda_+ \log_2(\lambda_+)) \tag{93}$$

Without any decoherence this again reduces back to the result of Ref.[5]. However, this description of the entanglement is more realistic due to the inclusion of the collisional decoherence. From Eq.(92) and Eq.(93) we make the following striking observations:
1.) By neglecting the decoherence factor we can see the following: When the effective phase (Φ_{eff}) is π we have $\lambda_\pm = \frac{1}{2}$, meaning that $S_{\text{VN}} = 1$, which indicates a maximum entanglement between the two systems. Similarly a phase of 2π will give rise to no entanglement ($S_{\text{VN}} = 0$) as we have $\lambda_+ = 1$ and $\lambda_- = 0$. These two statements are in agreement with the arguments made in Sec.(6). Also, as we are considering Φ_{eff} of at most around 1 rad ($< \pi$), we have that increasing the entanglement phase will give a higher entropy and thus a higher degree of entanglement. Which is why we want to maximize the entanglement phase for a given mass.
2.) We also observe that when the decoherence is maximum, $e^{-\gamma t} \to 0$, one also obtains $S_{\text{VN}} = 1$, such that the system is again maximally entangled. The difference is that now this maximum entanglement is due to the entanglement with the environment, which is consisted with arguments made in Sec.(4), and not with the desired system $\mathcal{S}_2$.
3.) We can also observe that larger decoherence rates lead to higher reductions of the second term of Eq.(92), implying a growth towards the maximum entanglement. However, as argued in point 2, this entropy is due to the interaction with the environment and not with the gravitational entanglement of the test masses.

As we want to measure only the entanglement of systems $\mathcal{S}_1$ and $\mathcal{S}_2$ and as the decoherence term is usually not completely understood, it might be wise to measure the entanglement differently and not with respect to the entropy. A more suitable way for this is, therefore, to measure the entanglement by measuring correlations between $\mathcal{S}_1$ and $\mathcal{S}_2$, since these correlations can also determine if the two systems are entangled. This can be accomplished by using an entanglement Witness, as in more detail will be discussed in the next

subsection. It is important to note that the entropy, and thus the entanglement phase, can still be used to describe the degree of entanglement of the two systems.

9.3 Entanglement Witness

In the original paper (Ref.[1]), it was suggested to measure the entanglement employing the entanglement witness ($\mathcal{W}$). This is a functional which can conclude if a system is entangled or separable as in Eq.(5). This functional is, as described in Sec.(6), based upon spin measurements in different bases of both test masses, from which one can determine from the expectation value if the systems are entangled or separable. The requirement on the expectation value is based on how $\mathcal{W}$ is build up [19], but in general, and also for the **QGEM**-protocol [26], it is such that when

$$\langle W \rangle = \mathrm{Tr}(\mathcal{W}\rho) < 0\,, \tag{94}$$

the systems are confirmed entangled and otherwise, $\langle \mathcal{W} \rangle > 0$, no conclusion can be drawn [19, 26]. ρ is again the reduced density matrix of the combined system.

For the original **QGEM**-protocol, the construction of $\mathcal{W}$ in terms of the complementary spin basis was such that the witness was composed to be $\mathcal{W} = I^{(1)} \otimes I^{(2)} - \sigma_x^{(1)} \otimes \sigma_z^{(2)} - \sigma_y^{(1)} \otimes \sigma_y^{(2)}$ [1, 26]. Here, the σ_i are the different pauli spin operators in the three spatial directions (x,y,z), with z the direction of the "spin-up" . The superscript (i) indicates in which system, $\mathcal{S}_1$ or $\mathcal{S}_2$, the corresponding measurement is taken. However, more recently, in Ref.[26], a more effective entanglement witness for the **QGEM**-protocol was found to be:

$$\mathcal{W} = I^{(1)} \otimes I^{(2)} - \sigma_x^{(1)} \otimes \sigma_x^{(2)} - \sigma_y^{(1)} \otimes \sigma_z^{(2)} - \sigma_x^{(1)} \otimes \sigma_z^{(2)} \tag{95}$$

With this construction of $\mathcal{W}$, one can just multiply it with the obtained expression of ρ of Eq.(83) and take the trace operation, of Eq.(94), to obtain just as shown in Ref.[26]:

$$\langle \mathcal{W} \rangle = \mathrm{Tr}(\mathcal{W}\rho) = 1 - e^{-\gamma t}(\sin \Delta\phi_{\uparrow\downarrow} + \sin \Delta\phi_{\downarrow\uparrow}) - \frac{e^{-2\gamma t}}{2}(1 + \cos\left(\Delta\phi_{\uparrow\downarrow} - \Delta\phi_{\downarrow\uparrow}\right)) \tag{96}$$

From this we see that higher decoherence rates actually increase the value of the expactation value of the witness, indicating that measuring the entanglement requires larger accumulated phases (the sin and cosine terms). Additionally, a more negative value of the witness will decrease the number of measurements needed to determine if quantum gravity exists [26], making larger negative values more suitable for the experiment, since this lowers the run-time.

From Eq.(96) one can make the distinction between high entanglement phases ($\Phi_{\text{eff}} \sim 1$ rad), and low entanglement phases ($\Phi_{\text{eff}} \sim 0.01$ rad). For high phases there is no direct correlation between the effective entanglement phase and the minimum value of $\langle \mathcal{W} \rangle$. However, it is still wise to maximize the effective entanglement phase in this limit as this will still give rise to a certain minimum mass for which the combination $\Delta\phi_{\uparrow\downarrow}$ and $\Delta\phi_{\uparrow}$ accumulate to the most optimal terms of the sines and cosines. Then, one can adjust the parameters of the experiment, as long as the requirements in Sec.(7) and Sec.(8) are not violated, such that the mass with the lowest decoherence rate attains these parameters. We will see, in Sec.(10.6), that the most optimal cases will still correspond to the cases where the mass is minimized for a given phase requirement.

However, in this thesis, we are more interested in the smaller phases as these are the phases one can obtain if one would apply more achievable experimental parameters of the futuristic experiment, such as achievable magnetic field gradients of 10^4 Tm^{-1}, together with masses one or two orders of magnitude lower than the proposed 10^{-14} kg. For these low phases, one can do a first-order Taylor expansion to obtain that Eq.(96) reduces to [26]:

$$\langle \mathcal{W} \rangle = \mathrm{Tr}(\mathcal{W}\rho) = 2\gamma t - \Phi_{\text{eff}} \tag{97}$$

This clearly shows the need to maximize the entanglement phase as this will minimize $\mathcal{W}$.

10 Comparison

As explained in Sec.(7), the current setup limits the possibilities in reducing the mass, since the minimum separation $(d-\Delta x)$ of the two closest states is limited by the potential ratio $\frac{V_{CP}}{V_G}$. However, for the modified setup we have this limitation by the strength of the Casimir force of the states with the plate relative to the magnetic force. In this section a comparison between the two setups will be provided by means of mass minimization for given phase requirements on the effective phase of Φ_{eff}=0.1,Φ_{eff}=0.01 & Φ_{eff}=1. In Sec.(10.1) and Sec.(10.2) this analysis will be done for the suggested experimentally demanding magnetic field gradient 10^6 Tm^{-1} for both setups. Following this section, in Sec.(10.3), the same analysis will be performed for the lower magnetic field gradients of 10^5 Tm^{-1} and 10^4 Tm^{-1}. In Sec.(10.5) the analysis of the decoherence induced by the environment, based on the theory of Sec.(4), will be performed in terms of the mass and magnetic field gradient for a range of environmental parameters. The comparison of both setups will be concluded by a comparison of $\langle \mathcal{W} \rangle$ in terms of the results obtained in the previously mentioned sections.

10.1 Mass minimization current setup

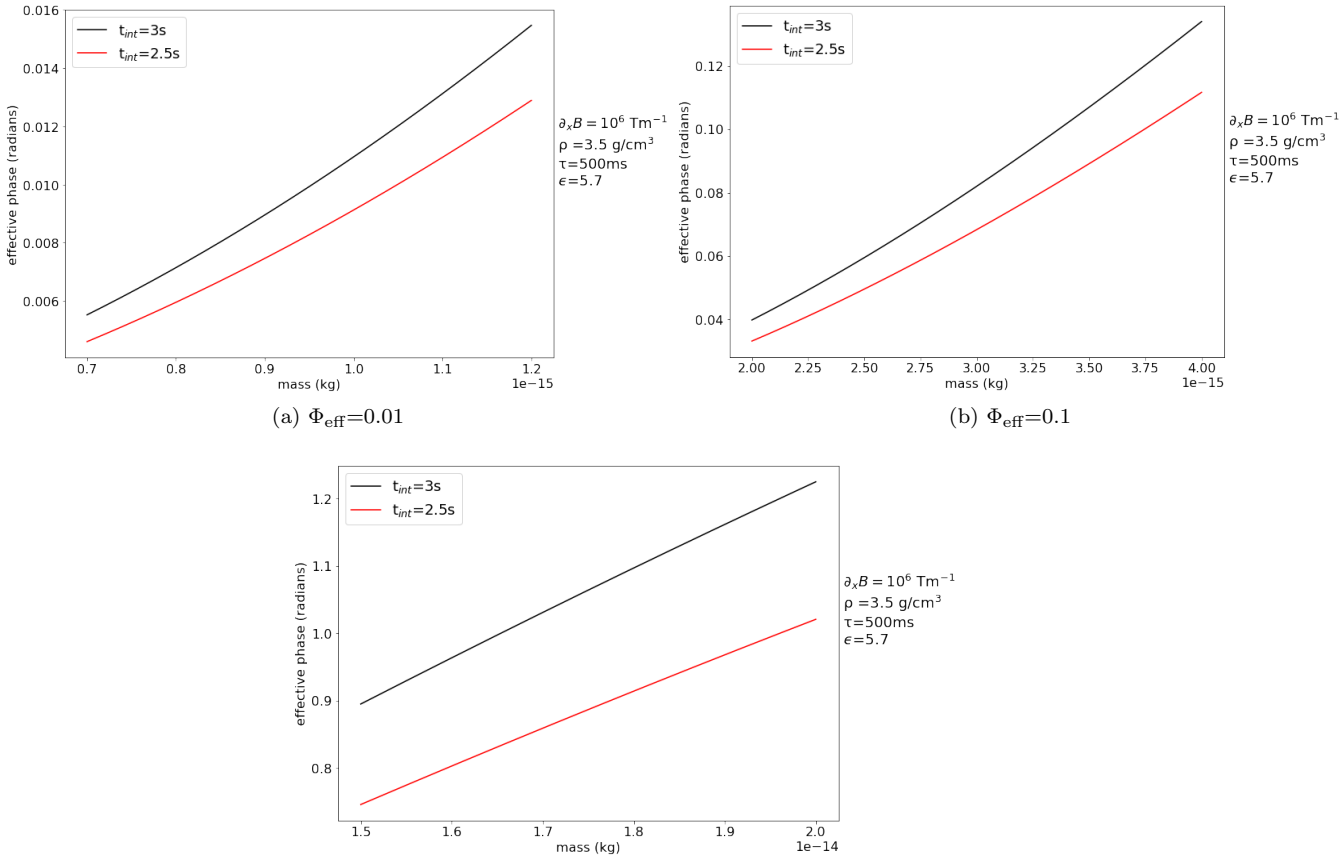

(a) Φ_{eff}=0.01

(b) Φ_{eff}=0.1

(c) Φ_{eff}=1

Figure 4: These figures display the maximum entanglement phase, generated in step 2 of the current setup, as a function of mass for the parameters indicated next to the graph. The optimal distances between the test masses was found to be $d-\Delta x \sim 157\mu$m in all cases.

From Eq.(63) it can be observed that for a given mass the maximum entanglement phase is given by the lowest value of $d-\Delta x$, however, as we saw from Eq.(73), this distance is for the current setup bounded from below by $(10\text{A})^{1/6}$. Hence, for a given mass, one has that the maximum phase is obtained by $d-\Delta x = (10A)^{1/6}$.

This will give us that the optimized distance d between the c.o.m's of the two diamond spheres can be expressed as:

$$d = \Delta x + (10A)^{\frac{1}{6}} \tag{98}$$

The superposition size Δx obtained in step 1 of the experiment was derived to be given by Eq.(54). Therefore, by using this expression and "plugging back in" the value of A, one has that the total expression for the c.o.m. separation distance d is given by:

$$d = \frac{g\mu_B \partial_x B}{2m}\tau^2 + \left(10\frac{23\hbar c}{4\pi G}(\frac{3}{4\pi\rho}\frac{\epsilon-1}{\epsilon+2})^2\right)^{\frac{1}{6}} \tag{99}$$

As suggested by prof A. Mazumdar, values for the magnetic field gradient in the range of 10^4-10^6 Tm^{-1} could be explored as well as an exploration of the interaction times ($\mathrm{t_{int}}$) in the range of 1-3 s. As explained earlier, a larger d, for a fixed distance $d-\Delta x$, will result in larger phase for a given mass, therefore, from Eq.(99), it is clear that the magnetic field gradient of 10^6 Tm^{-1} will result in the highest phase for a given mass. This magnetic field gradient is also the value that will be explored in this section. From Eq.(63) it is pretty straightforward to conclude that a higher $\mathrm{t_{int}}$ will give rise to a larger phase for a given mass [24]. This means that the interaction time of 3s generates the highest phase. However, it should be noted that this is larger than the suggested 2.5s of the Ref.[1], therefore, I will use both the value for 3s and 2.5s for the graphical visualization. The other interaction times will not be visually represented but can be of importance when the decoherence is sufficiently large with respect to the entanglement phase and will give solutions when the higher interaction times will not, as we will see in Sec.(10.6). Another value of importance is the time period of step 1 (and also step 3) of the protocol, which is τ, for which I will use a value of τ=500 ms as suggested in the original paper (Ref.[1]). Additionally, because diamond is used, we have a density of $\rho = 3.5$ g/cm^3 and a dielectric constant of ϵ=5.7 [1].

By substituting Eq.(99) and Eq.(54) in the expression for the effective phase, Eq.(63), the maximum effective entanglement as a function of mass will reduce to:

$$\Phi_{\mathrm{eff,max}} = \frac{Gm^2}{\hbar}t_{\mathrm{int}}\left(\frac{1}{(10A)^{\frac{1}{6}}} + \frac{1}{2\frac{g\mu_B\partial_x B}{2m}\tau^2 + (10A)^{\frac{1}{6}}} - 2\frac{1}{\frac{g\mu_B\partial_x B}{2m}\tau^2 + (10A)^{\frac{1}{6}}}\right) \tag{100}$$

This function has been graphically presented for a range of masses around the required phases as mentioned earlier for the values mentioned earlier. The results can be found in Fig.(4).

One can read of the minimum mass for a given phase requirement from Fig.(4). However, Eq.(100) could also have been rewritten as function of mass to get the minimum mass for a given phase. This will result in the equation, after only using the positive mass solution, given by:

$$m = \frac{-3(10A)^{1/6}\Phi_{\mathrm{eff,max}}B - B\sqrt{(10A)^{1/6}\Phi_{\mathrm{eff,max}}((10A)^{1/2}\Phi_{\mathrm{eff,max}} + 16DB^2)}}{2((10A)^{1/2}\Phi_{\mathrm{eff,max}} - 2DB^2)} \tag{101}$$

Here B=$2\frac{g\mu_B\partial_x B}{(\frac{\tau}{2})^2}$ and D=$\frac{Gt_{\mathrm{int}}}{\hbar}$. Using the same parameters as used for the results of Fig.(4) and with $\Phi_{\mathrm{eff,max}}$=0.01,0.1 and 1 rad, we will get the minimum masses as displayed in Tab.(1) of App.(A). These values match the ones, one can read off from Fig.(4).

10.2 Mass minimization modified setup, conducting plate

As explained in Sec.(8), we have for the modified setup that the only significant force that alters the motion of is the attractive Casimir force of the nearest states with respect to the conducting plate. The force is given by Eq.(77), which will result in the equation of motion of these states given by:

$$\ddot{x} = \frac{F_{\mathrm{casimir}}}{m} = -\frac{3}{2m\pi}\left(\frac{\epsilon-1}{\epsilon+2}\right)\frac{R^3}{x^5}\hbar c = -\frac{9\hbar c}{8\pi^2\rho}\left(\frac{\epsilon-1}{\epsilon+2}\right)\frac{1}{x^5} = -\frac{Z}{x^5} \quad [m/s^2] \tag{102}$$

[24] It should be noted that this is only the case as we are considering entanglement phases far below the phase of $\Phi_{\mathrm{eff}} \sim 2\pi$, which is obviously the upper-bound of a phase.

Here, m is again the mass of the test mass, ρ its corresponding density and $Z = \frac{9\hbar c}{8\pi^2\rho}\left(\frac{\epsilon-1}{\epsilon+2}\right)$. This second order differential equation in x can be solved numerically by utilizing expression of the second order differential equation:

$$\ddot{x} = \frac{x(t+\Delta t) - 2x(t) + x(t-\Delta t)}{(\Delta t)^2} \tag{103}$$

Here, Δt is a constant time interval taken sufficiently small. With this expression the equation of motion of the sphere reduces to:

$$x(t+\Delta t) = -\frac{Z}{x(t)^5}(\Delta t)^2 + 2x(t) - x(t-\Delta t) \;\rightarrow\; x_{n+1} = -\frac{Z}{x_n^5}(\Delta t)^2 + 2x_n - x_{n-1} \tag{104}$$

This function can be iterated to give the relative position x_n of the states with respect to the plate at a time $n\Delta$t. From Fig.(3), we see that the initial separation of the nearest state with respect to the center of the plate can be expressed as by $(d-\Delta x)/2$. Additionally, by denoting the thickness of the plate, as mentioned in Sec.(8), by W we have a separation of $(d-\Delta x)/2 - W/2$ of the inner states with the edge of the plate. As the states are stationary at the beginning of step 2 their initial velocity is zero[25]. This will mean that the two initial positions needed to solve Eq.(104) are given by:

$$x_0 = (d-\Delta x)/2 - W/2 \quad \& \quad x_1 = x_0 + v_0 \cdot \Delta t = x_0 \tag{105}$$

Using the expression for the superposition size, Eq.(54), one has that Eq.(104) can now be iterated for the same parameters as done for the current setup for a given mass and distance d. However, the condition imposed in Eq.(79) should also be implemented. Therefore, the iteration is stopped whenever this requirement is violated. This means that for values of m and d for which the requirement is violated before the final interaction time is reached, the interaction time would obviously be shorter to not violate the requirement.

Eq.(104) gives the relative position of the state with respect to the plate as explained before. However, for further analysis, it is more use-full to use the horizontal travelled distance of the state with respect to the initial separation of this state, x_0, this "extra" distance travelled during the free fall is depicted by s in Fig.(3). By also "slicing" this distance s up in different time intervals, one has that at a time $n\Delta t$ the value of s_n can be expressed as:

$$s_n = x_0 - x_n \tag{106}$$

With this expression we can observe from Fig.(3), that the relative distances between the different states at a time nΔt are given by:

$$(x_{|\uparrow\rangle_1} - x_{|\uparrow\rangle_2})_n = (x_{|\downarrow\rangle_1} - x_{|\downarrow\rangle_2})_n = d - s_n \quad (x_{|\uparrow\rangle_1} - x_{|\downarrow\rangle_2})_n = d + \Delta x \quad (x_{|\downarrow\rangle_1} - x_{|\uparrow\rangle_2})_n = d - \Delta x - 2s_n \tag{107}$$

By taking the infinitesimal limit of Δt one has a steady phase evolution during the time period Δt for a certain distance s_n. By implementing the obtained distances of Eq.(107) in the phase evolution, Eq.(63), one gets that the steady phase evolution during the time interval of Δt at a position s_n is given by:

$$\Phi_{\text{eff,n}} = \frac{Gm^2}{\hbar}\Delta t\left(\frac{1}{d-\Delta x-2s_n} + \frac{1}{d+\Delta x} - 2\frac{1}{d-s_n}\right) \tag{108}$$

Then one can take a Riemann sum over all attained values s_n to get the total accumulated effective phase during the free fall:

$$\Phi_{\text{eff}} = \frac{Gm^2}{\hbar}\Delta t\sum_n\left(\frac{1}{d-\Delta x-2s_n} + \frac{1}{d+\Delta x} - 2\frac{1}{d-s_n}\right) \tag{109}$$

For a fixed value of $d-\Delta x$ there are, for different masses, no changes in s_n[26]. If we than also fix the mass, similar to the current protocol, one has for the same reason as for the current setup that the highest

[25] The attraction of the plate with respect to the plate can be neglected during step 1 of the experiment as the magnetic field is several orders of magnitude larger at all times in step 1 for the relevant parameters.

[26] As we saw that the acceleration is mass independent, see Eq.(102). For this statement the acceleration requirement is not taken into account as this would lower the total accumulated summation when this requirement is violated.

magnetic field gradient will give the best results. However, for smaller interaction times we can start at smaller initial separations then for the higher interaction times as smaller values of s_n can be achieved before the acceleration requirement, Eq.(79), is violated and thus before the iteration is stopped. Consequently, the differences in results for interaction times are less significant than for the current setup. This is why the whole 1-3s region will be graphically displayed.

From Eq.(109), and the iteration equations, Eq.(104) & Eq.(106), and the acceleration requirement of Eq.(79), one can see that for a given mass the only factor that influences the other variable in the effective phase, which is s_n, is the distance d. A suitable expression for this distance would be:

$$d = \Delta x + NR \quad ; N \text{ is a positive (half) integer} \tag{110}$$

With this expression for d, Eq.(104) has been iterated using Eq.(54) and Eq.(116) for a range of values of N and a range of masses and these results have been implemented in Eq.(109) using Eq.(106). The python code used for this can be found in App.(C) and the results for the most optimal cases of N for the same phase requirements and for the same parameters as for the current setup can be found in Fig.(5).

From these figures, we observe first of all that all lines, depending on N and t_{int}, terminate at a certain minimum mass (corresponding to the lowest phase). These masses are characteristic for when the iteration of Eq.(104) transitions from being stopped due to violation of the acceleration requirement, Eq.(79), to being stopped because the given interaction time is reached. As the masses below the lowest mass have their iteration stopped because of the acceleration requirement they should, therefore, have a shorter interaction time than the ones indicated by their label. Therefore, those masses are not suitable for the experiment for the given interaction times and values of N indicated by their respective labels and are for that reason not displayed. Masses above the minimum mass are, on the other hand, allowed values for the experiment as they do not violate the acceleration requirement. To see this, one can rewrite the acceleration requirement in terms of the separation between one of the inner states and the plate (x):

$$\frac{a_{\text{casimir}}}{a_{mag}} \leq 0.1 \Rightarrow x \geq \left(\frac{90\hbar c}{6\pi} \left(\frac{\epsilon - 1}{\epsilon + 2} \right) \frac{R^3}{g\mu_B \partial_x B} \right)^{1/5} \tag{111}$$

This equation tells us that, to not violate the acceleration requirement, the separation of the state with respect to the plate should always be larger than $\left(\frac{90\hbar c}{6\pi} \left(\frac{\epsilon-1}{\epsilon+2} \right) \frac{R^3}{g\mu_B \partial_x B} \right)^{1/5}$, let's call this minimum separation the minimum distance. As this minimum distance scales with $R^{3/5}$ and the initial separation of the state with the plate ($(d - \Delta x - W)/2$) scales with R[27] one has that when the mass, and thus R, is increased, the states move further from the plate than the minimum distance of the acceleration requirement does. By also noting that the acceleration towards the plate is independent of the size/mass of the test masses, one has that higher masses, after the free fall, will be further from the plate than lower masses, since they are initially placed further from the plate due to the scaling with R. There is a "certain mass" for which the initial $(d-\Delta x-W)/2$ separation is such that after the free fall the separation of the state with respect to the plate coincides with the minimum distance. Therefore, as the acceleration is independent of size/mass and $(d - \Delta x - W)/2$ scales faster than the minimum distance, an increase of mass with respect to the "certain mass" will give, after the free fall, a larger distance of the states with the plate than the minimum distance. Thus, a stopping of the iteration due to the time limit is reached, and these masses are allowed to use for the experiment for the given values indicated in the graph. Vice versa we have due to the size-independent acceleration and the faster scaling of the initial separation with respect to the minimum distance that smaller mass with respect to the "certain mass" will give a separation of the state with respect to the plate, after the free fall, smaller than the minimum allowed distance. Therefore, these masses are disallowed to use for the given parameters in the graph as they violate the acceleration requirement. This is why the curves in the graph have a minimum mass (corresponding to the lowest phases) as lowering the mass will give no viable solutions for the experiment and are, therefore, not displayed.

[27] It should be stressed that this scaling of R of $(d - \Delta x - W)/2$ is not a physical result, but is purely coming from the numerical method, as to highlight the minimum achievable for the phase requirements, as will be explained later on.

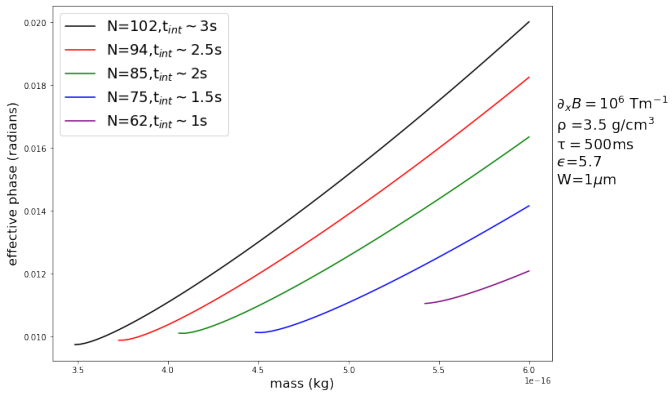

(a) Φ_{eff}=0.01

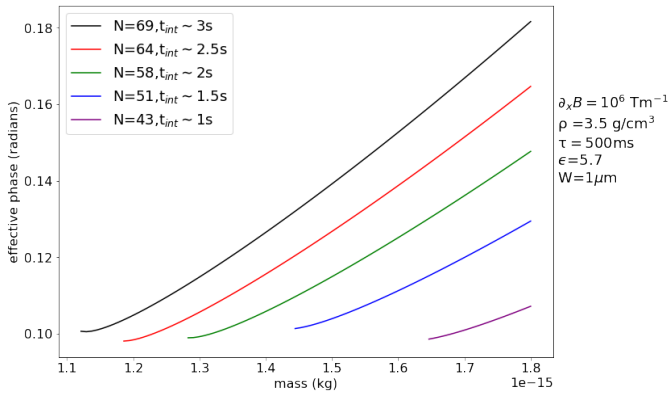

(b) Φ_{eff}=0.1

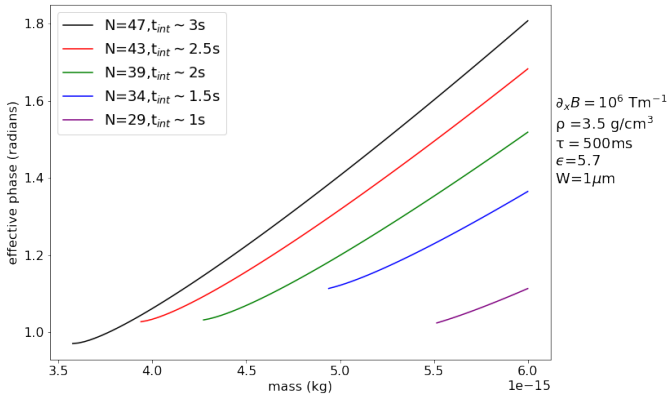

(c) Φ_{eff}=1

Figure 5: These figures display the maximum entanglement phase generated during step 2 of the modified set-up of the **QGEM**-protocol as a function of mass, for different values of N, and for the indicated phase requirements of the sub-graphs. N is related to the test mass separation d before step 1 of the experiment is carried out, by $d = \Delta x + NR$. The lowest mass with the lowest phase, for a given N & t_{int}, characterizes the mass for which the acceleration requirement is barely met. Hypothetical masses below this mass are, therefore, disallowed and cannot be used for the experiment. All masses above the minimum mass, as displayed in the graph, are, on the other hand, usable.

One wants to go to a scenario in which the initial separation of the test masses, d, is such that the acceleration requirement is barely met after a given interaction time, t_{int}, as this will give the shortest distances, s_n, between the nearest state with respect to the plate and hence give the largest effective phase. Therefore, one wants the minimum mass (with the lowest phase) to coincide with the given phase requirement as this will, therefore, minimize the mass for that phase. This is why the lowest masses are very close to the given phase requirement in the plots of Fig.(5). The minimum masses for a given phase requirement and given interaction, which can be read of from Fig.(5), are displayed in Tab.(1). One should also note that the lower the mass, the shorter the initial separation of the state with respect to the conducting plate is, due to the smaller value of NR. This is mainly because the acceleration of the Casimir force is mass-independent, while the acceleration due to the magnetic field is inversely proportional to the mass. This means that the acceleration of the magnetic field is stronger for lower masses and we can get closer to the plate without violating Eq.(79). For the smallest mass of around $3.5 \cdot 10^{-16}$ kg, the closest distance with respect to the edge of the plate will be around 8μm, or $28R$.

Lastly, we have to check whether the assumption that the most outer states of Fig.(3) are stationary holds

with the new Casimir force introduced by the conducting plate. As is clear from Fig.(3), the distance of the outer states with respect to the plate is $\frac{d+\Delta x}{2} - W/2$. By using Eq.(110), one gets a separation of:

$$(x_{|\uparrow\rangle_1} - x_{\text{Plate}}) = (x_{|\downarrow\rangle_2} - x_{\text{Plate}}) = \frac{2\Delta x + NR}{2} - \frac{W}{2} \tag{112}$$

From this expression it is clear that when $2\Delta x + NR$ has the smallest values, the separation is the smallest and the Casimir force will, thus, be the most significant. Therefore, if we check that the acceleration due to the Casimir force is insignificant for the mass corresponding to the smallest value of $2\Delta x + NR$ for the masses of Fig.(5)/ Tab.(1), it will be insignificant for all the masses in our mass region. From Eq.(54) it is clear that, for a given magnetic field gradient of 10^6 Tm^{-1}, Δx is the smallest for the largest mass. From Fig.(5) we see that the largest mass is approximately $5.7{\cdot}10^{-15}$, corresponding to $\Delta x \sim 407\mu$m. Even if we neglect the contribution of NR in Eq.(112) we would already end up with a negligible acceleration of $\sim 10^{-12}$ m/s^2 [28], where use has been made of Eq.(102). As this Δx is, as mentioned before, the smallest value for our mass region, we have a negligible acceleration of the outer masses towards the plate for all situations in Fig.(5), justifying the assumption.

10.3 Lower magnetic field gradients

In the previous sections we assumed a magnetic field gradient of 10^6 Tm^{-1}, however, as mentioned in Ref.[1], achieving such high magnetic field gradients can only be achieved when the test masses are very close to the magnetic source with a very precise separation of 10μm, which requires four different magnets co-moving with the test masses at a very precise (same) speed during the free-fall [1]. Additionally one needs to account for distortion of the motion of the test masses due to the Casimir force with the magnets and for patch-potentials for such small separations. However, lower magnetic field gradients, such as 10^4 Tm^{-1}, are favorable as they can be achieved in normal laboratories [1] and allow for a much larger separation of the states with the magnetic source, having a significant reduction in the effects of the Casimir force and patch potentials. Consequently, it would not be mandatory to apply the advanced futuristic setup of the high magnetic field gradient and, therefore, this section will deal with exploring the comparison of both setups for magnetic field gradients of lower magnetic field gradients of 10^5 Tm^{-1} and 10^4 Tm^{-1}.

10.3.1 Current setup

Following the same procedure for the current setup as in Sec.(10.1), the effective phase has been computed for a mass region of 10^{-14}-10^{-12} kg for the magnetic field gradient of 10^5 Tm^{-1} and the result is displayed in Fig.(6).

From Fig.(6), we observe that the effective entanglement phase approaches a certain value, which depends on the interaction time. However, with our maximum interaction time of 3s, we cannot get much higher than a phase of $\Phi_{\text{eff}} \sim 0.05$ rad. This implies that phase requirements of 0.1 and 1 rad will never be reached, limiting the experiment to be measured for the requirement of $\Phi_{\text{eff}} \sim 0.01$ rad. The physical reason that the higher phase requirements cannot be reached is that for this lower magnetic field gradient the magnetic field is unable to split the superposition of the test mass, for masses which would normally lead to entanglement of the desired requirement, to a significant size required to generate a significant differences in phase evolution of the state combinations, to overcome the closest separation of states of 157μm. For a mass of 10^{-14} kg we have that Δx is approximately 20μm, which is one order of magnitude smaller than the 157μm of the closest state separation. Consequently, we have that the gravitational interaction of all test masses will approximately be the same, and will even be more so for higher masses as they have a smaller superposition size. Therefore, they will not increase the effective entanglement phase as normally would be the case. One can see this mathematically by approximating Eq.(100). By substituting back in $\Delta x = \frac{g\mu_B \partial_x B}{2m}\tau^2$, Eq.(100)

[28] One can also safely neglect the contribution of $\frac{W}{2}$ as this is only 0.5μm which is negligible with respect to the superposition size.

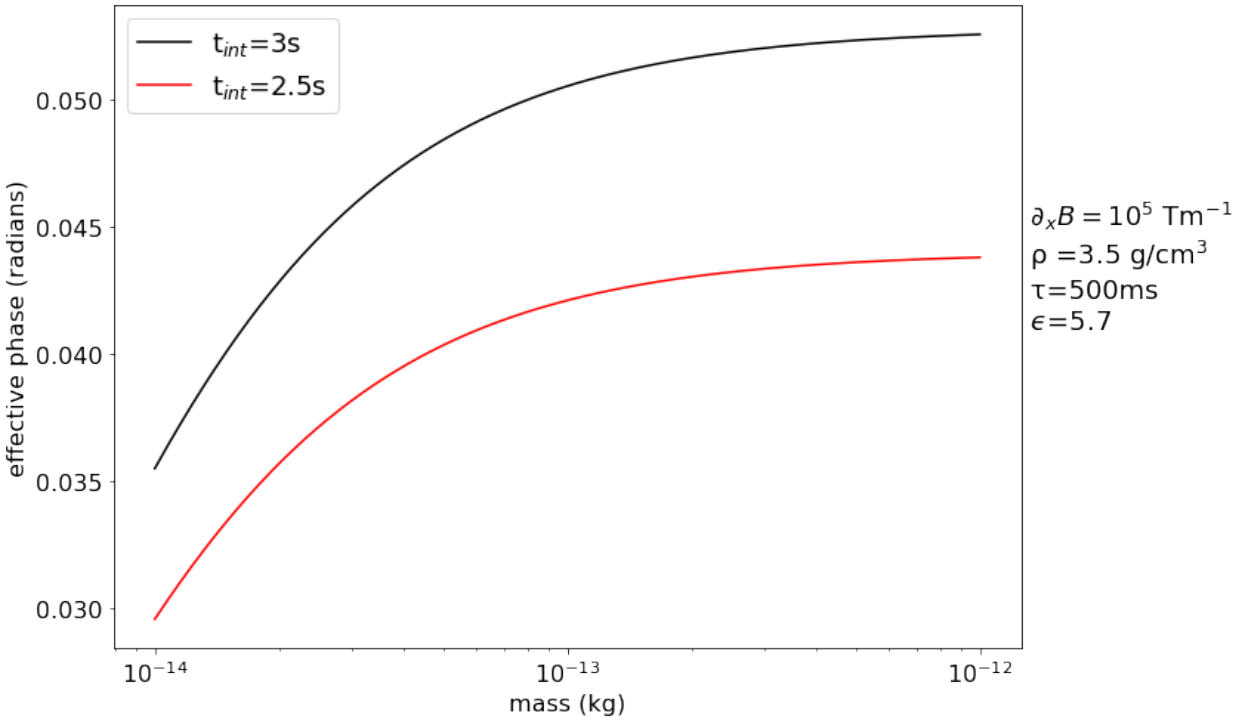

Figure 6: This figure displays the maximum entanglement phase ,generated during step 2, of the current setup of the **QGEM**-protocol as a function of mass for the parameters indicated next to the graph. The optimal distance between the test masses, before the splitting of step 1, was found to be $d - \Delta x \sim 157\mu$m. It should be noted that the mass axis is on a logarithmic scale.

can be rewritten as:

$$\Phi_{\text{eff,max}} = \frac{Gm^2}{\hbar} t_{\text{int}} \frac{1}{(10A)^{\frac{1}{6}}} (1 + \frac{1}{2\frac{\Delta x}{(10A)^{\frac{1}{6}}} + 1} - \frac{2}{\frac{\Delta x}{(10A)^{\frac{1}{6}}} + 1}) \tag{113}$$

As argued before $\Delta x << (10A)^{\frac{1}{6}}$, hence we can approximate the two fractions in the bracket by a geometric series $(1/(1-x) = \sum_0^\infty x^n)$. Expanding this up to second order (n=2) for both fractions will give us

$$\Phi_{\text{eff,max}} = \frac{Gm^2}{\hbar} t_{\text{int}} \frac{1}{(10A)^{\frac{1}{6}}} \left(1 + 1 - 2\frac{\Delta x}{(10A)^{\frac{1}{6}}} + \left(2\frac{\Delta x}{(10A)^{\frac{1}{6}}}\right)^2 - 2\left(1 - \frac{\Delta x}{(10A)^{\frac{1}{6}}} + \left(\frac{\Delta x}{(10A)^{\frac{1}{6}}}\right)^2\right)\right) , \tag{114}$$

this reduces further to:

$$\Phi_{\text{eff,max}} = \frac{Gm^2}{\hbar} t_{int} \frac{1}{(10A)^{\frac{1}{6}}} \frac{2(\Delta x)^2}{(10A)^{\frac{2}{6}}} = \frac{2Gt_{int}}{\hbar(10A)^{\frac{1}{2}}} \left(\frac{g\mu_B \partial_x B}{2} \tau^2\right)^2 \tag{115}$$

This is just a constant and with the relevant values this constant coincides exactly with the values which can be read of from Fig.(6). The phase of 0.01 rad can, as we see from Fig.(6), be reached and with Eq.(101), one will obtain that this phase is reached for the masses shown in Tab.(2).

One can do a similar procedure for the magnetic field gradient of 10^4 Tm^{-1} and one will obtain that with Eq.(115) the phase will not get higher than $5.2{\cdot}10^{-4}$ rad. Consequently, with this setup, and this magnetic field gradient, a phase of 0.01 rad cannot be reached or even approached closely.

10.3.2 Modified setup

For the modified setup we have to check, again, whether the acceleration of the outer states, of Fig.(3), due to the Casimir force with respect to the plate can be neglected. We will see that the highest mass, and thus the lowest superposition size, for an interaction time in the order of seconds, is $0.95{\cdot}10^{-14}$ kg. For such a mass and the lower magnetic field gradient of 10^5 Tm^{-1} we get a lower initial separation with the plate as indicated by Eq.(112). For a mass of $0.95{\cdot}10^{-14}$ kg and with N=26, as we will see, this will, by using the initial separation, lead to an acceleration of approximately $0.01/R$ s^{-2}, where use has been made of Eq.(102). Consequently, one can again neglect the acceleration of the outer states ($|\uparrow\rangle_1$ and $|\downarrow\rangle_2$) with the similar arguments made in in Sec.(10.2). With this assumption the iteration follows the same procedure as in Sec.(10.2), where only the value of the magnetic field gradient is one order of magnitude lower, this will result in Fig.(7).

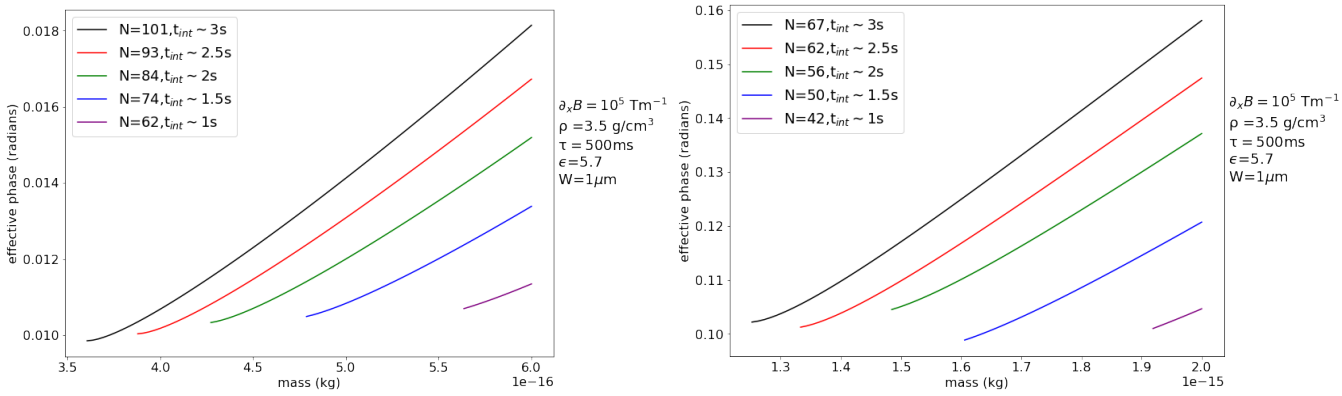

(a) Φ_{eff}=0.01 (b) Φ_{eff}=0.1

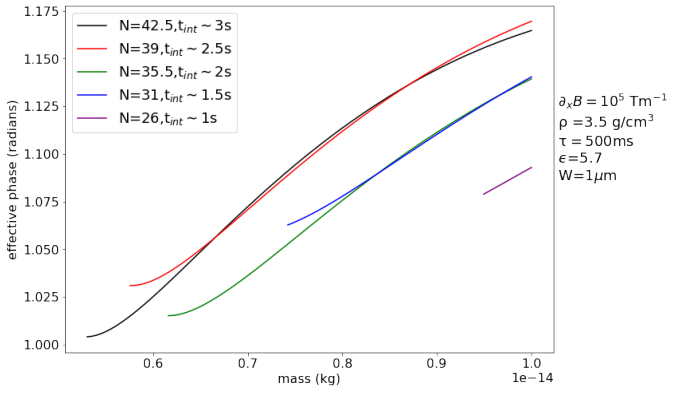

(c) Φ_{eff}=1

Figure 7: These figures display the maximum entanglement phase generated during step 2 of the modified set-up of the **QGEM**-protocol as a function of mass for different values of N, for the indicated phase requirements of the sub-graphs. N is related to the test mass separation d before step 1 of the experiment is carried out, by $d = \Delta x + NR$. The lowest mass with the lowest phase, for a given N & t_{int}, characterizes the mass for which the acceleration requirement is barely met. Hypothetical masses below this mass are, therefore, disallowed and cannot be used for the experiment. All masses above the minimum mass, as displayed in the graph, are, on the other hand, allowed to be used.

From Fig.(7) we observe that we can go up to phases of 0.1 and 1 rad, which was not possible for the current setup. The physical reason for this is that although Δx is much smaller than what one could achieve with the higher magnetic field gradient, we still have a reasonable superposition size compared to the initial separation of the closest states, which is at most the same order of magnitude as the superposition size. Furthermore,

the inner states also get attracted to the plate during the free fall, therefore, the superposition size is even more enhanced during this period. Consequently, we have, due to these two reasons, that the gravitational interaction between the different state combinations of the two systems can be sufficiently be distinquished from one another. This has the result that the second and third term of the effective phase, Eq.(118), are relatively low with respect to the first term, instead of being approximately the same. Henceforth, we still are able to generate significant entanglement phases. This is also possible because the separation of the closest states $(d - \Delta x)$ is one order of magnitude lower than before, since we can now go up to a separation in the order of 10μm, instead of the 157μm of the current setup. This makes the terms in the bracket for the effective phase already an order of magnitude larger for a given mass and, therefore, already gives an advantage for what is possible for the required phases.

One can also observe that figure c of Fig.(7) has a relatively small increase in phase after the minimum mass (with the lowest phase) compared to the other figures. This has mainly to do with the way the solution has been iterated, but has also to do with the limitation of the experiment. For the iteration, use has been made of the dynamic parameter NR, this parameter is, therefore, larger for the higher masses. This makes the considered initial separation between the test masses larger for higher masses. This will have several negative effects on the phase of higher masses. All negative influences of an increased mass are:
1.) First of all this larger initial separation of the states, due to NR, will lead to a less effective enlargement of the superposition size as the acceleration of the Casimir force, Eq.(102), is smaller. Thus, making the three terms in Eq.(118) more similar to one another.
2.) Larger separations of the test masses, again due to NR, with the lower Casimir acceleration also has the consequence that the inner states are not as close to each other as before. This implies that the magnitudes of the terms in the brackets in Eq.(118) are smaller.
3.) The last negative effect of higher masses is independent of this dynamic parameter but is because a higher mass leads to a smaller Δx, meaning that the terms in the brackets of Eq.(118) are similar to one another and thus lowers the phase.
It is important to realise that point 1 and 2 are purely iteration effects and point 3 is a purely physical effect. The three points mentioned above all lower the term in the bracket of Eq.(118), however, one also notes that a higher mass will increase the common factor outside of the bracket, because of the m^2 proportionality. Normally this effect is much larger than the 3 points mentioned above and this is why for other plots the phase increases more rapidly. However, in this case, the three terms have a relatively larger negative contribution on the phase, leading to a much smaller increase of the effective phase. If one were to go to higher masses than indicated in the figure, one would see a decrease in the phase, due to the larger contribution of the three points on the phase than the m^2 proportionality.

One should, again, note that the minimum masses are forced to coincide around the phase requirement as this maximizes the interaction time. Other values of N, would lead the minimum mass to coincide with other phases than the required phase and, therefore, as explained in the previous section, the masses that will correspond to the phase requirement are not optimal.

For the even lower magnetic field gradient of 10^4 Tm^{-1} we have to check, again, whether the assumption of stationary outer states will hold. For the masses of the phase requirement of 0.01, this assumption is still valid. However, as we will see later on, we will go up to masses of around 10^{-14} kg, and $d = \Delta x + 33 \cdot 10^{-6}$ m, see Fig.(9), to get to a maximum phase. For these masses, the acceleration of the outer states is approximately 0.3 μm/s^2, which is, with the acceleration time of 3s, in the order of the radius of the test mass. Therefore, one has to include the Casimir attraction of the plate on the outer states, $|\uparrow\rangle_1$ & $|\downarrow\rangle_2$ of Fig.(3).

This procedure can be modelled similar to what was done for the inner states in Sec.(10.2), where only the initial condition will be different. From Fig.(3), one can deduce that the initial conditions of the outer states are given by:

$$x_0^{(2)} = (d + \Delta x)/2 - W/2 \quad \& \quad x_1^{(2)} = x_0^{(2)} + v_0^{(2)} \cdot \Delta t = x_0^{(2)} \tag{116}$$

Here, $x_0^{(2)}$ is used for the distance of the outer states with the plate, instead of x_0, to distinguish from the position of the inner states. Following the same procedure as for the inner states, one obtains the change of

the distance for the outer states similar as for the inner states to be:

$$r_n = x_0^{(2)} - x_n^{(2)} \tag{117}$$

With this effective distance change of the outer states (r_n), we have that the second term of Eq.(109) will be different. Additionally, by observing Fig.(3), with now the outer states also moving inwards, we get that the expression of the effective phase becomes:

$$\Phi_{\text{eff}} = \frac{Gm^2}{\hbar}\Delta t \sum_{n=0}^{N}\left(\frac{1}{d-\Delta x-2s_n}+\frac{1}{d+\Delta x-2r_n}-2\frac{1}{d-s_n-r_n}\right) \tag{118}$$

Using this expression for the effective phase and following the same procedure of the iteration as done in Sec.(10.2), one obtains the result of Fig.(8) for a magnetic field gradient of 10^4 Tm^{-1}. It should be stressed that for these masses we also could have used the effective phase equation, with corresponding iteration, of Eq.(118), since here the acceleration of the outer states is, also, only $0.01/R$ s^{-2} and can for that reason also be neglected.

As we can see from Fig.(8), there is only a plot for a phase of 0.01 rad, this is because the other phase requirements could not be reached. This is already hinted by the fact that the increase of the phase after the minimum mass in Fig.(8) is not as steep as we are used to and this decrease of steeping can, again, be explained by the previously mentioned arguments used for the last plot of the magnetic field gradient of 10^5 Tm^{-1}.

However, we can get very close to an effective phase requirement of 0.1 rad. To show the maximum phase we can achieve, a slight altercation of the iterative expression of d, of Eq.(110), will be made and is given by:

$$d = \Delta x + N \cdot 10^{-6} \quad [\text{m}] \tag{119}$$

The reason for this is to have an equal separation for all masses, making the maximum independent on the way the iteration has been carried out, since we are no longer interested in observing the minimum mass. This makes it easier to find the actual maximum as the separation between the closest states is now the same for all masses. By using different values for N, in steps of 0.5, for the same iteration methods as before, we will get the results for the value of N which results in the highest maximum of the phase, as displayed in Fig.(9).

The transition from solid to dashed line indicates the transition from allowed masses to masses that are disallowed to use for the experiment for the indicated parameters. Additionally, the maxima correspond to the highest entanglement phases that can be generated by this setup of the **QGEM**-protocol, for the indicated parameters. The maxima have again an iterative explanation but is, in this case, not due to the way the iteration is carried out but is due to the violation of the acceleration requirement as will now be explained. The acceleration caused by the Casimir force is, as we saw previously in Eq.(102), independent on the size/mass of the test masses. Consequently, all masses are accelerated to the same extend for a given initial separation with the plate, so one might think that higher masses will automatically generate a higher phase as the distances will be the same. However, one should also remember that we implemented the condition that the acceleration caused by the Casimir force should be at a maximum of one-tenth of the magnetic field acceleration, see Eq.(111). This resulted in a minimum separation of the state with respect to the plate. From Eq.(111) one can see that increasing the mass will increase the minimum allowed separation distance of the inner state with the plate. With this in mind, it is pretty straight forward to conclude that, with the mass-independent acceleration, there is for a fixed distance d a maximum mass in which the acceleration requirement is barely met after the interaction time is reached. Therefore, higher masses have their iteration stopped before this time is reached, having that the summation of Eq.(118) is automatically lower as the final few terms which would normally be there are not included. This iterative effect together with that the superposition size is smaller, meaning a less effective separation as mentioned previously and a smaller difference between the bracket terms, are together larger than the m^2 proportionality which causes the maximum. It is also good to realise that these masses are disallowed for the indicated interaction times, since theiritteration is stopped before the interaction time is reached. Also, logically, all masses below the maximum have

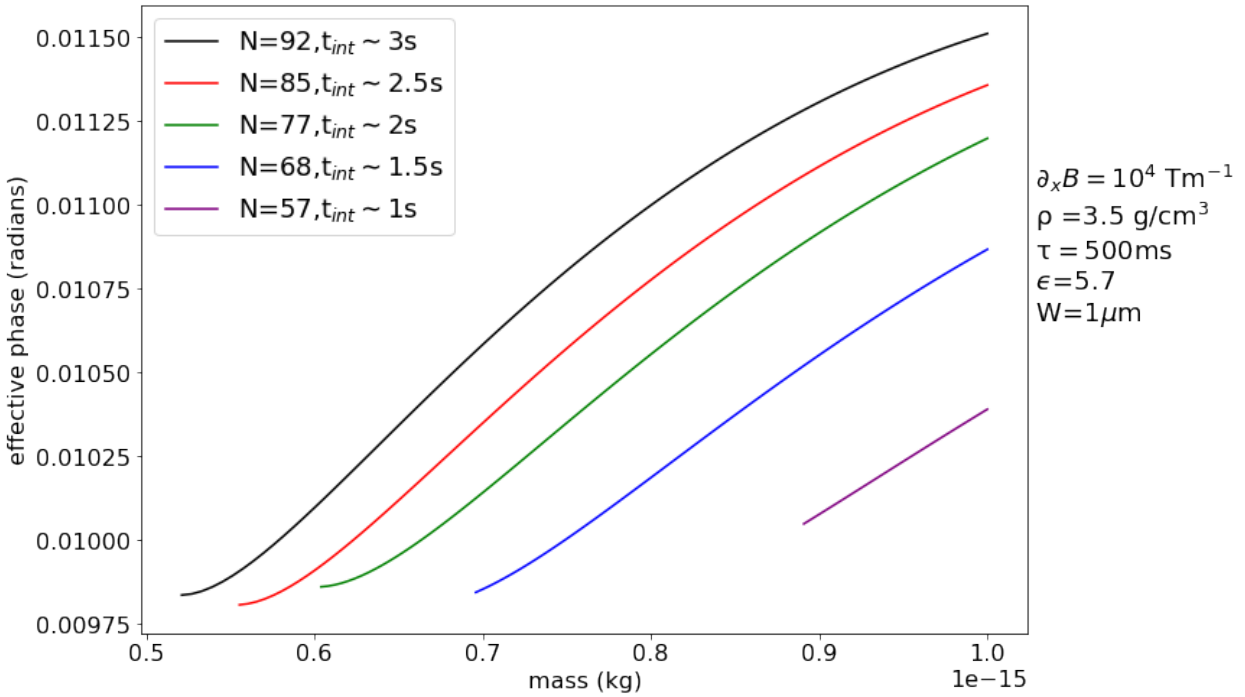

Figure 8: This figures displays the maximum entanglement phase generated during step 2 of the modified setup of the **QGEM**-protocol as a function of mass for different values of N, for a phase requirement of $\Phi_{\text{eff}} = 0.01$ Rad. N is related to the test mass separation d before step 1 of the experiment is carried out, by $d = \Delta x + NR$. The lowest mass with the lowest phase, for a given N & t_{int}, characterizes the mass for which the acceleration requirement is barely met. Hypothetical masses below this mass are, therefore, disallowed and cannot be used for the experiment. All masses above the minimum mass, as displayed in the graph, are, on the other hand, allowed to be used.

their iteration not stopped due to violation of the acceleration requirement and are, therefore, allowed values.

Choosing a higher value of N will lead to the peak shifted to the right towards higher masses. Choosing this higher value of Nhas three effects on the phase:
1.) An increase in phase due to the m^2 proportionality.
2.) A decrease in phase because the test masses are separated further from each other at all times during the free fall.
3.) A decrease in phase due to smaller Δx, leading to a smaller effective phase as mentioned previously.
It turns out that the "battle" between point 1 and points 2 & 3 leads to the highest peak for the given N displayed in Fig.(9). One can make the opposite arguments for a lower value of N. This makes that the indicated values of N are actually the ones corresponding to the largest entanglement phases one can achieve with this modified setup for this particular magnetic field gradient.

One should note that these maximum phases are an upper bound estimation. One can infer, by comparing the last value of the iteration of Eq.(106) with the value of Δx of Eq.(54), that for masses around 10^{-14} kg, Δx is the same order of magnitude as the maximum value of s, meaning that there is already a significant Casimir interaction during step 1 of the experiment. This implies that the separation of the test masses should be somewhat further, lowering the maximum phase by a small amount, not much as the acceleration of the magnetic field is still stronger here. The maximum here was just to show what is in general possible for the modified setup, but will not be used further on in this thesis as we are only interested in the phase requirement values. However, for setting up this experiment, one can do a similar analysis done in the rest

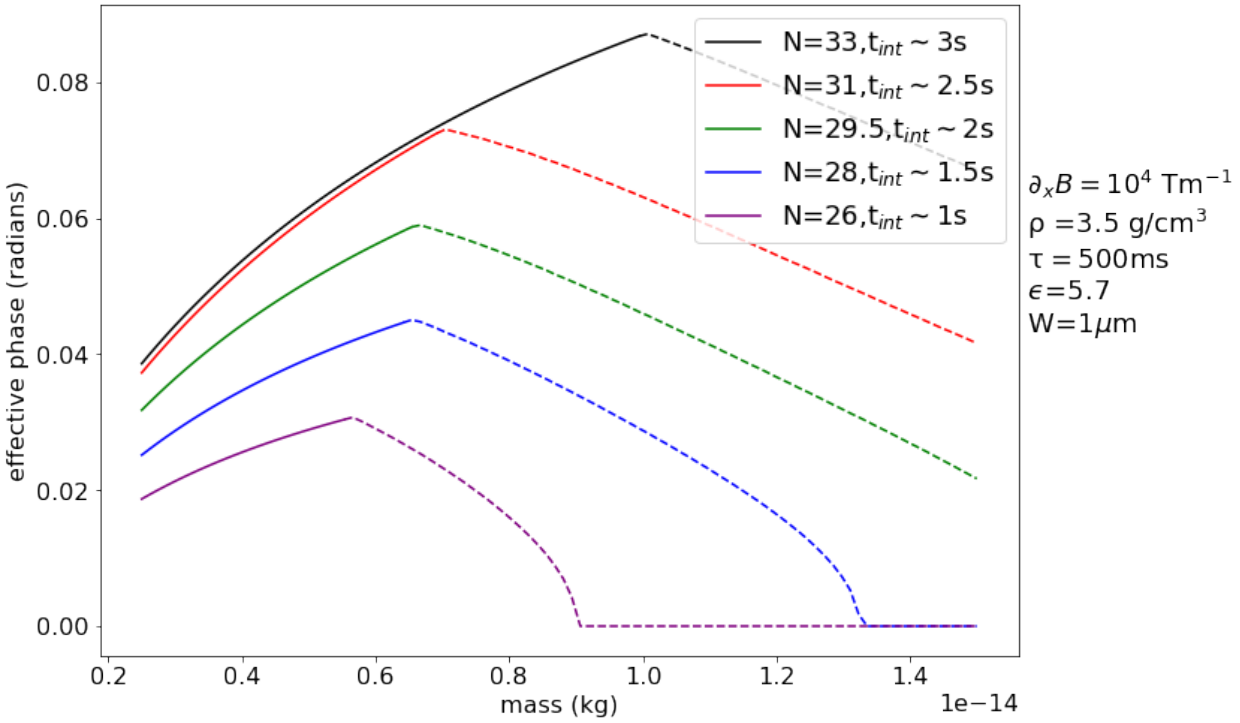

Figure 9: This figure displays the maximum entanglement phase generated during step 2 of the modified setup of the **QGEM**-protocol as a function of mass, for different values of N for the maximum possible phase. N is related to the test mass separation d before step 1 of the experiment is carried out, by $d = \Delta x + N \cdot 10^{-6}$ m. The transition from solid to dashed line characterizes the mass for which the acceleration requirement is barely met. Masses above this transition are disallowed and cannot be used for the experiment for the indicated interaction times and value of N. All masses below this transition, on the other hand, are allowed to be used.

of the thesis if one wants to maximize the phase.

The results of the minimum masses for a given phase requirement for the lower masses for both setups can be read off from the figures and all results are also concluded in Tab.(2) and Tab.(3) of App.(A).

I want to stress again that for the phase requirement of $\Phi_{\text{eff}} \sim 0.01$ rad together with the magnetic field gradient of 10^4 Tm^{-1} for the modified setup, the acceleration of the outer states can safely be neglected as this is important for the rest of the analysis.

10.4 Comparison minimum mass

Tab.(1), of App.(A) shows the relevant values for the mass minimization for a given phase requirement for the magnetic field gradient of 10^6 Tm^{-1}, as graphically displayed in Fig.(4) and Fig.(5). From Tab.(1) and comparing Fig.(4) with Fig.(5) we see that with a perfect conductor in between the nearest states much smaller masses can be reached for a given phase requirement as the separation between the closest states can be made much smaller. It is also clear that the larger the phase requirement, the more significant this effect is, because for a phase requirement of 0.01 rad and an interaction time of 3s we have a ratio of $\frac{m_{\text{current}}}{m_{\text{conducting plate}}} \approx 2.7$, whereas for a requirement of 0.1 rad we will have $\frac{m_{\text{current}}}{m_{\text{conducting plate}}} \approx 3$ and for a requirement of 1 rad we have $\frac{m_{\text{current}}}{m_{\text{conducting plate}}} \approx 4.7$. We also observe that for a given phase requirement the shorter interaction times of 1s for the modified setup are generating lower masses than interaction times of 3s for the

current setup. This will give an even more suitable option in terms of decoherence as we will see later on. However, it should be noted that the for the modified setup we assumed the plate to be a perfect conductor, but realistically perfect conducting materials do not exist and there will still be some electromagnetic waves propagating through the plate, giving rise to the presence of a small Casimir force between the nearest states, this assumption will be discussed in Sec.(13.2).

For a magnetic field gradient 10^5 Tm^{-1} we can only compare the 0.01 phase requirement as the current setup is unable to generate higher phases as we saw earlier. The mass ratio for this requirement for this is $\frac{m_{\text{current}}}{m_{\text{conducting plate}}} \approx 4.5$. We also observe that an effective phase requirement of 0.1 for the modified setup already gives better results than the 0.01 phase requirement of the current setup. For a magnetic field gradient 10^4 Tm^{-1} we only can go to modified setup, meaning that for laboratory allowed gradients we are limited, as we will see in Sec.(10.6), by conducting the experiment with the modified setup only. This already shows that the modified setup is far better equipped to utilize these lower gradients.

The discussion above shows qualitatively the favorability of the modified setup with regards to the current setup, however, it is not quantitatively discussed what the impact of this will be in terms of the measurability of the entanglement. In Sec.(10.6), we will see how much the modification of the setup would benefit the measurability of the quantum nature of gravity with the **QGEM**-protocol. However, first, the analysis of the collisional decoherence will be performed in the next section as this is also a significant contribution to the detectability as we saw in Sec.(9).

10.5 Impact on decoherence

In both the current and the modified setup we are, during all the steps of the experiment, dealing with two superpositions of two test masses. Therefore, the scattering model for the decoherence derived in Sec.(4) will be used as this model deals with the decoherence of such a system[29]. For this, one can, as derived in that section, use Eq.(38) to model the decoherence of the off-diagonal elements for the ever-changing superposition size.

This decoherence term for the **QGEM**-protocol depends on two kinds of particles: gas molecules and thermal photons[30]. The impact of this decoherence source depends on the environmental temperature (T_e), the number density of the gas (n_V), the internal temperature of the test masses (T_{int}), the size of the test masses (R) and the size of the superposition (Δx). In this thesis we stick to the suggested internal temperature of 0.15K in Ref.[1] and we will look at how this decoherence source can be modeled in terms of the environmental parameters (T_e and n_V), and the experimental parameters (R and Δx) and how this would affect the experiment. For the environmental parameters, we consider the external temperatures range of 1-4K and the number density range of $10^7 - 10^8$ m^{-3} [31].

10.5.1 Short- and long-wavelength approximations

To determine if we are dealing with short- or long-wavelength particles/photons, the wavelength of the environmental particles should be determined and compared to the superposition size of the test masses. For air molecules, inside the ultra-high vacuum setting of the experiment [1], we are dealing with gaseous particles, which we assume to have to the same composition as in the air. The thermal wavelength of such thermal molecules is given by [6]:

$$\lambda_{\text{air}} = \sqrt{\frac{2\pi\hbar^2}{m_{\text{air}} k_b T_e}} \tag{120}$$

[29] There are also other decoherences of the test masses, such as spin decoupling of the test masses, but these have already sufficient coherence times for internal temperatures around 77K, whereas we are dealing with a internal temperature of only 0.15K and should not be of a problem [1, 34] as lower temperatures give longer coherence periods. Another form of decoherence, which is very hypothetical, are the collapse models and this will be discussed in Sec.(12).

[30] Influences of photons from the environment outside the experiment, such as CMB- radiation, can easily be shielded from playing part in the decoherence of the system.

[31] As these ranges corresponds roughly to the pressure of 10^{-15} suggested in [1]. The ideal gas law can easily be applied in this scenario as the molar volumes considered make inter-molecular interactions and sizes of the molecules negligible.

To analyse which wavelength limit to apply, the lowest external temperature of 1K will be used as this maximizes the wavelength. Taking the typical mass of an air molecule to be 28.97 amu and assuming the gas to be in thermal equilibrium with the environment, one would obtain a wavelength of $\lambda \sim 0.32$ nm. Such a superposition size is in step 1 of the experiment in the worst case (using Eq.(51) for the highest masses and lowest magnetic field gradients) already reached after a couple of milliseconds. Therefore, after at most a couple milliseconds, the short wavelength limit for the superposition of states in step 1 of the experiment can already be applied. For step 3 of the protocol we have a similar period at the end where the wavelength is larger than the separation size Δx. Therefore, we get in the worst case, again, a time of the order of milliseconds where the total superposition is not larger than the wavelength of the environmental air molecules. However, the total duration of the experiment, with the created superposition, is at least $2\tau + t_{int} = 2 \cdot 0.5 + 1 = 2$ s [32], which is three orders of magnitude larger than the order of the millisecond. Consequently, we can safely assume the short wavelength limit for the scattering of the environmental air molecules to be applicable. As higher external temperatures will only lead to shorter wavelengths of the air molecules (Eq.(120)), we have that for higher external temperatures this assumption is even more valid.

In the scattering model we assumed, for photons, only scattering of the environmental photons. However, absorption of environmental photons and emission of photons from the test mass will also give "which-path" information loss of the system and should also be taken into account in the decoherence. The decoherence from these two sources can, luckily, be modeled similarly to the scattered photons [6].

The thermal wavelength of photons, which are present due to emission of blackbody radiation of the apparatus and the test masses, can be expressed as [6]:

$$\lambda_{\text{photons}} = \frac{\pi^{2/3}\hbar c}{k_b T_{e,(\text{int})}} \tag{121}$$

For the environmental scattering of photons, which are again assumed to be in thermal equilibrium with the environment, we have that the temperature is the external temperature and for temperatures of a few Kelvin this corresponds to a wavelength in the order of mm. The largest superposition size that is achieved for our mass region is the one corresponding to the smallest mass with the highest magnetic field gradient, which for the values of Tab.(1) are at most in the order of mm (by using Eq.(54))[33]. This implies that for the extreme cases the wavelength and the superposition size are of the same order, meaning that the long-wavelength limit is a loose estimate for this extreme case. However, the long-wavelength will still give an upper-bound estimate to the solutions [1, 6] for such cases. Additionally, the long-wavelength limit is still valid for masses which are an order of magnitude larger and/or magnetic field gradients of an order of magnitude smaller as we took an extreme case. Therefore, the long-wavelength limit will be applied to these kinds of photons.

Besides the scattering photons, as was explained before also decoherence due to the absorption of environmental photons. These absorbed photons have the same environmental temperature as the scattered photons, hence we can also apply the long-wavelength limit for the absorbed photons. Although the term "scattering" constant sounds weird for these absorbed photons, I will use it for expressing the decoherence rate of this interaction.

Another type of photons, that cause decoherence, are the photons that emission from the test masses [6]. The wavelength of these photons depends on the internal temperature and as this temperature has been set to 0.15K, we have that the wavelength is one order of magnitude larger than the environmental photons, since the wavelength is inversely proportional to the temperature, see Eq.(121. Consequently, the long-wavelength limit is even more applicable for these kinds of photons and will, therefore, be used.

[32] The at least statement comes from the fact that for the modified setup the superposition size is enhanced to $\Delta x + s$, meaning that τ should be larger in step 3 of the experiment to bring the superposition back. Also for t_{int} the lowest value of 1s of Tab.(1) is used to get another at least statement. This means that our assumption is even more valid in general.

[33] To be more precise one also has to include the extra superposition size created by s_n of figure 2. However, this is, at most, one order of magnitude smaller than Δx and makes, therefore, no significant contribution to the argument.

By applying the short- and long-wavelength limit for the relevant air molecules and black-body photons, one obtains using Eq.(37) and Eq.(39) the decoherence factor of:

$$\int \gamma_k \mathrm{d}t = \sum_k \gamma_k \Delta t = \Gamma_{\mathrm{air}} t + \sum_{i=1}^{3} \Lambda_i \int (x_{|\uparrow\rangle_k} - x_{|\downarrow\rangle_k})^2 \mathrm{d}t \quad ; \quad \Lambda_1 = \Lambda_{sc} \quad , \quad \Lambda_2 = \Lambda_e \quad , \quad \Lambda_2 = \Lambda_a \tag{122}$$

Here, Λ_{sc} is the scattering constant of the scattered environmental photons, Λ_a that of the absorbed photons, Λ_e that of the photons of the emission of the test mass, and Γ_{air} is the scattering rate of air molecules. $(x_{|\uparrow\rangle_k} - x_{|\downarrow\rangle_k})$ denotes the distance between the states of the superposition inside a single interferometer at a time $t = k$. This distance is not constant during the experiment as this distance changes in step 1 and 3 of both the current and modified setup as well as in step 2 of the modified setup.

10.5.2 Parameter influence total decoherence

The scattering constant for air molecules can be expressed in terms of the scattering rate and its thermal wavelength [6], giving:

$$\Gamma_{\mathrm{air}} = \lambda_{\mathrm{air}}^2 \Lambda_{\mathrm{air}} \tag{123}$$

A derivation of the scattering constant for air molecules can be found in App.(B.1) and can also be found in section 3.4.2 of Ref.[7]. Then, combining Eq.(170) of App.(B.1), with the wavelength of the air molecules, Eq.(120), gives the scattering rate of the gas molecules:

$$\Gamma_{\mathrm{air}} = \left(\sqrt{\frac{2\pi\hbar^2}{m_{\mathrm{air}} k_b T_e}} \right)^2 \frac{4R^2}{3\hbar^2} \frac{N}{V} \sqrt{\pi m_{air}} \left(2 k_b T_e\right)^{3/2} = \frac{16\pi n_V R^2}{3} \sqrt{\frac{2\pi k_b T_e}{m_{\mathrm{air}}}} \tag{124}$$

This expression is similar to expression (27) in Ref.[6] by applying the ideal gas law and noting that the mean velocity is given by $\sqrt{3k_bT_e/m}$.

The expressions for the scattering constant of the interacting photons of Eq.(122) are derived/given in App.(B.2) and can also be found in [6, 7] and are given by:

$$\Lambda_{sc} = 8!\zeta(9) \frac{8cR^6}{9\pi} \left(\frac{k_b T_e}{\hbar c}\right)^9 \mathrm{Re}\left(\frac{\epsilon - 1}{\epsilon + 2}\right)^2 \quad ; \quad \Lambda_{(e)a} = \frac{16\pi^5 c R^3}{189} \left(\frac{k_b T_{(i)e}}{\hbar c}\right)^6 \mathrm{Im}\left(\frac{\epsilon - 1}{\epsilon + 2}\right) \tag{125}$$

As mentioned earlier, $(x_{|\uparrow\rangle_k} - x_{|\downarrow\rangle_k})$ is a dynamic quantity, hence γ_k is dynamic and different for all steps of the experiment. Therefore one has to integrate/sum Eq.(122) differently for all steps of the experiment. Additionally, one should also distinguish between both the current and the modified setup as the decoherence of step 2 and step 3 require a different evaluation. Consequently, the evaluation of the decoherence factor will be done for two cases. The first case is the case that during the free fall the superposition size, Δx, is constant during the free fall, which is true for the current setup and is also a good estimate for the modified setup of the experiment with a magnetic field gradient of 10^6 Tm^{-1}. The second case is that the superposition size changes during the free fall, which is a small perturbation for the modified setup for a magnetic field gradient of 10^4 Tm^{-1} and the higher masses for the magnetic field gradient of 10^5 Tm^{-1} as here the largest value of s_n is one order of magnitude smaller than the superposition size.

For the first case it can analytically be derived that the decoherence factor of Eq.(122) reduces to:

$$\exp\left[-\int \gamma_k \mathrm{d}t\right] = \exp\left[-\left[\Gamma_{\mathrm{air}}(t_{\mathrm{int}} + 2\tau) + 2a^2 \left(\frac{\tau}{2}\right)^4 \sum_{i=1}^{3} \Lambda_i \left(\frac{46}{15}\frac{\tau}{2} + 2t_{\mathrm{int}}\right)\right]\right] \tag{126}$$

Here, a is the acceleration of a single state and is given by Eq.(50). The derivation of this formula can be found in App.(B.3). It should also be noted that this expression is exact for the current setup of the

QGEM-protocol and is a very sufficient first order estimate of the modified setup with the conducting plate for the highest magnetic field gradient.

Important to observe from Eq.(126) is that one can infer from the definitions of Γ_{air}, Λ_i, and a of Eq.(124), Eq.(125) and Eq.(50) that the dependence of the decoherence factor on the size of the test mass is given by:

$$\exp\left[-\int \gamma_k \mathrm{d}t\right] \propto \exp\left[-(C_1 R^2 + C_2 + (C_3 + C_4)R^{-3})\right] \tag{127}$$

The relevant constant for the size dependence are C_1,C_3 and C_4, where $C_1 \propto n_V T_e^{1/2}$,C_3&$C_4 \propto (\partial_x B)^2 T^6_{(i),e}$ and C_2, which arises from the combination of Λ_{sc} and a, is just a constant. We can simplify this proportionality even further to:

$$\exp\left[-\int \gamma_k \mathrm{d}t\right] \propto \exp\left[-C_1 R^2 (1 + \frac{C_3 + C_4}{C_1}\frac{1}{R^5})\right] ;$$
$$C_1 = \frac{\Gamma_{\text{air}}(t_{\text{int}} + 2\tau)}{R^2} \quad , \quad C_{(3)4} = 2\left(aR^3\right)^2 \left(\frac{\tau}{2}\right)^4 \left(\frac{46}{15}\frac{\tau}{2} + 2t_{int}\right)\frac{\Lambda_{(e)a}}{R^3} \tag{128}$$

If one has that $1 > \frac{C_3+C_4}{C_1}\frac{1}{R^5}$ in the mass region for $\partial_x B = 10^6$ Tm^{-1} [34], then the decoherence factor would dominantly increase with the exponential of the square of the radius. Vice versa, one would have that the decoherence factor would decrease with the exponential of R^{-3}. It should be noted that this is truly due to the fact that higher masses will have smaller superposition sizes, thus decreasing decoherence for the photon terms, for the same acceleration periods but have, on the other, larger sizes, which increases all constants/scattering rates. If one were to consider the same superposition size for all masses, then one would obtain, as one would expect, that the decoherence will always decrease with a decrease in size of the test mass.

In the original paper (Ref.([1])), a pressure of 10^{-15} Pa was proposed, this corresponds with the ideal gas law, footnote 31, to a number density low to high in the order of 10^7 m^{-3}, depending on the temperature. Therefore, a range of number densities of $10^7 - 10^8$ m^{-3} will be considered. For this number density range and a temperature of 1 K, we have that $\frac{C_3+C_4}{C_1}\frac{1}{R^5}$ ranges in the considered mass region from the order of 10^{-1} to the order of 10^{-5}. Consequently, we have an increase in decoherence by an increase in mass. However, if one would have the largest considered external temperature of 4K, one would go to a scenario like depicted in Fig.(10).

From this figure, one can observe that for masses roughly below $5 \cdot 10^{-15}$ kg ,the decoherence would decrease with an increase of mass, since $1 < \frac{C_3+C_4}{C_1}\frac{1}{R^5}$, and as this is a large amount of the mass range we are considering, $\langle \mathcal{W} \rangle$ of Eq.(96) would increase with an increase of mass. This is undesirable as we want $\langle \mathcal{W} \rangle < 0$ to be able to detect quantum gravity. The calculation of the entanglement witness with taking this into account will be done in the next section. It can be shown that altering the interaction time in the 1-3s regime will not have any noticeable effect on the results of Fig.(10).

For the second case, which applies to the lower magnetic field gradient of 10^4 Tm^{-1} of the modified setup and the masses around a phase of 1 rad for 10^5 Tm^{-1} for this setup, we have that the constant Δx assumption is loose and the change of s_n should be taken into account. The expression for this is derived in App.(B.3.2) and is given by:

$$\exp[-\sum_k \gamma_k \Delta t] = \exp\Bigg[- \Bigg[\Gamma_{\text{air}}(t_{\text{int}} + \tau + \tau_1) + \sum_{i=1}^{3}\Lambda_i \left(\frac{46}{15}a^2\{\left(\frac{\tau}{2}\right)^5 + \left(\frac{\tau_1}{2}\right)^5\} + 4a^2\left(\frac{\tau}{2}\right)^4 t_{int} + \sum_k (4a\left(\frac{\tau}{2}\right)^2 s_k + s_k^2)\Delta t\right)\Bigg]\Bigg] \tag{129}$$

[34] This corresponds to masses in between $3.5 \cdot 10^{-16} - 2 \cdot 10^{-14}$ as can be inferred from Tab.(1).

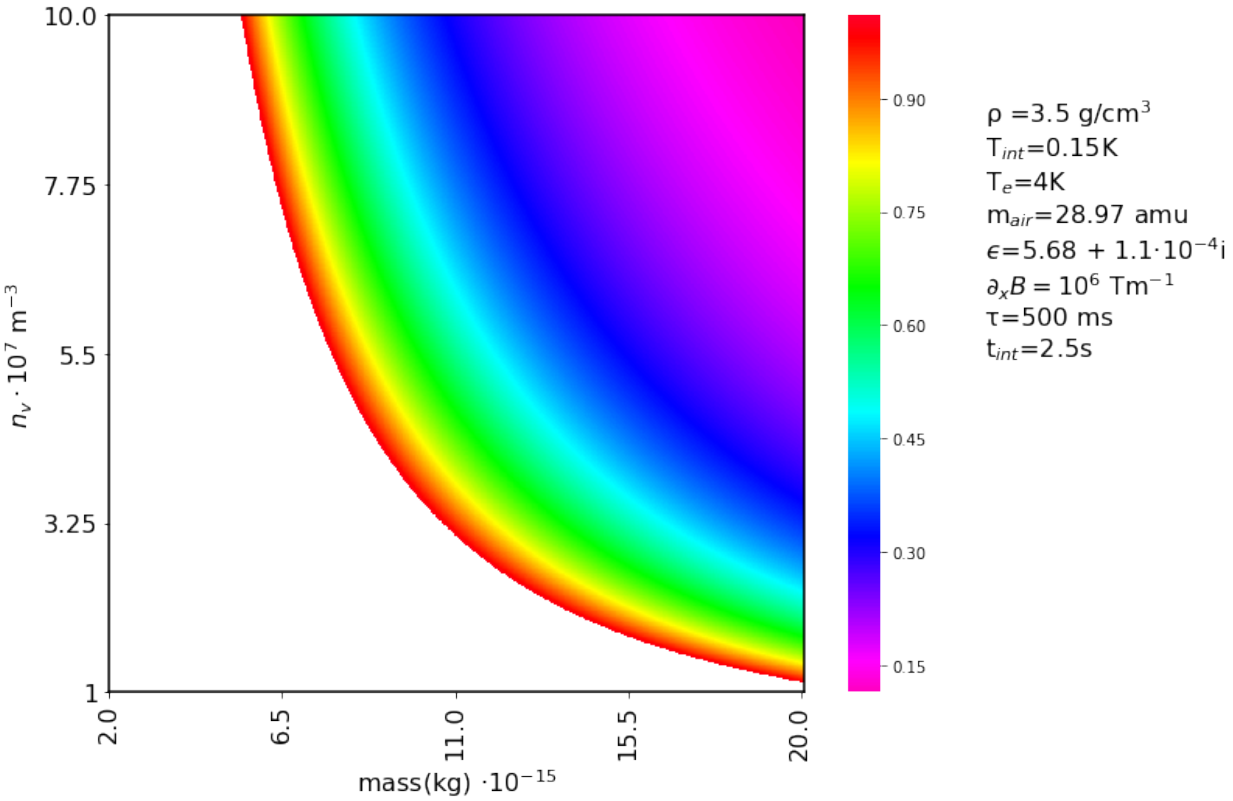

Figure 10: Heatmap of the $\frac{C_3+C_4}{C_1}\frac{1}{R^5}$ ratio for different values of n_V and the mass. The colorcode indicates the value of this ratio for the parameters next to the colorcode. The white region indicates the region in which $\frac{C_3+C_4}{C_1}\frac{1}{R^5} > 1$. It should be stressed that by changing the interaction time in the region 1-3s, the results will not have a noticeable effect on the results of the graph.

Here, $\tau_1 = 2\sqrt{\left(\frac{\tau}{2}\right)^2 + \frac{s_{k_{\max}}}{2a}}$ [35] and we see that with $s_{k_{\max}} << \Delta x$ we retrieve Eq.(126). In this expression it is assumed that the inner states instantaneously turn around after the free fall, so when the magnetic field is turned back on. More on this assumption will be discussed in Sec.(13.3). Important to observe is that s_n evolves differently for all masses (given in Tab.(2) and Tab.(3)) of the modified setup, since all these masses have a different initial distance with the plate, as NR is different. However, one could still do the analysis for if the decoherence would increase by an increase of mass by considering s_n to cause a small perturbation on Eq.(128). As one can show that in these cases s_n is at most one order of magnitude smaller than Δx, hence, one can still compute the $\frac{C_3+C_4}{C_1}\frac{1}{R^5}$ ratio. For a magnetic field gradient of 10^5 Tm^{-1}, one would obtain Fig.(11) for the temperature of 4K for this ratio. It can be shown that altering the interaction time in the 1-3s regime will not have any noticeable effect on the results of Fig.(11).

From Fig.(11), one can observe that for almost the whole mass range we get an increase in decoherence due to an increase in mass. As we also have that the ratio is smaller than 0.01, the inclusion of s_n in the superposition size would not result in the ratio becoming bigger than 1 for these masses, as s_n was a small perturbation. Therefore, we still have an increase in decoherence for an increase in mass.

[35] $s_{k_{\max}}$ is the value of s_n at the end of the free fall period and was denoted by s in Fig.(3). This value is automatically also the largest value of s_n.

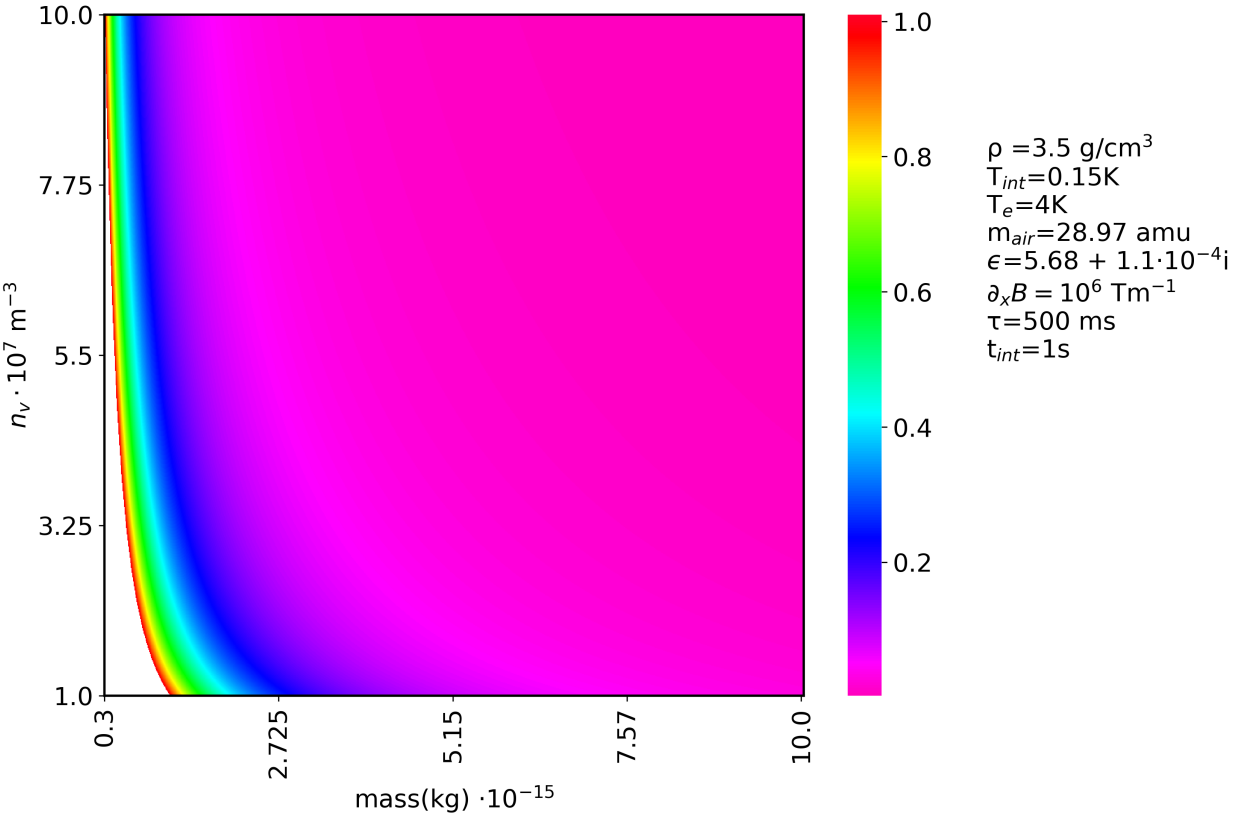

Figure 11: Heatmap of the $\frac{C_3+C_4}{C_1}\frac{1}{R^5}$ ratio for different values of n_V and mass. The colorcode indicates the value of this ratio for the parameters next to the colorcode. The white region indicates the region in which $\frac{C_3+C_4}{C_1}\frac{1}{R^5} > 1$. It should be stressed that by changing the interaction time in the region 1-3s, the results will not have a noticeable effect on the results of the graph.

For a magnetic field gradient of 10^4 Tm^{-1}, for the relevant mass range of Tab.(3), we have that the ratio ranges from 10^{-2} to 10^{-3}, for the largest external temperature of 4K, indicating that here we also have an increase in decoherence for an increase in mass.

10.6 Resulting Entanglement Witness

In this section the results obtained for phase maximization and the decoherence effects of the previous subsections will be used and combined to give the expression for the measurable entanglement witness shown in Sec.(9), to check for which parameters the entanglement can be measured. The environmental parameters will be in the ranges discussed in Sec.(10.5) and the parameters for magnetic field gradients, masses, and interaction times are the ones used in Sec.(10.1) up to Sec.(10.4). First, the analysis will be done for the current setup to see what the possibilities currently are. After that, it will be shown how the modified setup can be used to overcome the limitations of the current setup.

10.6.1 Expectation value witness current setup

From the phase part of Eq.(100), one can split the effective phase up into the two effective phases desired by the expression of $\mathcal{W}$, Eq.(96). Consequently, these two phases read:

$$\Delta\Phi_{\downarrow\uparrow} = \frac{Gm^2}{\hbar} t_{int} \left(\frac{1}{(10A)^{\frac{1}{6}}} - \frac{1}{\frac{g\mu_B \partial_x B}{2m}\tau^2 + (10A)^{\frac{1}{6}}} \right) , \tag{130}$$

and

$$\Delta\Phi_{\uparrow\downarrow} = \frac{Gm^2}{\hbar} t_{int} \left(\frac{1}{2\frac{g\mu_B \partial_x B}{2m}\tau^2 + (10A)^{\frac{1}{6}}} - \frac{1}{\frac{g\mu_B \partial_x B}{2m}\tau^2 + (10A)^{\frac{1}{6}}} \right) \tag{131}$$

For a more realistic picture one should also include the phase generated during step 1 and step 3 of the experiment. These "extra" phases are derived in App.(B.4) and are given by:

$$\Delta\Phi_{\downarrow\uparrow,e} = 2\frac{Gm^2}{\hbar} \left(-\frac{\ln\left(\frac{\left|\frac{a\tau}{2} - \sqrt{ad}\right|}{\frac{a\tau}{2} + \sqrt{ad}}\right)}{2\sqrt{ad}} + \frac{2}{\sqrt{4d_1 a - (a\tau)^2}} \arctan\left(\frac{a\tau}{\sqrt{4d_1 a - (a\tau)^2}}\right) - \frac{\tau}{d} \right) \tag{132}$$

and

$$\Delta\Phi_{\uparrow\downarrow,e} = 2\frac{Gm^2}{\hbar} \left(\frac{\arctan\left(\frac{a\tau}{2\sqrt{ad}}\right)}{\sqrt{ad}} - \frac{1}{\sqrt{(a\tau)^2 + 4ad_2}} \ln\left(\frac{-a\tau + \sqrt{(a\tau)^2 + 4ad_2}}{a\tau + \sqrt{(a\tau)^2 + 4ad_2}}\right) - \frac{\tau}{d} \right) \tag{133}$$

Since we now have the total relevant phase evaluations given by Eq.(130), Eq.(131), Eq.(132), and Eq.(133), one can calculate the expectation value of the entanglement witness for the experiment with Eq.(96). In previous sections we argued that phase maximization would lead to the lowest value, e.g. more negative, of $\langle \mathcal{W} \rangle$. To see this, the value of $\langle \mathcal{W} \rangle$ has been computed for different values of d, which still do not violate the potential requirement of Eq.(73), for the magnetic field gradient of 10^6 Tm^{-1} together with the different interaction times for the relevant mass region and the results are shown in Fig.(12). Note that the decoherence is, for the the moment, neglected ($\gamma = 0$), since we are here purely interested in the response of the entanglement witness to the phases.

From Fig.(12), one can observe that for all the interaction times the most negative values of the witness, for the relevant masses, is indeed achieved for the distance corresponding to the maximization of the phase. Additionally, the minimum is also achieved for the lower masses. This is useful for the low external temperatures as we discussed in Sec.(10.5) that smaller masses give smaller decoherence effects, therefore, this distance is the most suitable separation of the closest states. However, in Sec.(10.5) we also saw that for higher external temperatures, the experiment is more favorable for the higher masses for this high magnetic field gradient. From Fig.(12), one sees that for the absolute highest masses and for the larger interaction times (2 and 3s), higher values of d give better results, therefore, these options will be taken into consideration for the higher external temperatures in the rest of the analysis of this section.

By considering the environmental decoherence of the system, we can use the derived expression of the decoherence factor of Sec.(10.5), which is given by Eq.(126), together with the relevant phase equations (Eq.(130), Eq.(131), Eq.(132), and Eq.(133)), in the expectation value of $\mathcal{W}$, Eq.(96). For the magnetic field gradient of 10^6 Tm^{-1} one would obtain, for the discussed ranges of n_V and m, the results for a temperature of 1K as depicted in Fig.(13). The white area corresponds to parameter combination which leads to a value of $\langle \mathcal{W} \rangle > 0$ and these combinations are therefore not allowed. One should note that this figure displays the results for the interaction time which gives rise to the most negative values of $\langle \mathcal{W} \rangle$ and as discussed, based on the results of Fig.(12), the most suitable distance of d, which is the minimum distance of $d = \Delta x + (10A)^{1/6}$.

We see that with these parameters the entanglement can easily be measured with the best results for a mass of $8.4 \cdot 10^{-15}$ kg, corresponding to $\langle \mathcal{W} \rangle \sim -0.26$ as a lower value of the witness corresponds to fewer measurements needed to confirm the results [26]. One would for temperatures of 2 and 3K still find allowed values for $\langle \mathcal{W} \rangle$. One can also show that for the lowest number density of 10^7 m^3 the lowest mass that will give $\langle \mathcal{W} \rangle < 0$ is for a mass of around 10^{-15} kg, but this corresponds to a superposition size in the order of millimeters.

For the temperature of 4K one will find that there are no parameter combinations that will give $\langle \mathcal{W} \rangle < 0$ for interaction times of 2-3s. One can see this by noting from Fig.(10) that, first of all, the decoherence of

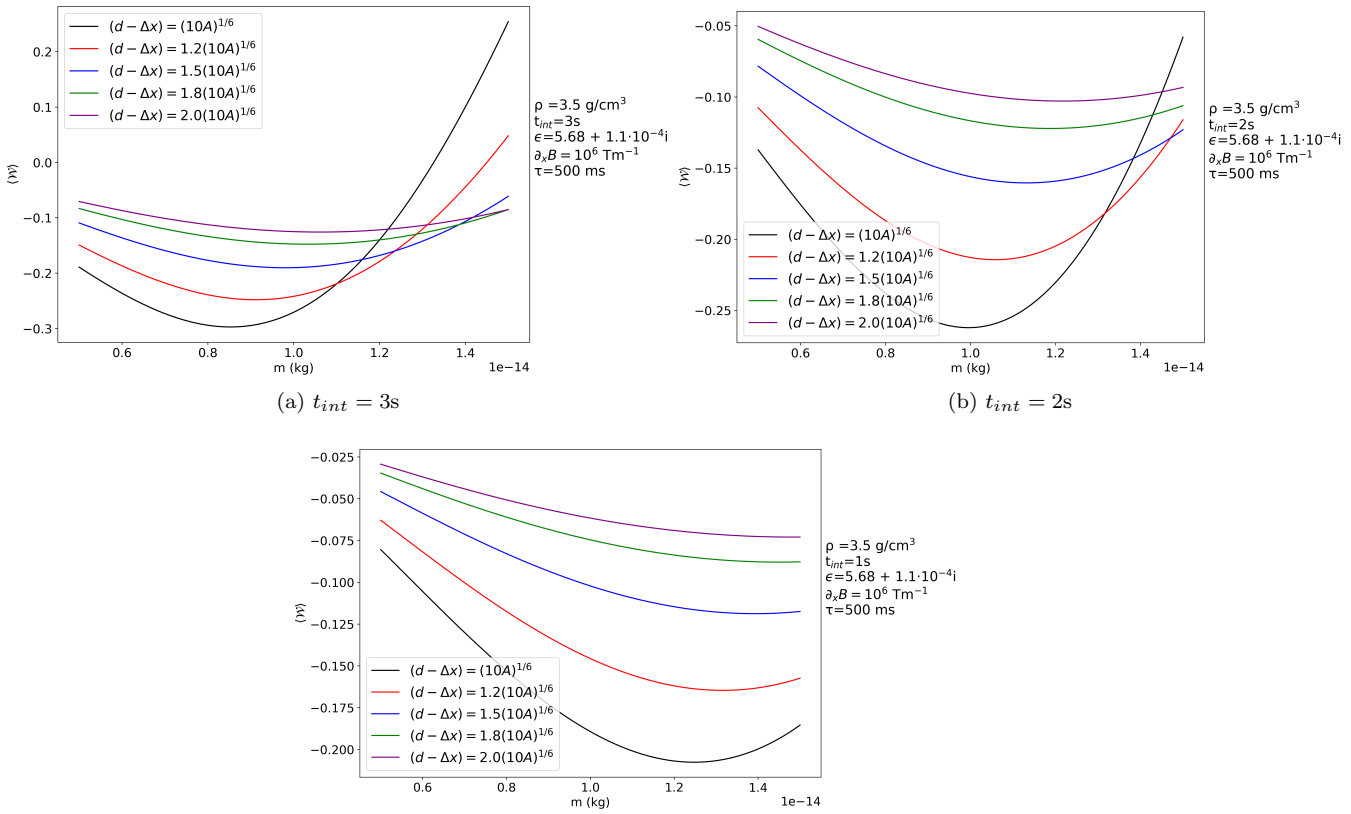

(a) $t_{int} = 3$s

(b) $t_{int} = 2$s

(c) $t_{int} = 1$s

Figure 12: These figures display $\langle \mathcal{W} \rangle$ for the relevant mass region of the current setup of the QGEM-protocol for different separations indicated by the label, for the parameters indicated next to the graph. We indeed observe that $d - \Delta x = (10A)^{1/6}$ will give the best results. However, as we can see, this is not the most viable option for all masses, which can be of importance if one takes into the account the results of the previous sub-section.

thermal photons for the masses considered becomes around the same order as decoherence induced by the scattering of air molecules. Therefore, to have measurable results, one has to have lower number densities[36] to combat the increased decoherence. Consequently, from Fig.(10), one can observe that this implies that one has to go for higher masses to minimize the decoherence, for example masses above around $1.4{\cdot}10^{-15}$ kg. However, from Fig.(12) one sees that to have optimum results for these masses, one has to go larger values of d, which leads to much smaller values of $\langle \mathcal{W} \rangle$. This effect, together with the previously mentioned increased magnitude of the decoherence, makes $\langle \mathcal{W} \rangle > 0$, having that the entanglement is not measurable. For the interaction time of 1s, on the other hand, we see from Fig.(12) that for these higher masses, one still has reasonable values for the witness, making this option favorable. This point together with the fact that the overall decoherence factor is lower, as this is proportional to $e^{t_{\text{int}}}$, makes that one finds allowed values for the witness for lower interaction times. It was again found that the best values for the witness correspond to a distance of $d = \Delta x + (10A)^{1/6}$ and the result is displayed in Fig.(14). From this figure, one can observe that the options for this temperature are extremely limited in terms of the mass of the test masses and the number density of the environmental gas. The maximum value correspond to a value of $\langle \mathcal{W} \rangle \sim -0.046$ for a mass of $\sim 1.35{\cdot}10^{-14}$ kg. The minimum mass that allows for $\langle \mathcal{W} \rangle < 0$ occurs for a mass around 10^{-14} kg.

Problems also start to occur when the magnetic field gradient is lowered, as we saw that the gradient of

[36] With lower number densities, densities below $2{\cdot}10^7$ m^{-3} are meant, as we will see that below this number density measurable values are found for the lower interaction time 0f 1s, see Fig.(14).

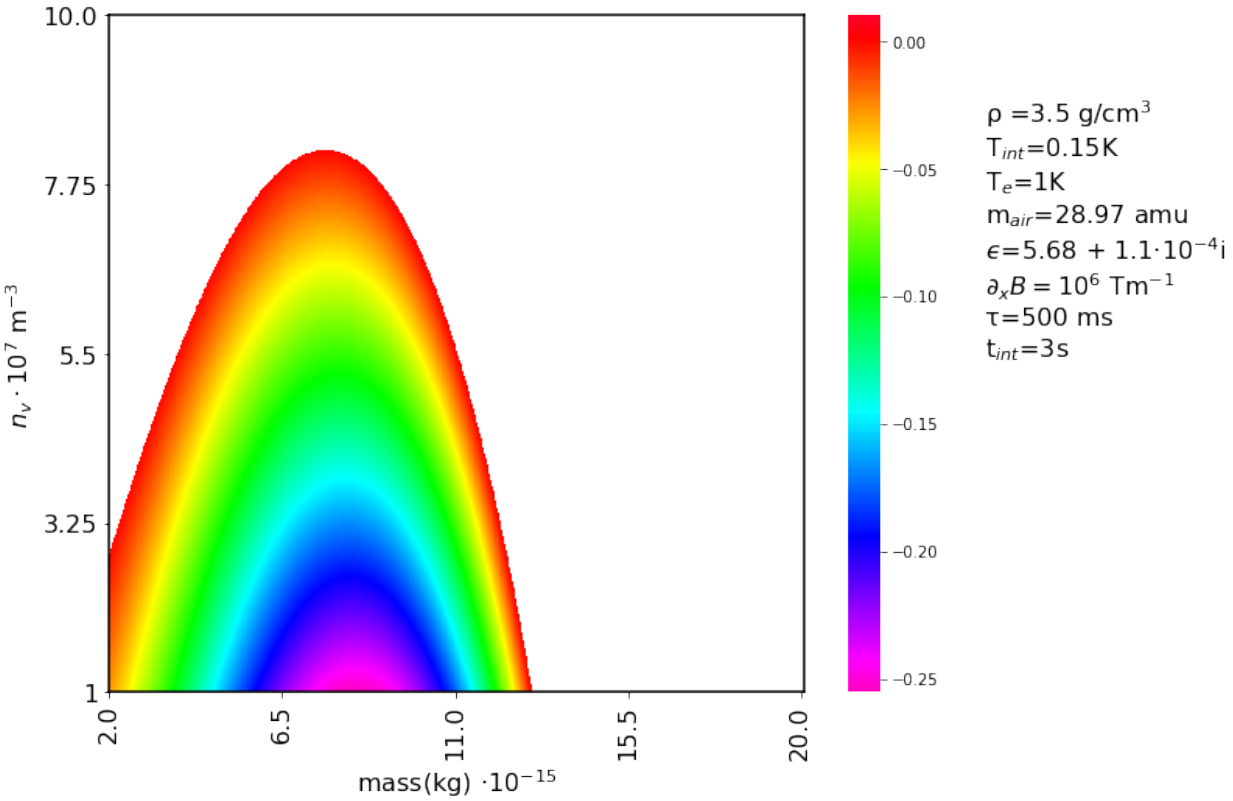

Figure 13: Heatmap of $\langle \mathcal{W} \rangle$ for a range of values of n_V and mass. The colorcode indicates the value of $\langle \mathcal{W} \rangle$ and the parameters used are given next to the colorcode. The white region indicates the region in which the expectation value is larger than zero. The most optimal witness value are in the pink region, with the most optimal value of $\langle W \rangle \sim -0.26$ for mass of $8.4 \cdot 10^{-15}$ kg.

10^5 Tm^{-1} does not generate sufficient entanglement phases for the relevant masses, see Fig.(6). If one would try to find $\langle \mathcal{W} \rangle < 0$ for the parameters we discussed, one would not find any allowed parameter combination that would satisfy this[37]. This implies that detection of the entanglement is not achievable with the current setup by lowering the magnetic field gradient by one order of magnitude with respect to the original proposal. One can see this as the effect that the decoherence is much stronger than the phase accumulation of the entanglement. This is mathematically visible by noting that for masses up to around 10^{-14} kg we have $\Delta\Phi_{\downarrow\uparrow}$ & $\Delta\Phi_{\uparrow\downarrow}$ around 0.1 rad. Consequently, we can safely expend the expression of the entanglement witness, Eq.(96), up to first order to get the result of Eq.(97). By changing the notation of γt to our expression for the dynamic decoherence constant, one has:

$$\langle \mathcal{W} \rangle = 2\gamma t - (\Delta\Phi_{\downarrow\uparrow} + \Delta\Phi_{\uparrow\downarrow}) + \mathcal{O}(n) = 2\int \gamma_k \mathrm{d}t - \Phi_{\mathrm{eff}} + \mathcal{O}(n) \tag{134}$$

This implies that for $\langle \mathcal{W} \rangle < 0$ one has satisfy the following condition:

$$\frac{\Phi_{\mathrm{eff}}}{2\int \gamma_k \mathrm{d}t} > 1 \tag{135}$$

This ratio has been evaluated using Eq.(126) for the decoherence factor and the sum of Eq.(130), Eq.(131), Eq.(132), and Eq.(133) for the effective phase. The ratio has been computed for the environmental parameters in which decoherence would attain the minimum value ($n_V \sim 10^7 \mathrm{m}^{-3}$ and T_e=1K), to get the largest

[37] One can again show that without decoherence the best witness value is again obtained for $d = \Delta x + (10A)^{1/6}$.

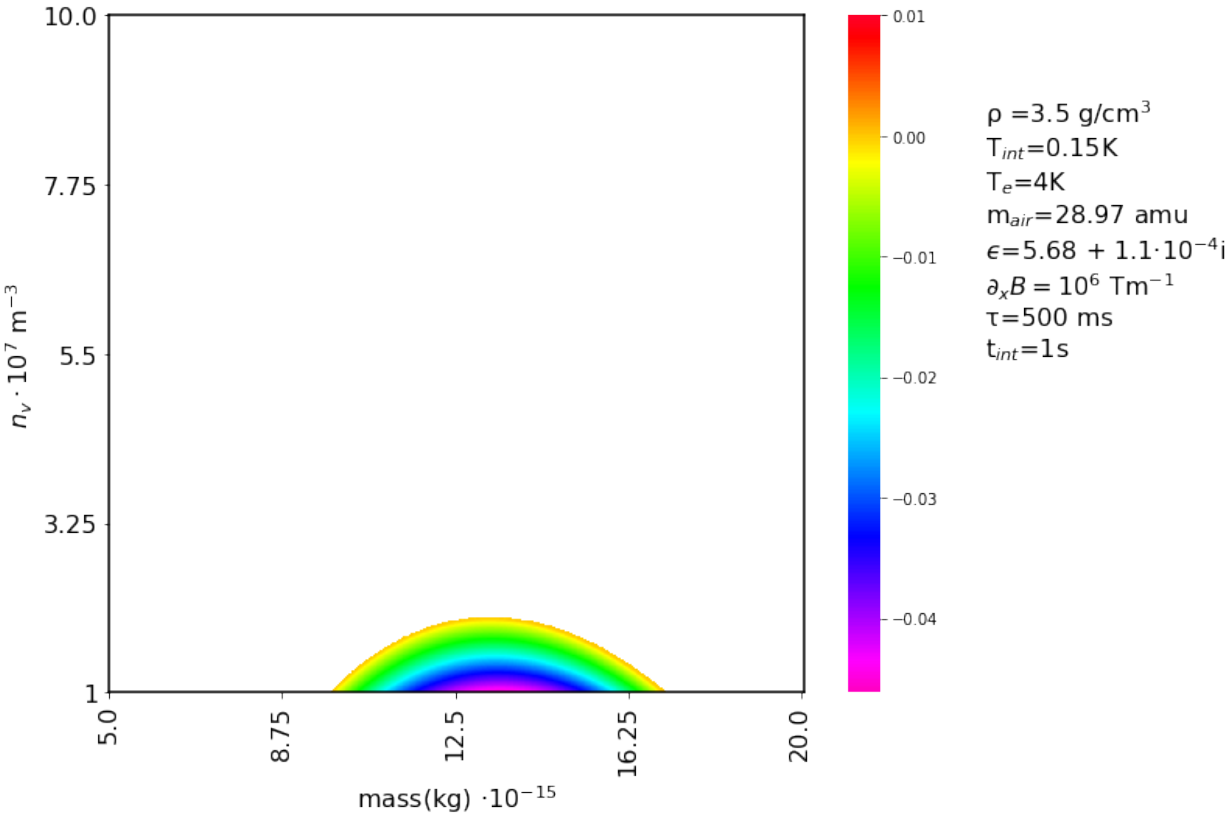

Figure 14: Heatmap of $\langle \mathcal{W} \rangle$ for a range of values of n_V and mass. The colorcode indicates the value of $\langle \mathcal{W} \rangle$ and the parameters used are given next to the colorcode. The white region indicates the region in which the expectation value is larger than zero. The most optimal witness value are in the pink region, with the most optimal value of $\langle \mathcal{W} \rangle \sim -0.046$ for mass around 10^{-14} kg.

value of the LHS of Eq.(135) and the result is displayed in Fig.(15) for different interaction times. From this figure, one can observe that this ratio rarely approaches one and, therefore, the entanglement of the test masses cannot be measured. The maximum of the graph however, corresponds to a value of 1.05 for a mass of $4.3 \cdot 10^{-15}$ kg, which might suggest that we have $\langle \mathcal{W} \rangle < 0$. However, one should keep in mind that we just used an approximation of the witness value, if one would compute the actual value of the witness, for these parameters, without approximation, one would find $\langle \mathcal{W} \rangle \sim 0.002 > 0$. This means that detection of the entanglement is still impossible. Consequently, one cannot go to the low magnetic field gradient of 10^5 Tm^{-1} for the current setup of the **QGEM**-protocol.

For a magnetic field gradient of 10^4 Tm^{-1} the results are even worse. This can be seen by following the same procedure and by observing that the phase accumulation is in the order of 10^{-4} rad (much lower than the 10^{-1} rad of 10^5 Tm^{-1}) and that the decoherence is the same as for 10^5 Tm^{-1}, since the decoherence of air molecules is the dominant term, see Sec.(10.5). Thus, one cannot go to lower magnetic field gradients, which are achievable in laboratories, with the current setup. Consequently, one is limited in using the magnetic field gradient of 10^6 Tm^{-1} in order to detect quantum gravity with the current setup of **QGEM**.

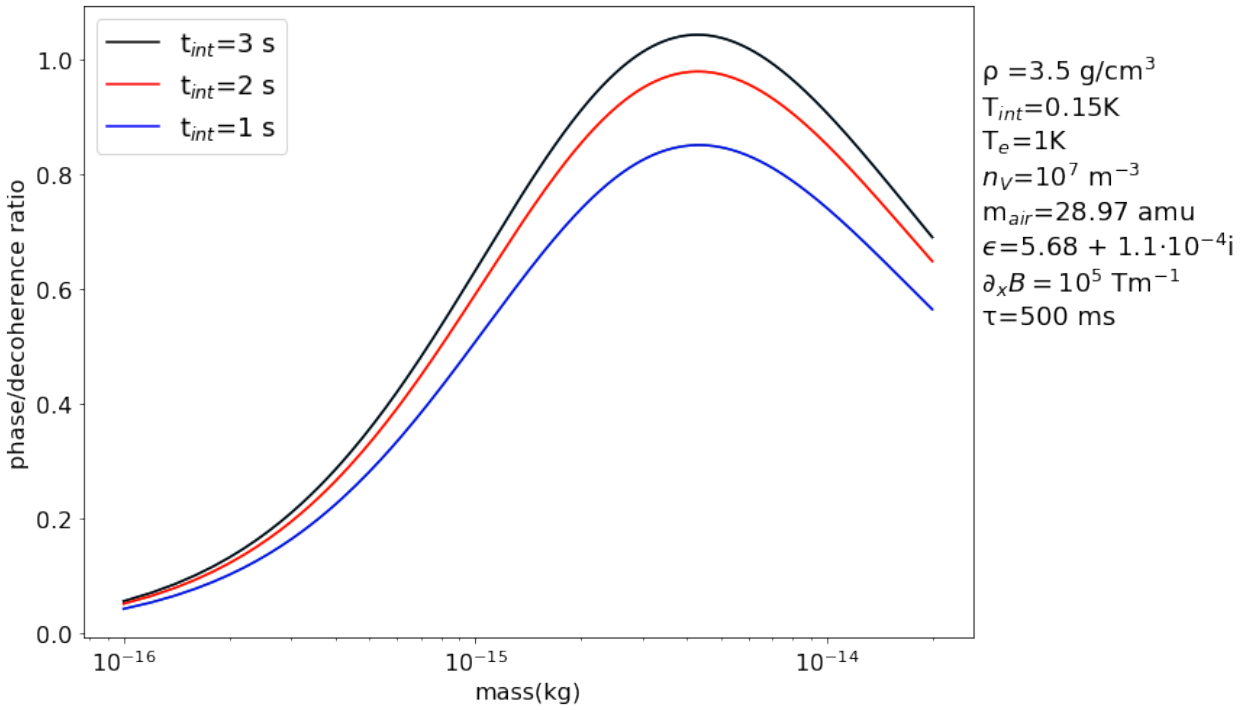

Figure 15: Graph of the ratio of Eq.(135) as a function of mass for the current setup for the parameters indicated next to the figure. That the phase/decoherence ratio is smaller than 1 means that the entanglement and thus quantum gravity can not be measured. The result that the peak for $t_{\rm int}$ is above 1.0 is slightly misleading as here entanglement is also not measurable, since this graph results from an approximation.

10.6.2 Solution of the modified setup

As we saw, the current setup is limited by high magnetic field gradients and partially limited by low temperatures. However, as we saw in Sec.(10.2) up to Sec.(10.4) the proposed modified setup generates significant phases for lower masses then the current setup and can even generate phases in the order of 0.01 rad for masses in the order of 10^{-16} and 10^{-15} kg. This will, as will be shown in this section, be sufficient to generate $\langle \mathcal{W} \rangle < 0$ for measuring the entanglement of both systems. For the higher temperature solution we focus on the mass of $6 \cdot 10^{-15}$ kg with $N = 29$ & $t_{\rm int} = 1$s as depicted in Fig.(5). For the lower magnetic field gradient we stick to a mass of 10^{-15} kg with $N = 57$ & $t_{\rm int} = 1$s, since this parameter combination is capable of generating a phase of order 0.01 rad as can be seen from Fig.(8).

As explained in App.(B.4), we can express the effective entanglement phase generated in step 1 of the experiment, similar to the current setup, by the sum of Eq.(132) and Eq.(133)[38]. For step 3 of the experiment we have the extra entanglement phase displayed by the same expressions, but now with $\tau \rightarrow \tau_1$ and $d \rightarrow d - s_{\rm max}$, see footnote 38. For the free fall period, the effective phase is displayed by Eq.(109) in Sec.(8) from which we can see that:

$$\Delta\Phi_{\downarrow\uparrow} = \frac{Gm^2}{\hbar}\Delta t \sum_{n=0}^{N} \left(\frac{1}{d - \Delta x - 2s_n} - \frac{1}{d - s_n} \right) \tag{136}$$

and

$$\Delta\Phi_{\uparrow\downarrow} = \frac{Gm^2}{\hbar}\Delta t \sum_{n=0}^{N} \left(\frac{1}{d + \Delta x} - \frac{1}{d - s_n} \right) \tag{137}$$

[38] These equations should be divided by two, to account for the fact that step 1 and step 3 are now considered separately. For the expression of step 3 it is assumed, just as in Sec.(10.5), that the inner states instantaneously turn around after the free fall, so when the magnetic field is turned back on. More on this assumption will be discussed in Sec.(13.3).

The mass of $6 \cdot 10^{-15}$ kg has been chosen as this is around the point in which increasing the mass will have negative effects on the decoherence ratio for high values n_V, as shown in Fig.(10), because such high densities are easier to achieve as they correspond to lower pressures. $N = 29$ & $t_{\text{int}} = 1s$ were chosen as these are allowed combination, as we saw in Fig.(5) of Sec.(8), and this would give better results then the higher interaction times with the higher N. With these parameters one can compute, just as is done in the previously section, the value of $\langle W \rangle$ with Eq.(129) for the decoherence term and the equations Eq.(132), Eq.(133), Eq.(136) and Eq.(137) for the relevant phases, with the altercations explained above Eq.(136). This will for the discussed ranges of n_V and T_e result in Fig.(16). From this figure, one can observe that for all values in the discussed ranges we have allowed values of $\langle \mathcal{W} \rangle$. Consequently, the entanglement is measurable for the higher temperatures combined with the higher number densities, whereas for the current setup we are limited by probing lower densities for these temperatures. Additionally, we can observe from Fig.(16) that the values of $\langle \mathcal{W} \rangle$ are significantly lower than for the current setup, implying that fewer measurements are needed to determine the quantumness of gravity [26]. The lowest value of the witness for these parameters corresponds to $\langle W \rangle \sim -0.5$. One can also show that for the lowest temperature of 1K one can go up to a number density of $\sim 3.7 \cdot 10^8$ m^{-3}.

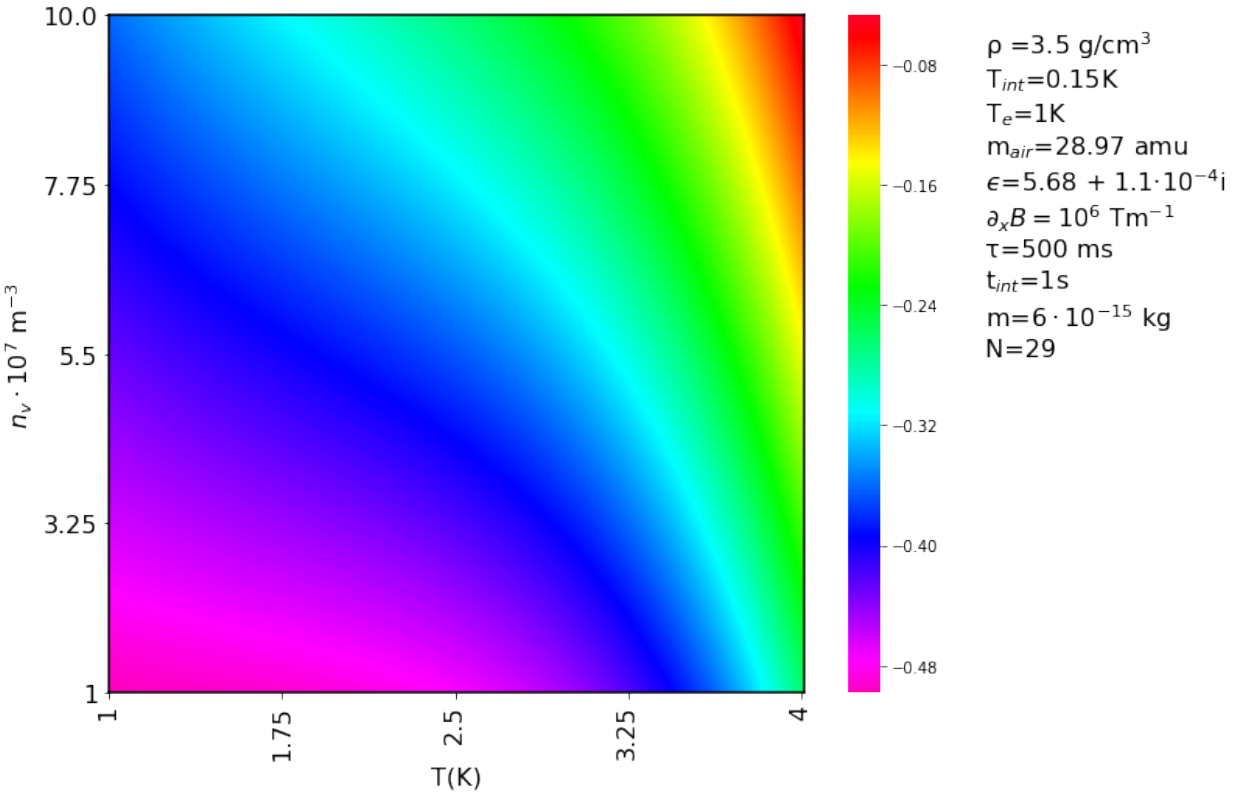

Figure 16: Heatmap of $\langle \mathcal{W} \rangle$ of a range of n_V and temperature for the modified setup. The color-code indicates the value of this expectation for the parameters next to the color-code. The indication that there is not a white region indicates that $\langle \mathcal{W} \rangle < 0$ at all times for these parameters. The best results are, ofcourse, obtained for the lowest number density and temperature considered, giving a witness value of $\langle W \rangle \sim -0.5$.

For the lower magnetic field gradient with the mass of 10^{-15} kg, $N = 57$ & $t_{\text{int}} = 1s$, we have that $\Delta\Phi_{\downarrow\uparrow}$ & $\Delta\Phi_{\uparrow\downarrow}$ are both in the order of 0.01 rad, after all steps of the experiment are completed, so one can still expand Eq.(94) to obtain the requirement of Eq.(135). However, now that we fixed the parameters of the test

masses and the separation between the states, we have that Φ_{eff} is fixed, giving us that with the equations mentioned briefly before we have[39]:

$$\sum_k \gamma_k \Delta t < \frac{\Phi_{\text{eff}}}{2} \sim 0.076 \tag{138}$$

With this limitation on the decoherence rate, one can, using the derived expression of Eq.(129), compute for what parameters of n_V and T_e the requirement of Eq.(138) is violated. This is graphically shown in Fig.(17), where all values of n_V below the black dotted line are allowed values. From this figure, one can observe that for all temperatures of our discussed range we have values of n_V in the discussed range which give suitable solutions for measuring the entanglement. This means that we have a huge advantage by using this modified setup as we are now able to measure the entanglement of the test masses by gravity for laboratory allowed magnetic field gradients.

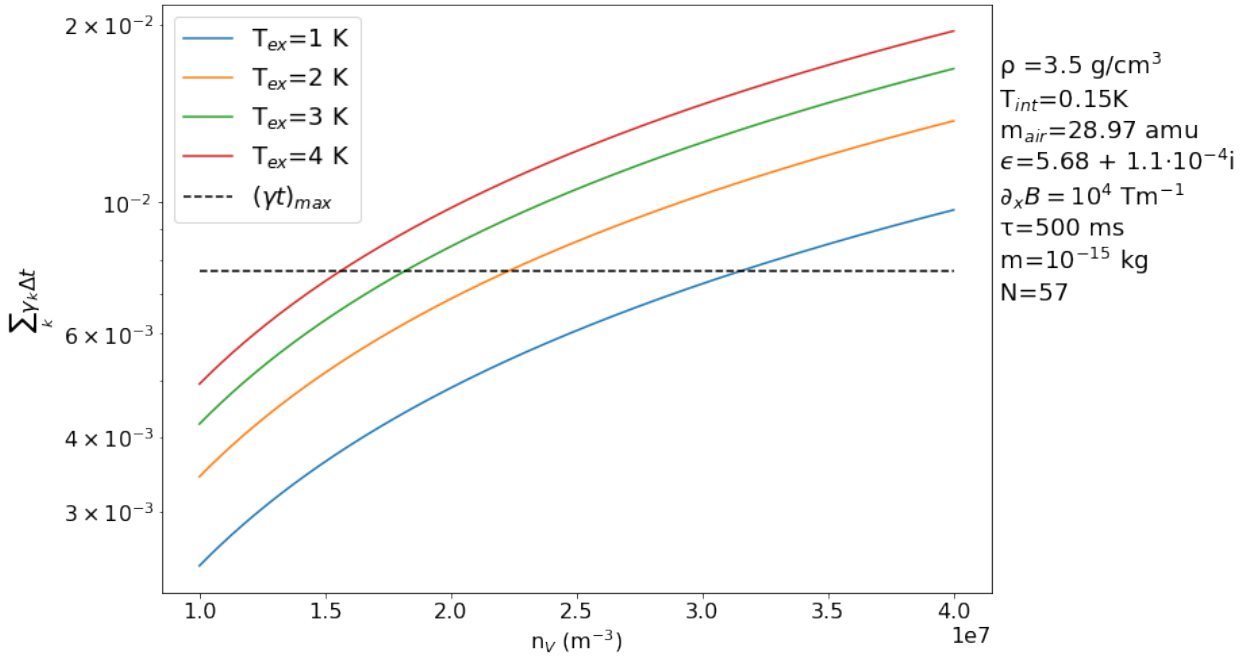

Figure 17: Graph of the decoherence factor for different temperatures as a function of the the number density of the gas together with the maximum allowed decoherence factor (black dotted line). The number density region displayed, is the lower portion of the considered range and the different curves indicate the different external temperatures in the considered range. All parameter combinations below the maximum allowed decoherence factor can be used for the detection of quantum gravity with the modified setup.

One can compute the values of $\langle \mathcal{W} \rangle$ for the allowed parameter combinations and one would logically find the most negative value for the parameters of $n_V = 10^7$ m^{-3} and T_e=1K. This most optimal value corresponds to $\langle \mathcal{W} \rangle \sim -0.01$, which is one order of magnitude smaller than for the gradient of 10^6 Tm^{-1}. Consequently, one needs to perform more measurements to determine or exclude the quantum nature of gravity.

From the analysis done in this section it is good to take away that for the current setup one could only achieve measurable entanglements with a large superposition size, ~ 230 μm, together with a relatively larger mass of $m \sim 10^{-14}$ kg. To achieve this, one needs a relatively high magnetic field gradient of 10^6 Tm^{-1}, which requires and advanced setup with co-moving magnets relatively close to the test masses. The most optimal

[39]Note that we have $\Phi \sim 0.152$, which is greater than the $\Phi_{\text{eff}} \sim 0.1$ obtained in Sec.(10.3). This is because the phase evolution in step 1 and 3 of the experiment has not been accounted for in Sec.(10.3).

results are obtained for the most negative value of the entanglement witness, which corresponds to an optimal mass of $\sim 8 \cdot 10^{-15}$ kg for an external temperature of 1K and $m \sim 1.4 \cdot 10^{-14}$ kg for an external temperature of 4K. Additionally, we saw that we are limited by a number density of $n_V \sim 8 \cdot 10^7$ m^{-3} for the temperature of 1K and already by $n_V \sim 2 \cdot 10^7$ for the temperature of 4K. If one would hypothetically implement the proposed modified setup for this enthusiastic gradient of 10^6 Tm^{-1}, one can implement higher and thus easier achievable gas densities of 10^8 m^{-3} for all temperatures of 1K-4K. Furthermore, one can double the expectation value of the witness and thus measure the entanglement with fewer measurements. However, the most striking result of the modified setup is that one can create a measurable entanglement with only a superposition size of $\sim 20\mu$m which can be created with a magnetic field gradient which is laboratory allowed and is two orders of magnitude smaller than for the current setup. This result corresponds to a mass of 10^{-15} kg and is achievable as long as the number density of the gas is relatively low, $n_V < 1.5 \cdot 10^7$ m^{-3} for T$_e$=4K and $n_V < 3 \cdot 10^7$ m^{-3} for T$_e$=1K. From Fig.(17), one can observe that other decoherence sources are not causing any problems as long as the decoherence rates for these sources are in the order of $\gamma \sim 10^{-3}$ s^{-1} or lower.

11 Deviation from Newtonian gravity

As mentioned in Sec.(6.4), the quantum gravitational potential used in this thesis does not provide a solution for the $1/r$ singularity of the gravitational potential. Currently, we only have upper-bounds on the distances in which the $1/r$ potential is valid [15], and we have no confirmation of a deviation from that potential. In Ref.[15] the upper-bound for the Yukawa gravitational potential of

$$V_G = \frac{Gm^2}{r}\left(1 + \alpha \cdot \exp\{-r/\lambda\}\right) , \tag{139}$$

was shown for different values of α and λ. For α=1 the upper-bound corresponds to $\lambda = 56\mu$m [15], which is in the order of the distances used in the modified setup of the **QGEM**-protocol, such that it is possible that deviations from the $1/r$ potential are of importance. In this section, it will be analyzed how the actual deviation of the gravitational potential can potentially be probed better with the newly proposed modified setup and how this would affect the experiment itself. For this, the potential will be treated as a result of a solution for the Ultra-Violet (UV)-dispersion, which arises from a quantum field theory approach [5]. However, the arguments for the Yukawa potential follow the same line of arguments.

For the modelling of the gravity in the UV region, the results of the infinite derivative ghost free theory of gravity (IDG) of Ref.[5] will be used. According to the results of this paper, one has that the Feynman propagator of the Graviton is given by:

$$\Pi_{\mu\nu\rho\sigma}(k) = \exp\left\{-\frac{k^2}{M_s^2}\right\}\left(\frac{\mathcal{P}^2_{\mu\nu\rho\sigma}}{k^2} - \frac{\mathcal{P}^0_{s,\mu\nu\rho\sigma}}{2k^2}\right) \tag{140}$$

Here, M_s is the fundamental scale of non-locality. By following the same method as in Sec.(6.4) the gravitational potential between the two test masses will as shown in Ref.[5] reduce to:

$$V_{\text{IDG}} = \frac{Gm^2}{x}\text{erf}\left(\frac{M_s x}{2}\right) \quad ; \quad \text{erf}(y) = \int_0^y e^{-t^2}\,\text{d}t \tag{141}$$

Here erf indicates the error function. From this expression we see that M_s indicates the distance at which V_{IDG} starts to deviate from the the Newtonian potential energy. This is, because the error function is equal to one for distance roughly above $y = 1$ and approaches $\frac{2y}{\sqrt{\pi}}$ for values of $y < 1$. Consequently, in these limits, Eq.(141) reduces to:

$$x > \frac{2}{M_s}\,;\, V_{IDG} = V_G \quad x < \frac{2}{M_s}\,;\, V_{IDG} = \frac{Gm^2 M_s}{\sqrt{\pi}} \tag{142}$$

Here, V_G is the Newtonian potential used throughout the thesis. From this we see that depending on the value M_s, we can get a deviation from the Newtonian gravity potential, where this deviated potential is a constant one. This deviation implies that the entanglement phases of Eq.(100) and Eq.(109) will differ from there usual expression. Assuming, for the moment, that only the closest states experience a real change in this altercation of the newtonian potential, one has for the current setup:

$$\Phi_{\text{eff}} = \frac{Gm^2}{\hbar} t_{\text{int}} \left(\frac{1}{d-\Delta x} \text{erf}\left(\frac{M_s(d-\Delta x)}{2} \right) + \frac{1}{d+\Delta x} - 2\frac{1}{d} \right) \tag{143}$$

and for the modified setup:

$$\Phi_{\text{eff}} = \frac{Gm^2}{\hbar} \Delta t \sum_n \left(\frac{1}{d-\Delta x-2s_n} \text{erf}\left(\frac{M_s(d-\Delta x-2s_n)}{2} \right) + \frac{1}{d+\Delta x} - 2\frac{1}{d-s_n} \right) \tag{144}$$

These equations will differ from Eq.(100) and Eq.(109) depending on the strength of the value of M_s in the error function. If the value of M_s is such that we have $(d-\Delta x) < \frac{2}{M_s}$, or $(d-\Delta x-2s_n) < \frac{2}{M_s}$ for the modified setup, then the error function will give a significant contribution to the entanglement phase and will. Therefore, this will alter the measurements of the entanglement witness and the entropy, and will, consequently, be different from the Newtonian case. Currently, the value of M_s ,for this theory, is not known [14]. However, by translating this value to the $\lambda = 56\mu$m and $\alpha = 1$ case for the Yukawa potential, M_s can be derived to have a minimum value of M_s=0.004 eV [14]. This corresponds then to a value of $2/M_s \sim 10^{-4}$ m$\sim 100\mu$m in the error function, meaning that if the $d-\Delta x$ seperation is below this value, one could expect significant changes in the measured entanglement witness and the entropy. For the current setup one is limited by a separation of the closest states of $d-\Delta x \sim 157\mu$m, see Eq.(73). This will give us that the error function becomes $\text{erf}\left(\frac{M_s(d-\Delta x)}{2}\right) \sim 0.994$. This is a small effect, however, as denoted in Ref.[5], this will change both the entropy and the expectation value of the entanglement witness of the current setup by only 0.001 [5]. Measuring such differences in the theoretical and experimental values of the witness/entropy could give an indication of truth of UV-dispersion theories of gravity and is therefore an additional aspect which can be probed with the protocol. However, one should note that in order to accomplish this, all decoherence sources should be completely understood as they also alter the witness value. One should keep in mind that this deviation of 0.001 is only true when the M_s is given by the lower-bound value of M_s. If the theory is true, M_s can also be larger than 0.004 eV, implying that the separation at which the error function kicks in is even lower, making the current setup ineffective to probe this theory. However, luckily for us, we can with the modified setup probe smaller separations and thus larger values of M_s. For the parameters surrounding the mass of $6 \cdot 10^{-15}$ kg of Sec.(10), where the relevant parameters are displayed in Fig.(16), one has a separation of the closest states of around 10μm. For the parameters surrounding 10^{-15} kg, as denoted next to Fig.(17), one will have the closest separation of around 19μm. These are both one order of magnitude smaller than the limiting separation of 157μm of the current setup. Therefore, one can probe values of M_s of one magnitude higher with the newly proposed modified setup. For the separation of 10μm, the distance at which the witness value starts to differ is for a value $M_s \sim 2/x \sim 0.04$ eV, therefore, one can probe values of M_s roughly up to this value. It is also good to observe that as the modified setup can always be set for distances in between 157μm and 10μm without violating any requirement, one can always probe this whole distance range in finding where M_s can optimally be found[40].

For the parameters surrounding the mass of the test mass of 10^{-15} kg and the gradient of 10^4 Tm^{-1}, this gravity model could, in principle, make measurements of the entanglement impossible, since we are limited to probe the entanglement for a separation of the closest states of 19μm. Implying that for low values of M_s, corresponding to a length of 56μm, the gravitational interaction of the closest states becomes significantly suppressed by the error function and approaches the constant of Eq.(142). As this closest separation is without the error function contribution the most dominant term of Eq.(145), one will have a significant

[40]It should be noted that this is only the case for the parameters surrounding the magnetic field gradient of 10^6 Tm^{-1}, as we saw that for the current setup this generates sufficient entanglement for the distance of 157μm (upper bound) and with the modified setup the distance can be brought down to 10μm (lower bound). Therefore, the whole range 157μm-10μm, generates sufficient entanglement and can be explored with the modified setup. The gradient of 10^4 Tm^{-1} is not suitable for this as we saw that we need the small separation of 19μm to generate a sufficient entanglement phase.

reduction of the entanglement phase when the error function is significant for the low values of M_s. This could have serious consequences on the expectation value of the entanglement witness as this could make the expectation value positive and, thus, makes it impossible to determine if entanglement occurred. To see when for which value of M_s measuring the entanglement becomes impossible, Eq.(145) is treated more generally to include the error function also for the second and third term, to read:

$$\Phi_{\text{eff,erf}} = \frac{Gm^2}{\hbar}\Delta t \sum_n \left(\frac{1}{d-\Delta x-2s_n}\text{erf}\left(\frac{M_s(d-\Delta x-2s_n)}{2}\right) + \frac{1}{d+\Delta x}\text{erf}\left(\frac{M_s(d+\Delta x)}{2}\right) - 2\frac{1}{d-s_n}\text{erf}\left(\frac{M_s(d-s_n)}{2}\right)\right) \tag{145}$$

One must also include the error function into the phase evolution during step 1 and step 3 of the experiment to give the accumulate discretized entanglement phase during the whole protocol. By using Eq.(193) and Eq.(195) of App.(B.4) we get with the inclusion of the the IDG potential a build up phase in step 1 of:

$$\Phi_{\text{eff},1} = \frac{Gm^2}{\hbar}\Delta t\left(\sum_{t=0}^{\frac{\tau}{2}}\left(\frac{1}{d-at^2}\text{erf}\left(\frac{M_s(d-at^2)}{2}\right)+\frac{1}{d+at^2}\text{erf}\left(\frac{M_s(d+at^2)}{2}\right)-\frac{2}{d}\text{erf}\left(\frac{M_s(d)}{2}\right)\right)+ \sum_{t=0}^{\frac{\tau}{2}}\left(\frac{1}{d+at^2-a\tau t-a\left(\frac{\tau}{2}\right)^2}\text{erf}\left(\frac{M_s\left(d+at^2-a\tau t-a\left(\frac{\tau}{2}\right)^2\right)}{2}\right)+ \frac{1}{d-at^2+a\tau t+a\left(\frac{\tau}{2}\right)^2}\text{erf}\left(\frac{M_s\left(d-at^2+a\tau t+a\left(\frac{\tau}{2}\right)^2\right)}{2}\right)-\frac{2}{d}\text{erf}\left(\frac{M_s(d)}{2}\right)\right)\right) \tag{146}$$

And for step 3 we have, as argued in Sec.(B.4), the same expression as for step 1 but with $d \to d - s_{max} = d'$ and $\tau \to \tau_1$. Henceforth, we have the build up phase during this step, including the IDG potential, of:

$$\Phi_{\text{eff},3} = \frac{Gm^2}{\hbar}\Delta t\left(\sum_{t=0}^{\frac{\tau_1}{2}}\left(\frac{1}{d'-at^2}\text{erf}\left(\frac{M_s(d'-at^2)}{2}\right)+\frac{1}{d'+at^2}\text{erf}\left(\frac{M_s(d'+at^2)}{2}\right)-\frac{2}{d'}\text{erf}\left(\frac{M_s(d')}{2}\right)\right)+ \sum_{t=0}^{\frac{\tau_1}{2}}\left(\frac{1}{d'+at^2-a\tau_1 t-a\left(\frac{\tau_1}{2}\right)^2}\text{erf}\left(\frac{M_s\left(d'+at^2-a\tau_1 t-a\left(\frac{\tau_1}{2}\right)^2\right)}{2}\right)+ \frac{1}{d'-at^2+a\tau_1 t+a\left(\frac{\tau_1}{2}\right)^2}\text{erf}\left(\frac{M_s\left(d'-at^2+a\tau_1 t+a\left(\frac{\tau_1}{2}\right)^2\right)}{2}\right)-\frac{2}{d'}\text{erf}\left(\frac{M_s(d')}{2}\right)\right)\right) \tag{147}$$

By implementing the sum of these phases in the analysis of the entanglement witness of Sec.(10.6), we have in this low phase limit:

$$\langle \mathcal{W} \rangle = 2\sum_k \gamma_k \Delta t - (\Phi_{\text{eff,erf}} + \Phi_{\text{eff},1} + \Phi_{\text{eff},3}) \tag{148}$$

Then, by doing the analysis for the most optimal environmental parameters of $T_e \sim 1$ K and $n_V \sim 10^7$ m^{-3}, as shown in Sec.(10.6), one will obtain $\langle \mathcal{W} \rangle$ as a function of M_s as displayed in Fig.(18). The red dotted line indicates the resulting value of $\langle \mathcal{W} \rangle$ in the linearized gravity model without the UV contribution as obtained in Sec.(10.6). From this we observe that for $M_s < 0.021$ eV, measuring the entanglement becomes impossible as $\langle \mathcal{W} \rangle > 0$. One can also observe that the expectation value of the witness approaches the obtained witness value of the 1/r potential of the obtained results of Sec.(10.6). One can explain this by noting that for high values of M_s, the non-locality occurs at distances smaller than the separation of the closest states in the

QGEM-protocol. Consequently, the error function approaches unity and the phase evolution, and thus the expectation value of the witness, is the same for both gravity models. The sudden increase around 0.01 eV can be explained by noting that this corresponds to around the region where the third term of $\Phi_{\text{eff,erf}}$ will not be suppressed by the error function. Therefore, only the first term (closest state interaction) is suppressed and the phase will logically be negative. Therefore, as we can see from Eq.(148), the expectation value of the witness will increase. The decrease after the maximum can be explained by noting that this corresponds to a value of M_s where the first term also starts to lose its suppression of the error function. Henceforth, the effective phase starts the become positive again, decreasing the expectation value of the witness.

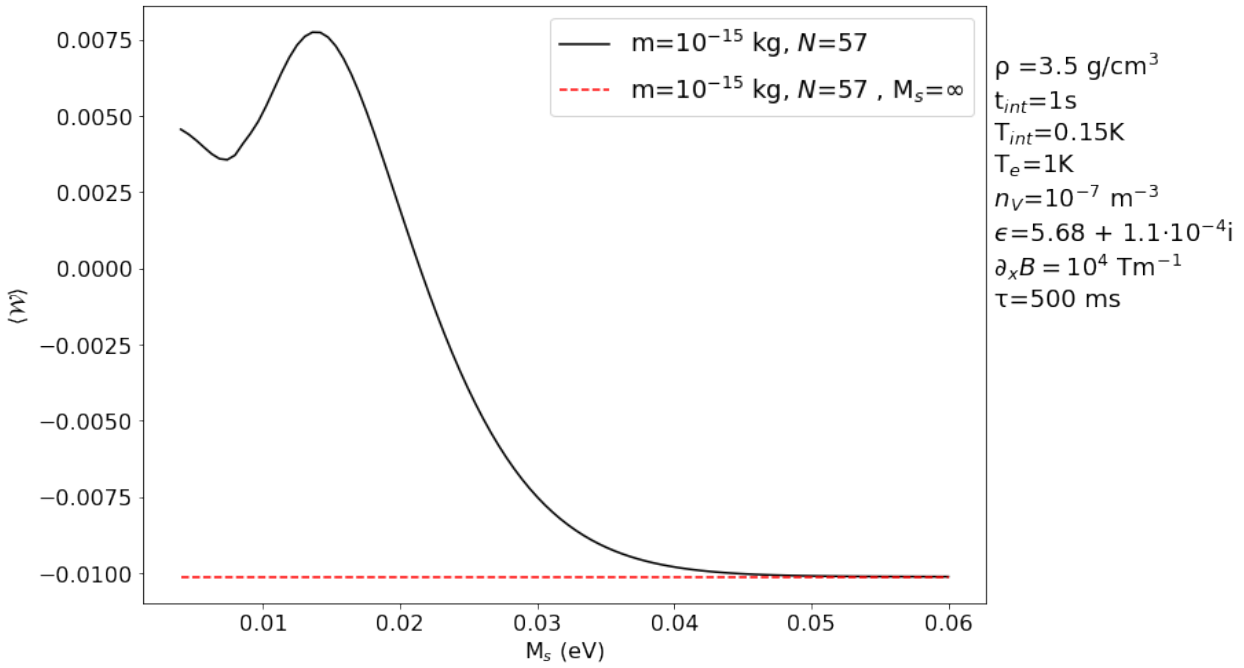

Figure 18: Graph of the expectation value of the entanglement witness as a function of the fundamental scale of non-locality for the parameters indicated next to the figure. The red dotted line represents the case of $M_s = \infty$ used previously, as this is the witness corresponding to the usual 1/r potential of Newtonian gravity. From the graph we observe that for $M_s < 0.021$ eV, quantum gravity can not be measured as $\langle \mathcal{W} \rangle > 0$.

12 Impact collapse models

The decoherence due to the scattering of environmental particles/photons is an experimentally proven concept of decoherence on a spatially separated superposition [7]. However, it is noteworthy to mention that, there could be another type of decoherence coming from the so-called collapse model which, up to now, only exists in theory. From quantum physics we know that if a measurement is performed on a superimposed system, the wavefunction of this system collapses to one of the states such that you only measure one state and not all states of the superposition [17]. This phenomena cannot be explained by the Schrödinger equation [7, 16]. Collapse models give a modification to the Schrödinger equation to explain this collapse phenomenon. Such collapse models form a serious problem for the **QGEM**-protocol, as we are dealing with mesoscopic test masses which, as we will see shortly, collapse to a definite state very quick with the collapse models, losing the superposition and, thus, gives serious restriction on the magnitude of the entanglement with the other test mass.

One such a collapse model is the Continuous Spontaneous Localization (CSL) model [6, 7, 16]. This model

adds a stochastic noise term to the Schrödinger equation [6, 7], while still obeying the laws of quantum physics [16]. This makes that the superposition randomly collapses into one of the superimposed states. This "randomness" gets enhanced the larger the system is, meaning that mesoscopic objects collapse, and thus localize, at a much faster rate [7, 16] than microscopic objects. Two other important parameters of the CSL model are the spatial correlation function of the noise (r_c) and the collapse strength (λ) [16]. The r_c term of the CSL model determines for which superposition size the noise can distinguish between the superimposed states, and, thus, gives an indication for which sizes the collapse becomes significant. This value of r_c is modeled to be 1μm [16], which is small compared to Δx of the **QGEM**-protocol of both setups and, therefore, gives already an indication of a fast decoherence in this model. The λ parameter gives an indication on the rate at which the superposition loses its coherence, which by different studies has been modeled to be either 10^{-16} Hz or 10^{-8} Hz [6, 16]. In Ref.[6], the coherence time of a superposition of macroscopic objects due to the CSL model was theoretically modeled, using the value of $\lambda = 10^{-16}$ Hz, to get a lower bound on the decoherence rates. In Sec.(10.6) we came to the exciting conclusion that, for the **QGEM**-protocol, we can reduce the mass and the superposition size by one order of magnitude together with a reduction of the magnetic field gradient by 2 orders of magnitude. However, a mass of $\sim 10^{-15}$ kg corresponds to a diameter of around 800 nm. From figure 10 of Ref.[6], we already see that for a diameter of 500 nm, the decoherence time is already 0.1 ms for a superposition 0.1 μm, whereas we demand a superposition size of $\Delta x \sim 20\mu$m to measure the entanglement, which would lead to even smaller coherence times for our larger test object with the even larger superposition size. Therefore, as we need coherence in the order of seconds, the current CSL-model makes the **QGEM**-protocol impossible to implement for both proposed setups.

Besides modeling of the CSL model, Ref.[6] also computed the decoherence rates for collapse models build upon wormholes smaller than the Planck scale induced by quantum gravity as well as a models based upon Newtonian gravity and upon the K-model. I will not go into detail of the physical derivation of these models. However, I will implement the results obtained in Ref.[6] for the decoherence of a macroscopic superposition, on to our parameters of the **QGEM**-protocol for both setups obtained in previous sections.

The collapse model based upon quantum gravity is based on the collapse/localization of the macroscopic object with tiny wormholes smaller than the Planck scale [6]. This model shows greater decoherence then the CSL model [6]. Therefore, if this model is true, it also makes the **QGEM**-protocol not achievable.

The collapse model based on Newtonian gravity is the decoherence caused by a potential of the form of the (Newtonian) gravitational interaction of the superimposed states [6]. As we saw that the linearized gravity model of Sec.(6.4) results in the same potential, the model will be the same. In the **QGEM**-protocol we are, for both setups, dealing with superposition sizes much larger than the size of the test mass. Therefore, according to Ref. [6], we get that the decoherence rate is independent of the superposition size, and is given by:

$$\Gamma = \frac{6Gm^2}{5R\hbar} = \frac{6G}{5\hbar}\left(\frac{4\pi\rho}{3}\right)^{1/3} m^{5/3} \tag{149}$$

Here, we already see a strong dependence on the mass of the test mass. For the total interaction time of $t_{int} + \tau + \tau_1$, we get the decoherence factor $\sum_k \gamma_k \Delta t$ of:

$$\sum_k \gamma_k \Delta t = \Gamma(t_{int} + \tau + \tau_1) = \exp\left[\frac{6G}{5\hbar}\left(\frac{4\pi\rho}{3}\right)^{1/3} m^{5/3}(t_{int} + \tau + \tau_1)\right] \tag{150}$$

For the parameters surrounding $m = 10^{-15}$ kg with the gradient of 10^4 Tm^{-1}, as depicted next to Fig.(17), one would obtain that $\sum_k \gamma_k \Delta t \sim 3.8$, which is 3 orders of magnitude larger than what is needed for the requirement of the decoherence of Eq.(138). Consequently, this model would also spoil the experiment, making it impossible to conduct the experiment[41].

[41] As the 10^{-15} kg mass is the lowest mass we could go to with both setups and the decoherence value for this collapse model is also too large for the higher phases, generated by the higher masses, this collapse model will, also, make measurements impossible for all cases of both setups. This can be shown by implementing this decoherence term in Eq.(96), by doing this one would find that for the considered parameters, for both setups, the entanglement witness would never be negative and, thus, measuring the entanglement is impossible.

The K-model is based on the collapse of the superposition due to the incompatibility of quantum physics, general relativity, and the structure of spacetime [6]. From figure 13 of Ref.[6] we can infer that, for the **QGEM**-protocol, with the minimum diameter of 800 nm, as argued before, the coherence time is already smaller than 0.1 s for a superposition size of 2 μm. However, for the **QGEM**-protocol, the superposition size is one order of magnitude larger and as the coherence time scales as $1/(\Delta x)^2$ we have that, if this model is true, the coherence time would again be too small to produce a detectable entanglement.

13 Extra considerations

13.1 Decoherence induced by the plate

In section 10.6 we saw that the modified setup will give better results around the proposed parameters in Ref.[1]. Furthermore, we saw that this modified setup can even generate measurable entanglements for laboratory achievable magnetic field gradients. However, this is all under the condition that the introduced conducting plate will not act as a significant decoherence source on the two superpositions. In Sec.(4) we saw that the decoherence on a system is defined by the leakage of the "which-path" information and, thus, by the overlap of the different states that the environment, which is the plate, can attain upon interaction with the system. Here, the system are the superpositions of the test masses. For the plate these environmental states are the possibility of (vibrational) excitation due to the force experienced by the test masses. In this section, we will see that for all the different state combinations (also valid for collapse to certain states), the deflection of the plate will be smaller than the ground-state spread of the plate. This is also the case if one takes into account a significant uncertainties of the placement of the test masses. Consequently, the plate will not be excited and, thus, no leakage of "which-path information" of the systems into the plate will occur. This implies that the plate will not act as a decoherence source. The analysis will be done for both the masses and their parameters suggested in Sec.(10.6)[42], but can in principle be done for all parameters.

The force of the conducting plate with respect to one of the states is as argued in Sec.(8) given by:

$$F_{\text{Casimir}} = -\frac{3}{2\pi}\left(\frac{\epsilon-1}{\epsilon+2}\right)\frac{R^3}{x^5} = -\frac{3\hbar c}{2\pi}\left(\frac{\epsilon-1}{\epsilon+2}\right)\frac{R^3}{x^5}\,[kg\cdot m/s^2] \tag{151}$$

In a real-life scenario both test masses will not be placed exactly at the same distance from the plate, as what is shown in Fig.(3), and this can cause there to be a net force acting on the conducting plate, resulting in a bending of the plate, which in turn can cause the plate to oscillate, possibly leading to excitation and thus "which-path" information loss. This oscillation of the plate is caused by the force of the inner states acting on the plate because, as we saw in the analysis of Sec.(10), the force on the inner states is dominant with regards to the outer states[43]. Another negative effect of the oscillation of the plate is that the force on the states oscillates with time and can cause serious problems for the experiment as this alters the phase evolution and causes a problem in bringing back the superposition, or collisions of the plate with the states can occur. Therefore, the geometrical parameters of the plate have to be chosen such that the bending will be negligible.

With the uncertainty of placement of the test masses, the argued decoherence can occur for force imbalances on the plate caused by four different kinds of combinations of states. Using the parameters of Fig.(3) we have force imbalances on the plate happening for the combination of states $|\downarrow\rangle_1|\uparrow\rangle_2$,$|\uparrow\rangle_1|\downarrow\rangle_2$ and the two similar contributions of $|\downarrow\rangle_1|\downarrow\rangle_2$ and $|\uparrow\rangle_1|\uparrow\rangle_2$. As the force on the plate for the combination $|\uparrow\rangle_1|\downarrow\rangle_2$ is obviously less significant than $|\downarrow\rangle_1|\uparrow\rangle_2$, we have that if we show that no decoherence will occur for the $|\downarrow\rangle_1|\uparrow\rangle_2$ state, then it will suffice to conclude that also no decoherence will occur for the $|\uparrow\rangle_1|\downarrow\rangle_2$ combination of states. The $|\uparrow\rangle_1|\downarrow\rangle_2$ combination, with the given placement uncertainty, is also the net effect of the bending of the plate, by summing over all the state combinations, since these two individual states are the only significant

[42] This corresponds to the mass of $6\cdot10^{-15}$ kg with $N=29$, $t=1$s and $\partial_x B = 10^6$ Tm^{-1} and to the mass of 10^{-15} kg with $N=57$, $t=1$s and $\partial_x B = 10^4$ Tm^{-1}

[43] To avoid confusions the "inner" states are the ones close to the plate, so $|\downarrow\rangle_1$ and $|\uparrow\rangle_2$ of Fig.(3), and the "outer" states are the ones the furthest from the plate, so $|\uparrow\rangle_1$ and $|\downarrow\rangle_2$ of Fig.(3).

"force-sources". The $|\downarrow\rangle_1 |\downarrow\rangle_2$ and $|\uparrow\rangle_1 |\uparrow\rangle_2$ contributions have the same magnitude of bending of the plate but opposite directions, so one can treat the possible decoherence similarly, hence only the $|\uparrow\rangle_1 |\uparrow\rangle_2$ combination will be taken into account for these two combinations. The force imbalances caused by these states will have the largest magnitude if the center of masses of both test masses are, with the given uncertainty in the placement, displaced both to the right or left of Fig.(3) and this will be used to maximize the bending. It is again important to stress that if the bending of the plate for all state combinations will not lead to excitation of the plate then there will be no way to tell from the plate in which states the superpositions are (as all state combinations will not alter the state of the plate) and, therefore, no extra decoherence term will act on the system. To model this, the wavefunction of the plate will be modeled as a harmonic oscillator [17], as we will see that the induced bending acts like an harmonic oscillator. Therefore, the bending of the plate will be compared to the corresponding ground state spread of the harmonic oscillator [35].

First let us define the directions in Fig.(3). Setting the axis along the length of the plate to be the z-axis, the axis perpendicular to this, on the paper, the x-axis, and the direction into the paper the y-axis. As the superimposed states of the test masses are all on the same line on the x-axis, as indicated in Fig.(3), we can assume the contribution of all forces of the states with respect to the plate to act as a point force on the plate along the x-axis. That this is a point force is also justified by the fact that plate is of an infinite extension in the z-axis compared to the sizes of the states. Therefore, we can approximate the bending of the plate to be caused by a point force along the x-axis. As the plate was assumed to be clamped at the ends of the z-axis, as described in the description of Fig.(3), which is reasonable to keep the plate at its place during the free fall, we get that the displacement/bending for such a point source at the midpoint is as derived in Ref.[36] given by:

$$\delta_d = \frac{FL^3}{192EI} \tag{152}$$

Here, E is the young modulus of elasticity of the plate, and I is the area moment of inertia of the cross-section perpendicular to the axis around which the plate is bend (z-axis), which is the xy plane of Fig.(3). It is also important to note that this is the displacement of the center of the plate, which is the maximum displacement possible. If the force acts on a different point along the length of the plate the resulting maximum displacement would be smaller [36]. However, by assuming the force to always act on the midpoint during the free fall we get an upper-bound on the bending of the plate.

As the force acts along the x-axis, we require the area moment of inertia to be I_y and assuming the plate to have a length of H along the y-axis we get:

$$I_y = \int_{-H/2}^{H/2} \int_{-W/2}^{W/2} x^2 dx dy = \frac{1}{12} W^3 H \quad ; \quad \text{W thickness of the plate along the y-axis} \tag{153}$$

For the **QGEM**-protocol, the thickness W is our fixed value, however, H is completely free as long as the infinite plate assumption holds. I_y is maximum, thus δ_d minimized, when we have a square plate, thus $H = L$. By substituting I_y with $H = L$ in Eq.(152) we get:

$$\delta_d = \frac{FL^2}{16EW^3} \tag{154}$$

For the next part of the analysis we assume that the uncertainty of the placement can range from 0 to $R/2$, with R the radius of the test mass. If we then denote this displacement by uR, with u ranging from $u = 0$ to $u = 0.5$, we get that the initial separation of the inner states of Fig.(3), before the free fall, can be denoted by $(d-\Delta x)/2 - W/2 \pm uR$. For the state combination $|\downarrow\rangle_1 |\uparrow\rangle_2$ the maximum displacement will then logically occur, as mentioned before, when both systems are placed an amount of uR to the right, or left but we will consider right for arguments sake, of Fig.(3), as this maximizes the difference in the Casimir force of the two states with respect to the plate. Consequently, for the maximum bending, we get an initial displacement of $(d-\Delta x)/2 - W/2 - uR$ for the state $|\downarrow\rangle_1$, and $(d-\Delta x)/2 - W/2 + uR$ for the $|\uparrow\rangle_2$ state, with respect to the plate.

The Casimir force of the plate with respect to the $|\downarrow\rangle_1$ state will act as an attractive force on the plate towards the left of Fig.(3), and for the $|\uparrow\rangle_2$ state we have an attractive force on the plate to the right,

causing a net force to act to the left or right on the plate. As the left system is closer to the plate, and thus has a higher attraction, this net force will be to the left. Furthermore, as the Casimir force goes as $1/x^5$ this net force will be the largest at the end of the free fall. Consequently, the point force of Eq.(154) obtains its maximum at the end of the free fall, and thus gives the largest displacement of the plate. Denoting the Casimir force of the plate with respect to $|\downarrow\rangle_1$ as $\mathbf{F}_{|\downarrow\rangle_1}$, and the Casimir force of the plate with respect to the $|\uparrow\rangle_2$ as $\mathbf{F}_{|\uparrow\rangle_2}$ we get a maximum deflection of[44]:

$$\delta_{d,max} = \frac{F_{max}L^2}{16EW^3} = \frac{|\mathbf{F}_{|\downarrow\rangle_1}(x(t_{int})) + \mathbf{F}_{|\uparrow\rangle_2}x(t_{int}))|L^2}{16EW^3} \tag{155}$$

For the combination of $|\uparrow\rangle_1 |\uparrow\rangle_2$, we only have the contributing force, acting on the plate, by the $|\uparrow\rangle_2$ state[45], therefore, with the same argument that the force is maximum at the end of the free fall, we have the bending of the plate given by:

$$\delta_{d,max} = \frac{F_{max}L^2}{16EW^3} = \frac{|\mathbf{F}_{|\uparrow\rangle_2}x(t_{int}))|L^2}{16EW^3} \tag{156}$$

As Eq.(154) is also proportional to L^2, it is also wise to go for less lengthy plates to lower the deflection, which can be achieved if we let the plate free fall with the test masses. In this limit, we can set the length of the plate to be 1 mm^3, as this is still 4 to 5 orders of magnitudes larger than the sizes of the test masses, implying that the plate is still of infinite extend with respect to the size of the test masses. Another important aspect of lowering the size of the plate is that it will reduce the cost of acquiring such plates.

In order to calculate the Casimir forces on the plate, one can just use the iteration technique of Eq.(104) of Sec.(10.2), with a small altercation on the initial placement d. As we model the situation for the uncertainty of placement to the right of Fig.(3) we have the initial condition of placement of Eq.(110) given by:

$$d = \Delta x + (N \pm u)R \tag{157}$$

Here, the + sign corresponds to the states of system 1, and the - sign to the states of system 2. Next, by using this new placement condition in the iteration technique described in Sec.(10.2), without the acceleration condition, one can compute the force exerted on the plate by both the $|\downarrow\rangle_1$ and the $|\uparrow\rangle_2$ states by inserting the last iterated value of Eq.(104) in the equation of the Casimir force, Eq.(151).

As we also fixed the values of L and W, the only variable left is the Youngs modulus (E). For this, I will assume, for the moment, that the plate is made out of pure copper. The modulus of copper was measured in Ref.[37] up to 4K to fit the behavior of 137-1.27·10$^{-4}T^2$ GPa, so for our external temperature range of 1-4K, we can take E$\sim$ 137 GPa. By taking E$\sim$ 137 GPa and the values and the iteration technique described earlier, the deflection of the center of the plate has been calculated for both the parameter combinations mentioned in the beginning of this section, for both the $|\downarrow\rangle_1 |\uparrow\rangle_2$ and the $|\uparrow\rangle_1 |\uparrow\rangle_2$ state combination, for the discussed uncertainty range, and the results can be found in Fig.(19).

From Fig.(19), one can observe that the deflection of the plate is at least 12 orders of magnitude smaller than the width of the plate, causing no harm-full force differences on the states. However, as mentioned before, this deflection should not cause the plate to go to an excited state as this can lead to decoherence on the two test masses. The possibility for this will now be analyzed.

As we are dealing with a high vacuum and the Casimir force will go away, since the states are accelerated away from the plate, to bring the superposition back, we have that the center of the plate will oscillate with a minimalistic damping. We can determine the stiffness (k) from Eq.(154), as $F = kx \rightarrow k = F/\delta_d$. Therefore

[44] It is good to note that I included the direction of the forces as I wrote bold letters for the force. If one were to use only the magnitudes one would have a minus sign between the forces as the directions of both forces are in opposite directions.

[45] This is because, as argued before, the magnitude of the force of the outer states is small compared to that of the inner states.

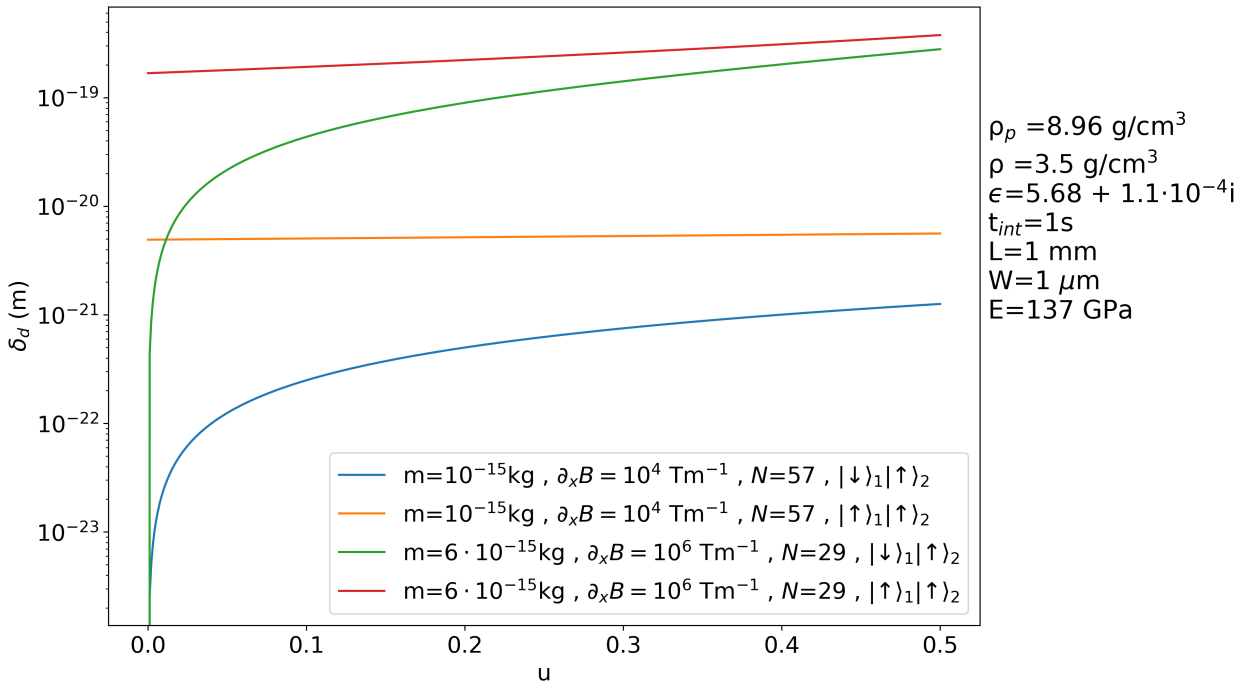

Figure 19: Deflection of the center of the plate due to uncertainty of test mass placement for an uncertainty ranging from 0 to $0.5R$ for the parameters and state combinations indicated by the respective labels. One can observe that the deflection of the plate is at least 12 orders of magnitude smaller than the thickness of the plate.

the induced bending is like an harmonic oscilattor, which follows the same force law, and as we know from a harmonic oscillator that the frequency of oscillation is $\omega = \sqrt{\frac{k}{m_p}}$, we will get an oscillation frequency of

$$\omega = \sqrt{\frac{k}{m_p}} = \sqrt{\frac{16EW^3}{mL^2}} = \sqrt{\frac{16EW^2}{\rho_p L^4}}\,, \tag{158}$$

where ρ_p is the density of copper, which is around 8.96 g/cm^3.

As mentioned before, the plate is modeled as a harmonic oscillator for which the spread of position of the states is given by [35]:

$$\Delta X = \sqrt{\left(n + \frac{1}{2}\right)\frac{\hbar}{m_p \omega}} \tag{159}$$

Here, m_p is the mass of the object modeled as the oscillator, which we assume to be the whole plate. n is an integer indicating the excited state, with $n = 0$ being the ground state. Then, if the deflection of the plate, caused by the different state combinations, is smaller than the ground state spread of the oscillator, the plate will not be found in one of the excited states as these positional spreads for excited states are larger with a constant positional spread/energy separation between excitations.

For the ground state spread we then have just:

$$S = \sqrt{\frac{\hbar}{2m_p\omega}} = \left(\frac{\hbar}{2\rho_p WHL\left(\frac{16EW^2}{\rho L^4}\right)^{1/2}}\right)^{1/2} = \frac{1}{W}\sqrt{\frac{L}{H}}\sqrt{\frac{\hbar}{2\rho_p\sqrt{16E}}} = \frac{1}{W}\sqrt{\frac{\hbar}{2\rho_p\sqrt{16E}}} \tag{160}$$

Where in the last line the square plate assumption, of $H = L$,is used. As this expression needs to be larger than the displacement due to bending, we get:

$$S > \delta_{d,max} \rightarrow \frac{1}{W}\sqrt{\frac{\hbar}{2\rho\sqrt{16E}}} > \frac{F_{\max}L^2}{16EW^3} \rightarrow \frac{W^2}{L^2} > \frac{F_{\max}}{(16E)^{3/4}}\sqrt{\frac{2\rho}{\hbar}} \tag{161}$$

If we fix W, as we have done in the analysis of the thesis, we get the requirement on the length to be:

$$\frac{W^2}{L^2} > \frac{F_{\max}}{(16E)^{3/4}}\sqrt{\frac{2\rho_p}{\hbar}} \rightarrow L < \left(\frac{1}{W^2}\frac{F_{\max}}{(16E)^{3/4}}\sqrt{\frac{2\rho}{\hbar}}\right)^{-1/2} \tag{162}$$

Here, $F_{\max}$ is the force experienced by the plate, depending on the combination of states, and is denoted by Eq.(155) or Eq.(156) for the relevant states. This maximum allowed length, in order for the displacement to be smaller than the ground state spread, is again computed for both the masses and their parameters for both the $|\downarrow\rangle_1|\uparrow\rangle_2$ and $|\uparrow\rangle_1|\uparrow\rangle_2$ combination, for the range of uncertainties and the result can be found in Fig.(20).

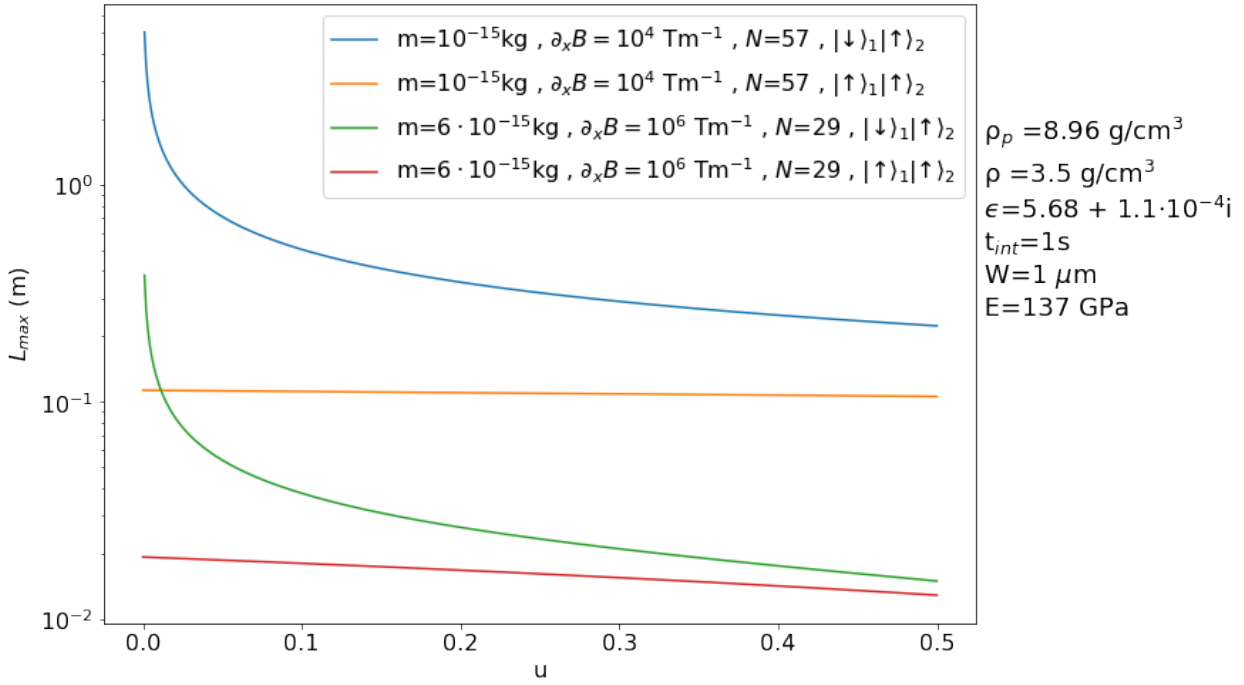

Figure 20: Maximum length of the plate to not be found in an excited vibrational state as a function of uncertainty of placement of the test masses for the different state combinations with their corresponding parameters, indicated by their respective labels. One can observe that for the parameters and state combinations surrounding the mass of 10^{-15} kg a plate of length 100 mm, will suffice for no decoherence to occur. Similarily for the mass of $6 \cdot 10^{-15}$ kg, this corresponds to a length of 10 mm. Consequently, the chosen length of 1mm is more then sufficient for both cases.

From Fig.(20), we observe that the maximum length never exceeds 10 mm for the parameters around the gradient of 10^6 Tm^{-1}, and for the parameters of the laboratory allowed magnetic field gradient of 10^4 Tm^{-1} we are not even exceeding the 100 mm range. Therefore, the chosen length of $L = 1$mm is an excellent choice for the experiment as this will give a deflection of the plate much smaller than the actual ground-state spread, having no excitation of the plate for all the different state combinations. Therefore, no "which-path" information will leak into the plate having that the plate does not act as a decoherence source on both systems.

13.2 Perfect Conductor

For the whole derivation of the modified setup with the conducting plate, the assumption of the perfect conducting plate has been made. A perfect conductor has an infinite conductivity, which cannot be achieved with normal materials. However, for materials with a high reflectivity over a great portion of the electromagnetic spectrum, this will be a pretty reasonable assumption. In the previous section we assumed the plate to be made out of copper as it is a very rigid material, copper has also a high conductivity at low temperatures [37]. However, copper is not a great reflector at low frequencies, so one might have to look for composite materials with for example aluminum or silver, which are considered to be good metallic reflectors, but have lower rigidities. Therefore, a composite material of the sort should have an elastic Young-Modulus,E, such that the length-limit of Eq.(162) is not violated as to have no decoherence source coming from the plate .

For such a composite plate the requirement should be that one has a strong reduction of the Casimir-Polder potential between the closest states, such that the gravitational force between the states is still the dominant force. For the parameters surrounding the mass of 10^{-15} kg with the magnetic gradient of 10^4 Tm^{-1}, one has the separation of the closest states during the free fall around $d - \Delta x \sim 24\mu$m. Consequently, when there is no plate in between the test masses the ratio of the gravitational potential over the Casimir-Polder potential has a magnitude of Eq.(72):

$$\frac{V_G}{V_{CP}} \sim 10^{-4} \tag{163}$$

Therefore, one needs the composite plate to screen the Casimir-Polder potential at least by a factor of 10^5 to have $\frac{V_G}{V_{CP}} > 10$. People have already shown on the Armstrong length scale that a sheet of graphene in between two silica plates, would shield the Casimir force according to a $1/x$ law, with x the separation between silica plate, see Ref.[38]. Extending this to our distance would already reveal a 10^5 reduction on the Casimir force. Although the materials and geometries are completely different with respect to the **QGEM**-protocol, it already shows the possibility in the strong reduction of the Casimir force.

Another method to obey the perfect conductor assumption is to let the metallic plate act as a tiny Faraday cage [39]. For this, we have an empty space (cavity) inside the plate itself, which makes sure that the electromagnetic waves cannot travel through this cavity [39]. This implies that there cannot be standing electromagnetic waves present between two states on opposite sides of the plate and thus annihilating the possible Casimir force between the two.

13.3 Bringing back the superposition

As mentioned throughout this thesis, one of the difficulties of this new, advanced, setup is that one has to be careful how the superposition is brought back in step 3 of the experiment, due to the acceleration of the inner states towards the conducting plate. At the end of the free-fall there is still a residual velocity of the states present due to the Casimir force, implying that when the magnetic field is switched back on there is still a residual velocity towards the plate. This means that the inner states, $|\downarrow\rangle_1$ and $|\uparrow\rangle_2$ of Fig.(3), do not instantaneously turnaround as assumed in the analysis of Sec.(10). Consequently, if one keeps the magnetic field gradient similar for both the inner and outer states of step 3, the superimposed states do not "meet" at the same place, having not a significant overlap of the wave-packets of the states, and we have no superposition that is brought back. This can, in principle, be solved by imposing a slightly inhomogeneous magnetic field gradient that is different for both the inner and outer states, such that they will meet at the end. This usually means that the inner states are subjected to a slightly higher gradient than the outer states.

However, we still have to check the instantaneously turnaround assumption to validate the results of Sec.(10). As we saw that only the inner states of Fig.(3) are significantly affected by the conducting plate, we have that when the magnetic field is switched back on, they will still feel the effect of the "pulling" force of the plate. The equation of motion for these states is, at the start of step 3 of the experiment ,similar to as

derived in Sec.(10.2) but with the addition of the magnetic field gradient:

$$\ddot{x} = \frac{F_{\text{Casimir}}}{m} + \frac{F_{\text{magnetic}}}{m} = -\frac{9\hbar c}{8\rho\pi^2}\left(\frac{\epsilon-1}{\epsilon+2}\right)\frac{1}{x^5} + \frac{g\mu_B\partial_x B}{m} \tag{164}$$

Where use has been made of Eq.(50) and Eq.(102). Using the same iteration technique as in Sec.(10.2) we obtain that this second-order differential equation can be solved by iterating:

$$x_{n+1} = -\frac{Z}{x_n^5}(\Delta t)^2 + 2x_n - x_{n-1} + \frac{g\mu_B\partial_x B}{m}(\Delta t)^2 \tag{165}$$

The initial conditions are determined by the end position and end velocity after the free-fall time of step 2. With these conditions, one can determine how long it would take for the state to come to a "hold" before it turns around and accelerates backward, to bring the superposition back. This stationary point can be determined using the same iteration technique as in Sec.(10.2) with our newly determined initial conditions. The python code used for this section can be found in App.(C). For the iteration, we assume, for the moment, that the magnetic field gradient is still the same as in step 1 of the experiment but, in reality, it should, as argued before, be slightly higher, which will only benefit the results. Using the parameters surrounding the mass of $6 \cdot 10^{-15}$ kg with the gradient of 10^6 Tm^{-1}, and the mass of 10^{-15} kg with the gradient of 10^4 Tm^{-1}, as used in the analysis of Sec.(10.6), one would then find that the turnaround times are 1 ms and 32 ms respectively. Although in the second case it seems significant, one has to remember that the total time of step 3 is one order of magnitude larger, and the total run time of the experiment is even two orders of magnitude larger. Therefore, this contribution would only alter the results of Sec.(10.6) by a very small perturbation. However, as mentioned before, one has to impose fluctuating gradients for the inner states to bring back the superposition which lowers the turn-time. For a doubling of the gradient, one would reduce the time of the turning point to 16 ms and for a quadrupling, this would already reduce to approximately 9 ms, justifying the assumption even more.

One can even get rid of the problem of turning point times and the need of inhomogeneous magnetic field gradients, by modifying the setup of the experiment even further. For this one implements the parallel setup proposed in Ref.[40]. With this setup, the superposition of the test masses are parallel to each other[46] instead of along the same line. This implies that the acceleration of the Casimir force induced by the plate will not alter the superposition size and one can use the same magnetic field gradient for the recombination of the superposition. Although this setup can for the same separation of the closest states generate larger entanglements, the test masses should initially be placed further from one another as there is also a significant acceleration towards the plate in step 1 and step 3 of the experiment and is present for all states. Consequently, the effectiveness of this setup depends on how fast the spin measurements on the test masses ,after recombination, can be taken as to have no collisions of the test masses[47]. The effectiveness of this setup is something to explore in further research as this setup ,if suitable, will make our life easier.

14 Discussion

In this thesis, it was shown that with the current setup of the **QGEM**-protocol, one cannot reduce the magnetic field gradient of 10^6 Tm^{-1} by even one order of magnitude, as one needs a large superposition size to generate a sufficient entanglement to overcome the limiting separation, of the closest states, $d - \Delta x$, of 157μm. This limiting separation was obtained under the assumption that the test masses are modeled as neutral atoms just as in Ref.[1]. Although the masses can be made relatively neutral [1], these masses still have a magnetic susceptibility [1]. Consequently, when the test masses are subjected to the magnetic field of the interferometer, the test masses will become magnetized. This will affect the obtained expression for the Casimir-Polder potential, Eq.(45), as this would alter the allowed electromagnetic wave modes in between

[46] So a single superposition is along the vertical direction and, thus, along the length of the plate of Fig.(3), instead of being on the same line on the horizontal axis of this figure.

[47] One can pull the plate away after the recombination of the test masses as this will not affect the entanglement anymore and one can, thus, lower the velocity of the test masses this way

the states which can alter the limiting separation distance of 157μm. This effect has not been taken into account in this thesis.

The decoherence on the system was modeled as to be a result of "which-path" information loss of the spatial superposition of a test mass by interaction, of the superposition, with the environmental gas and photons, and by the emission of black-body photons of the test mass itself. In this model, the internal temperature of the test mass of ~ 0.15K initially proposed in Ref.[1] was used, and a range of number densities of the environmental gas ,ranging from 10^7 to 10^8 m^{-3} , and an external temperature range of 1-4K were considered. The latter two parameters combined, correspond to pressures of $\sim 10^{-16} - 5 \cdot 10^{-15}$ which is around the original proposed pressure of 10^{-15} Pa [1]. To arrive at the model for this decoherence source several assumptions were made throughout the analysis of Sec.(4) and Sec.(10.5) under which: an isotropic medium, no recoil of the test masses and the applicability of short- and long-wavelength limits. For the isotropic medium assumption, one has to realize that the test masses alter the environment itself, as they influence the distribution of the environmental particles/photons, therefore, one test mass gives a perturbation on the hypothetical isotropic medium of the other test mass. As the thermal wavelength of the environmental photons is an order of magnitude larger than the distance between test masses, for the best scenarios of Sec.(10.6), scattering or emission of photons might influence the scattering on the other test masses during the free-fall period. This effect has not been taken into account in the analysis, but can be considered to cause a reasonable small perturbation on the results, as we are already dealing with a low-density environment and this effect depends on a specific angle of scattering. By treating the no recoil assumption as an elastic scattering between gas and test mass, one can show that, for the obtained masses $10^{-15} - 10^{-14}$ kg, this leads to a residual velocity around $10^{-27} - 10^{-28}$ m/s and is, thus, negligible as assumed. The relevant assumptions for the short- and long-wavelength limits used are as argued in Sec.(10.5) pretty reasonable, as we are dealing with a minimum mass of around 10^{-15} kg, for which the most "loose" upper-bound is for the environmental photons with the external temperature of 4K and the high magnetic field gradient of $\partial_x B \sim 10^6$ Tm^{-1}. For these parameters, the wavelength is in the same order as that of the superposition size, Δx, nevertheless, the long-wavelength limit still gives an upper-bound on the decoherence as argued in Ref.[6] and Sec.(10.5). Also, as this only a loose upper-bound for this extreme scenario and is acceptably valid for higher masses and lower gradients, the results are pretty accurate for the best case scenario's/parameters of the experiment.

With the validity of the above assumptions it was, with the maximization of the entanglement phase and the modeling of the decoherence of the above-mentioned model, shown that, with the entanglement witness of Ref.[26], the best results for measuring the quantum gravity induced entanglement are obtained for a mass of around $8 \cdot 10^{-15}$ kg for an external temperature, T_e of 1K, and a mass of $1.4 \cdot 10^{-14}$ kg for $T_e \sim 4$K. This corresponds to $\langle W \rangle \sim -0.26$ and $\langle W \rangle \sim -0.046$ respectively for the lowest number density of $n_V \sim 10^7$ m^{-3}. Entanglement can, for $T_e \sim$1K, be measured for $n_V < 8 \cdot 10^7$ m^{-3} and reduces to $n_V < 2 \cdot 10^7$ m^{-3} for $T_e \sim 4$K. However, as mentioned before, this current setup of the **QGEM**-protocol is due to significant entanglement of the test mass through the Casimir-Polder potential, at short distances, limited by the closest state separation of the states of 157μm. Therefore, large superposition sizes should be created, in the order of the closest separation of 157μm, to generate a significant gravitational induced entanglement. This makes it impossible to reduces the magnetic field gradient of the SG-interferometer used to split the spatial superposition even by one order magnitude, from 10^6 to 10^5 Tm^{-1}, to measure the entanglement of the test masses. It is also noteworthy that with $T_e \sim$1 K & $n_V \sim 10^7$ m^{-3}, one can go to a mass of 10^{-15} kg to have $\langle \mathcal{W} \rangle < 0$, but requires $\Delta x \sim$ 2mm which is a huge separation compared to the result of the modified setup which will now be discussed.

To overcome the limitation imposed by the Casimir-Polder potential a perfectly conducting plate was introduced between the two test masses, see Fig.(3), which screens the Casimir-Polder potential between the two systems. This allowed the test masses to come closer together, as one no longer has to worry about the entanglement of the test masses through the Casimir-Polder potential. This resulted that for the same enthusiastic magnetic field gradient of 10^6 Tm^{-1} one has no bound on the number density of the gas and the temperature in the considered ranges of $10^7 - 10^8$ m^{-3} and 1-4K. Also one has for the most optimal environmental parameters $\langle \mathcal{W} \rangle \sim -0.5$, which is double that for the current setup shown before and thus allowing for fewer measurements needed to determine the quantumness of gravity. For this result, the parameters

surrounding a mass of $6 \cdot 10^{-15}$ kg were used[48], and the dynamics of the states during the free-fall ,due to interaction with the newly introduced plate, were taken into account. The requirement on the dynamics was such that that the states should be in a position such that the strength of the attraction of the plate never exceeded an order of 0.1 of the magnetic field strength needed to bring the superposition back. However, the most intriguing effect of this modification of the setup, is that one can produce a measurable entanglement, $\langle \mathcal{W} \rangle < 0$, for a mass of 10^{-15} kg with only a superposition size of $\sim 23\mu$m [49]. This can be accomplished, utilizing laboratory allowed magnetic field gradients of 10^4 Tm^{-1}, which is a reduction of two orders of magnitude with respect to the current setup. This detection of quantum gravity is, as can be inferred from Fig(17), possible when $n_V < 3.1 \cdot 10^7$ m^{-3} for $T_e \sim 1$K, and $n_V < 1.6 \cdot 10^7$ m^{-3} for $T_e \sim 4$K. With the closer allowed separation of the closest states, one has with the newly proposed setup, as argued in Sec.(11), a better advantage in probing UV deviation theories of quantum gravity. For the theoretical model used in Ref.[5], this allows exploration of the fundamental scale of non-locality, M_s, up to around a value of ~ 0.04 eV. It should be noted that for the parameter space surrounding the mass of 10^{-15} kg, $M_s > 0.021$ eV in order to measure entanglement, whereas for current measurements M_s can be a minimum of $M_s \sim 0.004$ eV. One can make similar arguments for other models that try to explain the $1/r$ singularity of gravity, such as the Yukawa-potential approach.

Another issue that is not explored in this thesis, is the possibility for a fifth unknown force that can entangle the system, or which can make non-local operations. The former option can cause stronger entanglement than the gravitational entanglement causing deviations from the observed entanglement witness, and for the latter makes the LOCC assumption no longer valid.

With the introduction of the conducting plate, one can also encounter new problems with regards to decoherence, one of which is that the interaction with different state combinations of both test masses could induce vibrational excitation of the plate, leading to "which-path" information loss and thus decoherence effects. However, as argued in Sec.(13.1), if we fix the square plate by a length $L \sim 1\mu$m, and a width $W \sim 1\mu$m, there will not be vibrational excitation of the plate, and the plate will, therefore, not carry information about the superposition and, consequently, does not act as a decoherence source. One should note that the contribution of surface defects on the plate have not been analyzed in this thesis and should be explored for a real-life experiment. The plate itself also perturbs the environment and can, therefore, also alter the scattering of environmental photons/particles on the test masses, as they can scatter off the plate on to the test masses, and can increase the decoherence, on the other hand, the plate also shields environmental particles. Therefore, it can potentially also decrease the decoherence of the test masses. These effects have, quantitatively, not been taken into account in this analysis, but should be taken into account in further research.

As argued before, the environmental decoherence was taken into account to look at the possibilities for both setups. However, there are still other decoherence sources present during the experiment, such as decoherence of the spin decoupling of the NV-point of the test masses, magnetic polarization of the test masses, or collapse models. The coherence of the spin can, as argued in the original paper (Ref.[1]), for our internal temperature of 0.15K, based on the results of Ref.[34], easily be realized. The test masses will also be magnetized in the inhomogeneous magnetic field of the experiment, as pointed out in Sec.(6.1), this will, as argued and pointed out in Ref.[25], alter the trajectory of the states in creating the superposition, to an oscillatory motion. This limits the maximum superposition size which can be created far below the sizes needed to make the entanglement measurable. As argued in Sec.(6.1), we can make the change in trajectory due to this magnetization negligible by coating the diamagnetic diamond core of the test masses with paramagnetic/ferromagnetic materials. The material engineering aspect in achieving the optimal coating in terms of the number of layers, the thickness of the layers, and kind of coating materials, definitely needs further exploration, as this is an important aspect in creating a superposition of significant size in a laboratory. One can infer, from Fig.(17), that, if the other decoherence sources have an accumulative decoherence rate

[48] This corresponds to a free fall time of 1s, an initial separation of the test masses of $d \sim 408\mu$m, and a splitting period of $\tau = 500$ms.

[49] The other parameters corresponding to this possibility are: an initial separation of test masses of $d \sim 47\mu$m, and again an interaction time of 1s, and splitting time of $\tau = 500$ms.

in the order of 10^{-3} Hz, it will not give any trouble in the obtained results for the measurability of the entanglement. It was shown that with the current hypothesized collapse models, the decoherence imposed by current models, for the parameter space surrounding both the current and the proposed setup, would be too large to measure the entanglement between the two test masses.

Another issue to combat with the modified setup is that the interaction of the plate with the test masses causes a different trajectory, during the free-fall, of the superposed states of the test masses. Therefore, the magnetic field needs to have "extra" in-homogeneities in step 3 of the **QGEM**-protocol to bring the superposition back. One can also combat this by imposing the superposition of the test masses to be parallel to the length of the plate, such that Δx is not affected by the interaction with the plate, however, this approach requires further analysis. The effectiveness of this parallel setup relies on the speed in which spin measurements can be taken, but can in principle generate higher phases for a given separation of the test masses with respect to the plate. Furthermore, we saw the possibility for realising the assumption of the perfect conductor by looking at (composite) material for which the reduction of the Casimir-Polder potential between the closest states is such that the gravitational force is still the dominant entangling source. For the parameters surrounding the mass of 10^{-15} kg, this corresponds to a needed reduction of around 10^5 of the Casimir-Polder potential. Promising results for such a Casimir screening by a graphene sheet were already obtained in Ref.[38]. It should also be noted that for a reduction, but not complete annihilation of the Casimir-Polder force, the magnitude of the Casimir interaction between plate and states is lowered as the plate is not fully reflective to EM-waves. Consequently, the trajectory perturbation of the states becomes less significant, which is in favor for bringing the superposition back.

The last point to make is that, in the most optimal scenario, we can with the plate limit the superposition size to $\sim 23\mu$m for the magnetic field gradient of 10^4 Tm^{-1} with the mass of 10^{-15} kg. However, such a superposition size with such a mass is still unachievable with current possibilities of SG-interferometry [11, 12, 13]. Therefore, experimental possibilities are still out of reach for the experiment and improvements from this side are still needed for this challenging project. On the other hand, theoretical improvements can still be obtained from the design side. As mentioned before, one can look at the parallel setup to have sufficient phase evolution for lower superposition sizes, or one can look at multi-component entanglement. With this, it is meant that instead of two test masses we have let us say three or four test masses in a superposition, each in a separate compartment. All compartments are separated by Casimir screening plates, to increase the entanglement of the test masses and, thus, generating higher entanglement phases. Such designs might reduce the needed masses and superposition sizes even further. This is an important aspect which can be probed for further analysis to bring experiment and theory closer together for this exciting project.

15 Conclusion

In Ref.[1], a promising experiment to test the quantum nature of gravity was proposed, which consists of entangling two diamond, mesoscopic, test masses, which are both in a spatial superposition. The entanglement between the two test masses of the experiment, which was refered to as the **QGEM**-protocol, can only occur if gravity is of a quantum nature. Therefore the purpose of this protocol is to go after the detection of the gravitationally induced entanglement between the two test masses. However, in the current protocol, masses of $\sim 10^{-14}$ kg together with a superposition sizes of $\sim 200\mu$m are needed to prove the entanglement, which requires a magnetic field gradient of 10^6 Tm^{-1}. Such a high magnetic field gradient does not allow for laboratory allowed magnetic field gradients and requires co-moving magnets close to the test masses, leading to alteractions in the motion of the test masses, together with an increase in the decoherence of the test masses. Additionally, the parameters of the mass and superposition size are too far of a reach for state of the art Stern-Gernlach interferometers. In this thesis, the restriction on the parameters was shown by modeling the decoherence according to "which-path" information loss by interaction with the environment. This modelling together with the restriction of the Casimir-Polder potential, makes it for the current protocol

impossible to detect the entanglement for lower magnetic field gradients than the order of 10^6 Tm^{-1} [50]. As one needs a relatively large superposition size to create a significant entanglement to overcome the limited separation of the test masses induced by the Casimir-Polder potential. The Casimir-Polder interaction limits this separation as this is another quantum communicator which could entangle the system, which is not a desirable effect, as one wants the entanglement to come dominantly from the gravitational interaction. By imposing that the gravitational potential should be at least one order of magnitude larger than the Casimir-Polder potential, one has that the closest separation between states is limited by 157μm.

To overcome this limitation, a modification for the **QGEM**-protocol was proposed in this thesis, which consisted of the insertion of a perfectly conducting plate in between the test masses which ameliorates the Casimir-Polder interaction between those test masses by acting as a Faraday cage. Consequently, the entanglement can only occur through the gravitational force, allowing, in principle, for much smaller separations between the test masses. The introduced plate however, still generates a significant Casimir force between the plate and the different states of the test masses. This attractive force needs to be lower than the magnetic force required to bring the superposition back, giving rise to another limitation of the setup. Nonetheless, one is, even with this limitation, still able to detect the entanglement of the test masses for masses around $\sim 10^{-15}$ kg with superposition sizes of $\sim 23\mu$m. This is a huge improvement compared to the current protocol, as one can reduce both the mass and the superposition size by one order of magnitude. Additionally, one can create the superposition with a laboratory achievable magnetic field gradient of 10^4 Tm^{-1}, which is an astonishing two orders of magnitude lower than for the current setup and makes it easier to control the motion of the test mass. It was also shown that with this new setup, one has a better possibility to probe deviations from the known $1/r$ potential of gravity (provided that gravity is of a quantum nature). Since one can probe the entanglement for separations, between the test masses, of one order of magnitude smaller than for the current setup. Another aspect shown in this thesis is that the interaction of the spatially separated states of both test masses with the plate, does not lead to an extra decoherence source for a square plate of length 1mm and width 1μm, as such a plate will, for all state combinations, not get vibrational excited. Implying that no "which-path" information can leak into the plate as the plate cannot discriminate between the different state combinations of the test masses and, therefore, carries no information about those test masses.

Although we are now able to detect the entanglement for masses and superposition sizes one order of magnitude smaller than initially proposed, the new parameters are still too large for the current matter-wave interferometers. Therefore, improvements from both experimentalists and theorists should be made to bring the difference of the parameters space of the growing technology and the allowed parameter space closer together. Such that we tackle one of the most sought after questions of the century: "Can we tie gravity to quantum mechanics to obtain a *theory of everything*?"

16 Acknowledgements

I want to thank Mazumdar, Bose, and Marshman for insight-full discussions about the **QGEM**-protocol and its limitation and discussions about the screening of the Casimir-effect. I also want to thank the University of Groningen for allowing me to conduct my Bachelors thesis during the difficult times surrounding the ongoing pandemic.

17 Publication

Part of this Thesis was published on Arxiv in Ref [41]:
Thomas W. van de Kamp, Ryan J. Marshman, Sougato Bose, and Anupam Mazumdar. Quantum Gravity Witness via Entanglement of Masses: Casimir Screening. June 2020.

[50] This is by restricting the temperature of the environment to be in the Kelvin range and not go to lower number densities of the environmental gas of the order of 10^7 m^{-3} corresponding to pressures around 10^{-15} Pa.

References

[1] Sougato Bose, Anupam Mazumdar, Gavin W. Morley, Hendrik Ulbricht, Marko Toroˇ s, Mauro Paternostro, Andrew Geraci, Peter Barker, M.S. Kim, and Gerard Milburn. Spin Entanglement Witness for Quantum Gravity. *Phys. Rev. Lett.*, 119(24):240401, 2017.

[2] Steven Weinstein and Dean Rickles. Quantum gravity. In Edward N. Zalta, editor, *The Stanford Encyclopedia of Philosophy*. Metaphysics Research Lab, Stanford University, summer 2019 edition, 2019.

[3] Chiara Marletto and Vlatko Vedral. Gravitationally induced entanglement between two massive particles is sufficient evidence of quantum effects in gravity. *Physical review letters*, 119 24:240402, 2017.

[4] Charles H. Bennett, David P. DiVincenzo, Christopher A. Fuchs, Tal Mor, Eric Rains, Peter W. Shor, and John A. Smolin. Quantum nonlocality without entanglement. *Phys. Rev. A*, 59:1070, 1999.

[5] Ryan J. Marshman, Anupam Mazumdar, and Sougato Bose. Locality & Entanglement in Table-Top Testing of the Quantum Nature of Linearized Gravity. 7 2019.

[6] Oriol Romero-Isart. Quantum superposition of massive objects and collapse models. *Phys. Rev. A*, 84:052121, Nov 2011.

[7] M. A. Schlosshauer. *Decoherence and the Quantum-to Classical Transition*. Springer, 2007.

[8] H.B.G. Casimir and D. Polder. The Influence of retardation on the London-van der Waals forces. *Phys. Rev.*, 73:360–372, 1948.

[9] Marian Otter. *The Casimir Force a force out of nothing*. Rijksuniversiteit Groningen, May 31, 2006. https://www.rug.nl/research/zernike/education/topmasternanoscience/ns190otter.pdf.

[10] Asaf Szulc. *The Casimir Effect*. https://physics.bgu.ac.il/COURSES/QuantumMechCohen/Contributions/Casimir_Effect.pdf.

[11] C. Wan, M. Scala, G. W. Morley, ATM. A. Rahman, H. Ulbricht, J. Bateman, P. F. Barker, S. Bose, and M. S. Kim. Free nano-object ramsey interferometry for large quantum superpositions. *Phys. Rev. Lett.*, 117:143003, Sep 2016.

[12] Yair Margalit, Zhifan Zhou, Or Dobkowski, Yonathan Japha, Daniel Rohrlich, Samuel Moukouri, and Ron Folman. Realization of a complete stern-gerlach interferometer. *arXiv: Quantum Physics*, 2018.

[13] Shimon Machluf, Yonathan Japha, and Ron Folman. Coherent stern–gerlach momentum splitting on an atom chip. *Nature Communications*, 4:2424, 09 2013.

[14] James Edholm, Alexey S. Koshelev, and Anupam Mazumdar. Behavior of the Newtonian potential for ghost-free gravity and singularity-free gravity. *Phys. Rev. D*, 94(10):104033, 2016.

[15] Daniel J. Kapner, Tessa S. Cook, Eric George Adelberger, Jens H Gundlach, Blayne R. Heckel, Carolyn Hoyle, and H. Erik Swanson. Tests of the gravitational inverse-square law below the dark-energy length scale. *Physical review letters*, 98 2:021101, 2007.

[16] Angelo Bassi and Hendrik Ulbricht. Collapse models: from theoretical foundations to experimental verifications. *arXiv: Quantum Physics*, 504:012023, 2014.

[17] David J. Griffiths. *Introduction to Quantum Mechanics*. Pearson Prentice Hall, 2nd edition edition, 2004.

[18] Maximilian Schlosshauer. Quantum Decoherence. *Phys. Rept.*, 831:1–57, 2019.

[19] Anirban Pathak. *Elements of Quantum Computation and Quantum Communication*. Taylor Francis, Inc., USA, 1st edition, 2013.

[20] Klaus Hornberger and John E. Sipe. Collisional decoherence reexamined. *Phys. Rev. A*, 68:012105, Jul 2003.

[21] Andrei Tokmakoff. *5.74 Introductory Quantum Mechanics II*. Massachusetts Institute of Technology: MIT OpenCourseWare, Spring 2009. https://ocw.mit.edu License: Creative Commons BY-NC-SA.

[22] Dr David Tong. *Quantum Field Theory*. University of Cambridge Part III Mathematical Tripos, Michaelmas Term, 2006 and 2007. http://www.damtp.cam.ac.uk/user/tong/qft.html.

[23] Hye-Young Kim, Jorge O. Sofo, Darrell Velegol, Milton W. Cole, and Gautam Mukhopadhyay. Static polarizabilities of dielectric nanoclusters. *Phys. Rev. A*, 72:053201, Nov 2005.

[24] L.H. Ford. Casimir force between a dielectric sphere and a wall: A Model for amplification of vacuum fluctuations. *Phys. Rev. A*, 58:4279, 1998.

[25] Julen S Pedernales, Gavin W. Morley, and Martin B. Plenio. Motional dynamical decoupling for matter-wave interferometry. *arXiv: Quantum Physics*, 2019.

[26] Hadrien Chevalier, Adam J.W. Paige, and Min Seong Kim. Witnessing the non-classical nature of gravity in the presence of unknown interactions. 2020.

[27] Mark Thomson. *Modern Particle Physics*. Cambridge University Press, 2013.

[28] Luca Buoninfante. Ghost and singularity free theories of gravity. *arXiv: General Relativity and Quantum Cosmology*, 2016.

[29] Valeri Ligatchev. Morphology, acoustic phonon confinement, phonon-induced strain and dielectric permittivity of nominally undoped nano- and micro-crystalline diamond. In *ECS Transactions*. ECS, 2008.

[30] Angel Ibarra, Milagro Gonzalez, Rafael Vila, and Joaquin Molla. Wide frequency dielectric properties of cvd diamond. *Diamond and Related Materials*, 6:856–859, 04 1997.

[31] Jean-Michel Le Floch, Romain Bara, John G. Hartnett, Michael E. Tobar, David Mouneyrac, Damien Passerieux, Dominique Cros, Jerzy Krupka, Philippe Goy, and Sylvain Caroopen. Electromagnetic properties of polycrystalline diamond from 35 k to room temperature and microwave to terahertz frequencies. 2011.

[32] PhD D.G. Simpson. *Gauss's Law for Gravity*. Department of Physical Sciences and Engineering Prince George's Community College, Dec 6, 2006. http://www.pgccphy.net/ref/gravity.pdf.

[33] American Elements ®. Ultra thin copper nanofoil. https://www.americanelements.com/ultra-thin-copper-nanofoil-7440-50-8#section-properties CAS : 7440-50-8.

[34] Nir Bar-Gill, Linh M. Pham, Andrey Jarmola, Dmitry Budker, and Ronald L. Walsworth. Solid-state electronic spin coherence time approaching one second. *Nature communications*, 4:1743, 2013.

[35] University of Missouri-St. Louis. *Chapter 3: Extended Example: The Harmonic Oscillator*. http://web.mst.edu/~parris/QuantumOne.

[36] James M. Gere Barry J. Goodno. *Mechanics of Materials*. Mechanics of Materials (9e). Cengage Learning, 9th edition, 2018.

[37] N. Simon, Elizabeth Drexler, and R. Reed. Properties of copper and copper alloys at cryogenic temperatures. *NIST Monograph*, 177, 01 1992.

[38] Musen Li, Jeffrey R Reimers, John F. Dobson, and Tim Gould. Faraday cage screening reveals intrinsic aspects of the van der waals attraction. *Proceedings of the National Academy of Sciences of the United States of America*, 115:E10295 – E10302, 2018.

[39] David J. Griffiths. *Introduction to Electrodynamics*. Cambridge University Press, 4 edition, 2017.

[40] Hai Chau Nguyen and Fabian Bernards. Entanglement dynamics of two mesoscopic objects with gravitational interaction. *arXiv: Quantum Physics*, 2019.

[41] Thomas W. van de Kamp, Ryan J. Marshman, Sougato Bose, and Anupam Mazumdar. Quantum Gravity Witness via Entanglement of Masses: Casimir Screening. 6 2020.

A Relevant tables

Setup	$\mathbf{t_{int}}$ (s)	$\partial_x \mathbf{B}$ (Tm^{-1})	$\mathbf{\Phi_{eff}}$ (rad)	**minimum mass** (kg)$\cdot 10^{-14}$
Current	3	10^6	0.01	0.095
Current	2.5	10^6	0.01	0.105
Current	3	10^6	0.1	0.336
Current	2.5	10^6	0.1	0.375
Current	3	10^6	1	1.654
Current	2.5	10^6	1	1.960
Conducting Plate	3	10^6	0.01	~ 0.035
Conducting Plate	2.5	10^6	0.01	~ 0.037
Conducting Plate	2	10^6	0.01	~ 0.041
Conducting Plate	1.5	10^6	0.01	~ 0.045
Conducting Plate	1	10^6	0.01	~ 0.054
Conducting Plate	3	10^6	0.1	~ 0.111
Conducting Plate	2.5	10^6	0.1	~ 0.119
Conducting Plate	2	10^6	0.1	~ 0.128
Conducting Plate	1.5	10^6	0.1	~ 0.145
Conducting Plate	1	10^6	0.1	~ 0.165
Conducting Plate	3	10^6	1	~ 0.36
Conducting Plate	2.5	10^6	1	~ 0.39
Conducting Plate	2	10^6	1	~ 0.425
Conducting Plate	1.5	10^6	1	~ 0.49
Conducting Plate	1	10^6	1	~ 0.55

Table 1: Table displaying the minimum mass required for a given entanglement phase (0.01, 0.1 or 1 rad) to be met for a given interaction time and a magnetic field gradient of 10^6 Tm^{-1}. It should be noted that the given initial separation of the test masses are not indicated but can be found in Fig.(4) and Fig.(5).

Setup	$\mathbf{t_{int}}$ (s)	$\partial_x \mathbf{B}$ (Tm^{-1})	$\Phi_{\mathbf{eff}}$ (rad)	**minimum mass** (kg)$\cdot 10^{-14}$
Current	3	10^5	0.01	0.165
Current	2.5	10^5	0.01	0.196
Current	3	10^5	0.1	-
Current	2.5	10^5	0.1	-
Current	3	10^5	1	-
Current	2.5	10^5	1	-
Conducting Plate	3	10^5	0.01	~ 0.036
Conducting Plate	2.5	10^5	0.01	~ 0.039
Conducting Plate	2	10^5	0.01	~ 0.043
Conducting Plate	1.5	10^5	0.01	~ 0.048
Conducting Plate	1	10^5	0.01	~ 0.056
Conducting Plate	3	10^5	0.1	~ 0.126
Conducting Plate	2.5	10^5	0.1	~ 0.134
Conducting Plate	2	10^5	0.1	~ 0.148
Conducting Plate	1.5	10^5	0.1	~ 0.16
Conducting Plate	1	10^5	0.1	~ 0.192
Conducting Plate	3	10^5	1	~ 0.53
Conducting Plate	2.5	10^5	1	~ 0.58
Conducting Plate	2	10^5	1	~ 0.62
Conducting Plate	1.5	10^5	1	~ 0.74
Conducting Plate	1	10^5	1	~ 0.95

Table 2: Table displaying the minimum mass required for a given entanglement phase (0.01, 0.1 or 1 rad) to be met for a given interaction time and a magnetic field gradient of 10^5 Tm^{-1}. It should be noted that the given initial separation of the test masses are not indicated but can be found in Fig.(6) and Fig.(7).

Setup	$\mathbf{t_{int}}$ (s)	$\partial_x \mathbf{B}$ (Tm^{-1})	$\Phi_{\mathbf{eff}}$ (rad)	**minimum mass** (kg)$\cdot 10^{-14}$
Current	3	10^4	0.01	-
Current	2.5	10^4	0.01	-
Current	3	10^4	0.1	-
Current	2.5	10^4	0.1	-
Current	3	10^4	1	-
Current	2.5	10^4	1	-
Conducting Plate	3	10^4	0.01	~ 0.052
Conducting Plate	2.5	10^4	0.01	~ 0.055
Conducting Plate	2	10^4	0.01	~ 0.06
Conducting Plate	1.5	10^4	0.01	~ 0.07
Conducting Plate	1	10^4	0.01	~ 0.089
Conducting Plate	3	10^4	0.1	-
Conducting Plate	2.5	10^4	0.1	-
Conducting Plate	2	10^4	0.1	-
Conducting Plate	1.5	10^4	0.1	-
Conducting Plate	1	10^4	0.1	-
Conducting Plate	3	10^4	1	-
Conducting Plate	2.5	10^4	1	-
Conducting Plate	2	10^4	1	-
Conducting Plate	1.5	10^4	1	-
Conducting Plate	1	10^4	1	-

Table 3: Table displaying the minimum mass required for a given entanglement phase (0.01, 0.1 or 1 rad) to be met for a given interaction time and a magnetic field gradient of 10^4 Tm^{-1}. It should be noted that the given initial separation of the test masses are not indicated but can be found in Fig.(8).

B Derivations Sec.(10)

B.1 Scattering constant air molecules

This subsections consists of deriving the scattering constant for air molecules on the superposition following the procedure of Ref.[7].

The first step includes the assumption that the size of the test masses is much larger than the wavelength of the air molecules [7]. This is valid as the lowest mass in Tab.(1) corresponds to a radius in the order of at least $\sim$ 100 nm, while the wavelength of the air molecules was calculated to be in the order of $\sim$0.1 nm. With this assumption we can state that the differential cross-section ,$|f(q\mathbf{n}, q\mathbf{n}')|^2$, is constant and that the cross-section of scattering is just the geometrical cross-section of scattering [7]. This gives rise to $|f(q\mathbf{n}, q\mathbf{n}')|^2 = R^2/4$ [7]. With this we get that the second integral in Eq.(32) becomes:

$$\frac{\pi R^2}{6\hbar^2}\int_{-1}^{1} \mathrm{dcos}(\Theta)\,(1-\cos(\Theta)) = \frac{\pi R^2}{6\hbar^2}\left(\cos(\Theta) - \frac{\cos^2(\Theta)}{2}\right)\Big|_{-1}^{1} = \frac{\pi R^2}{3\hbar^2} \tag{166}$$

This gives rise to the scattering constant given by [7]:

$$\Lambda_{\mathrm{air}} = \frac{\pi R^2}{3\hbar^2}\int \mathrm{d}q\varrho(q)v(q)q^2 \tag{167}$$

By using the Maxwell-Boltzmann distribution for our gas of air molecules as denoted by equation 3.71 in Ref.[7] and substituting $v(q) = q/m$ back in we get:

$$\Lambda_{\mathrm{air}} = \frac{4\pi^2 R^2}{3m\hbar^2}\frac{N}{V}\frac{1}{(2\pi m k_b T)^{3/2}}\int_0^\infty \mathrm{d}q\, q^5 \exp\left(\frac{-q^2}{2mk_bT}\right) \tag{168}$$

By making the substitution $q^2/(2mk_bT) = x \rightarrow dq = (2mk_bT)/(2q)dx$ we get that the integral in the above equation becomes:

$$\int_0^\infty \mathrm{d}q\, q^5 \exp\left(\frac{-q^2}{2mk_bT}\right) = \frac{(2mk_bT)^3}{2}\int_0^\infty \mathrm{d}x\, x^2 e^{-x} = (2mk_bT)^3 \tag{169}$$

Substituting that in Eq.(168) we obtain:

$$\Lambda_{\text{air}} = \frac{4\pi^2R^2}{3m\hbar^2}\frac{N}{V}\frac{1}{(2\pi mk_bT)^{3/2}}(2mk_bT)^3 = \frac{4R^2}{3\hbar^2}\frac{N}{V}\sqrt{\pi m}\,(2k_bT_e)^{3/2} \tag{170}$$

Which is our final expression for the scattering constant of the air molecules in the **QGEM**-protocol. Note that I rewrote T by T_e to express that the temperature we are dealing with is the environmental temperature. It should also be noted that this expression reduces to the expression given in [6] if one applies to ideal gas law, which is valid for the low-density gas we are dealing with, as the conditions are for example more extreme than in outer space .

B.2 Scattering constants environmental photons

This derivation follows the one given in Ref.[7], so for a more detailed analysis I will refer the reader to section 3.4 of Ref.[7].

For photons, which are scattered upon interaction with the superimposed test masses, the differential cross-section can be written according to the Rayleigh law, which is given by equation 3.59 in Ref.[7][51]. This will have the result that the second integral in Eq.(32) becomes:

$$\frac{q^4R^6}{\hbar^6}\mathrm{Re}\left(\frac{\epsilon-1}{\epsilon+2}\right)^2\frac{\pi}{3}\int_{-1}^{1}\mathrm{d}\cos(\Theta)\,(1-\cos(\Theta)(1+\cos^2(\Theta)) \tag{171}$$

Where Re denotes the real part, this integral reduces to:

$$\frac{q^4R^6}{\hbar^6}\mathrm{Re}\left(\frac{\epsilon-1}{\epsilon+2}\right)^2\frac{\pi}{3}\left(\cos(\Theta)-\frac{\cos^2(\Theta)}{2}+\frac{\cos^3(\Theta)}{3}-\frac{\cos^4(\Theta)}{4}\right)\Big|_{-1}^{1} = \frac{q^4R^6}{\hbar^6}\mathrm{Re}\left(\frac{\epsilon-1}{\epsilon+2}\right)^2\frac{\pi}{3}\frac{8}{3} \tag{172}$$

Substituting that equation into the second integral of Eq.(32) together with $v(q) = c$ for photons one obtains:

$$\Lambda_{sc} = \frac{R^6}{\hbar^6}\mathrm{Re}\left(\frac{\epsilon-1}{\epsilon+2}\right)^2\frac{8\pi c}{9}\int_0^\infty \mathrm{d}q\,\varrho(q)q^6 \tag{173}$$

Using the Planck distribution for the thermal photons of the environment, one obtains the density as indicated by equation 3.63 of Ref.[7], where the assumption is made that the momenta of the thermal photons are isotropically distributed. By substituting that expression in our equation above we will arrive at:

$$\Lambda_{sc} = \frac{8cR^6}{9\pi\hbar^9}\mathrm{Re}\left(\frac{\epsilon-1}{\epsilon+2}\right)^2\int_0^\infty \mathrm{d}q\,\frac{q^8}{\exp[cq/(k_bT)]-1} \tag{174}$$

Then by making the substitution $x = cq/(K_bT) \rightarrow dq = \mathrm{d}x\, k_bT/c$ we obtain the expression:

$$\Lambda_{sc} = \frac{8cR^6}{9\pi\hbar^9}\mathrm{Re}\left(\frac{\epsilon-1}{\epsilon+2}\right)^2\left(\frac{k_bT}{c}\right)^9\int_0^\infty \mathrm{d}x\,\frac{x^8}{\exp[x]-1} \tag{175}$$

Using the zeta Riemann function ,$\zeta(n)$, as defined by equation 3.65 in [7] one obtains the final expression given by:

$$\Lambda_{sc} = 8!\zeta(9)\frac{8cR^6}{9\pi}\left(\frac{k_bT_e}{\hbar c}\right)^9\mathrm{Re}\left(\frac{\epsilon-1}{\epsilon+2}\right)^2 \tag{176}$$

[51] Here it should be noted that the real part of polarizibility of the sphere is already taken into account in Schlosshausser's expression.

Here I again changed T to T_e to express that we are dealing with the environmental temperature [6].

What changes for absorption of environmental photons and emission of photons from the test masses is that the differential cross-section used in obtaining Eq.(171) is different or that it describes the probability of emission. This will result that the "scattering" constants for absorption and emission and photons is according to Ref.[6] is given by:

$$\Lambda_{(e)a} = \frac{16\pi^5 cR^3}{189}\left(\frac{k_b T_{(i)e}}{\hbar c}\right)^6 \mathrm{Im}\left(\frac{\epsilon-1}{\epsilon+2}\right) \tag{177}$$

here T_i denotes the temperature of the test masses, because this is the temperature the thermal photons are emissioned around, and Im denotes the imaginary part of $\left(\frac{\epsilon-1}{\epsilon+2}\right)$.

B.3 Derivation total decoherence of the QGEM-protocol

In this section of the appendix the analytic expression for the total collisional decoherence of the experiment, for both setups, will be derived for both the case where the superposition size is constant during the free-fall as well as the case where this is not the case. This will be done by noting that the superposition evolves differently in all 3 parts of the experiment. The analysis first focuses on giving the second term of $\int \gamma_k \mathrm{d}t$ of Eq.(122).

B.3.1 Constant superposition size

This sub-subsection focuses on the case for the constant superposition size.

step 1: In this part of the experiment we have, for both setups, a constant acceleration of both states in the superposition , with the acceleration given by Eq.(50). For the acceleration part of the experiment we than have that $|x_{|\uparrow\rangle_k} - x_{|\downarrow\rangle_k}| = 2\cdot\frac{a}{2}t^2 = at^2$. This will give that we can write the second summation of the second term as:

$$(x_{|\uparrow\rangle_k} - x_{|\downarrow\rangle_k})^2 = a^2t^4 \tag{178}$$

This will give us that the integral of the second term can be evaluated as

$$\int (x_{|\uparrow\rangle_k} - x_{|\downarrow\rangle_k})^2 \mathrm{d}t = a^2\int_0^{\tau/2} t^4 \mathrm{d}t = \frac{a^2}{5}\left(\frac{\tau}{2}\right)^5 \tag{179}$$

During the deceleration period of this step we have, as argued in Sec.(6), the reverse of the magnetic field giving us that the dynamic superposition distance becomes $|x_{|\uparrow\rangle_k} - x_{|\downarrow\rangle_k}| = -at^2 + 2a\frac{\tau}{2}t + a\left(\frac{\tau}{2}\right)^2$, where the second term and third term are the initial velocity and superposition size caused by the acceleration period. This will give similar to the acceleration period that the integral for this part becomes:

$$\int (x_{|\uparrow\rangle_k} - x_{|\downarrow\rangle_k})^2 \mathrm{d}t = \int_0^{\tau/2}\left(-at^2 + 2a\frac{\tau}{2}t + a\left(\frac{\tau}{2}\right)^2\right)^2 \mathrm{d}t = -\frac{a^2}{5}\left(\frac{\tau}{2}\right)^5 + \frac{46}{15}a^2\left(\frac{\tau}{2}\right)^5 \tag{180}$$

Combining the expression for the acceleration and deceleration period we obtain that that during step 1 of the experiment the second term in Eq.(122) becomes:

$$\sum_{i=1}^{3}\Lambda_i \int (x_{|\uparrow\rangle_k} - x_{|\downarrow\rangle_k})^2 \mathrm{d}t = \sum_{i=1}^{3}\Lambda_i \frac{46}{15}a^2\left(\frac{\tau}{2}\right)^5 \tag{181}$$

Step 2: As argued before, for the modified setup, s_n is at most 2 orders of magnitude smaller than Δx for the high magnetic field gradient and the lower masses of the gradient of 10^5 Tm^{-1}. Therefore we can safely make the assumption that, during this step, we have a pretty much constant separation of Δx for both the

modified setup with the plate and the current setup. Therefore for a given interaction time t_{int} with the constant superposition size the second term of Eq.(122) becomes:

$$\sum_{i=1}^{3}\Lambda_i\int(x_{|\uparrow\rangle_k}-x_{|\downarrow\rangle_k})^2\mathrm{d}t=\sum_{i=1}^{3}\Lambda_i(\Delta x)^2t_{int}=\sum_{i=1}^{3}\Lambda_i 4a^2\left(\frac{\tau}{2}\right)^4t_{int} \tag{182}$$

In the last line use has been made of Eq.(54) and Eq.(50) from which it can be seen that $\Delta x=2a\left(\frac{\tau}{2}\right)^2$.

Step 3 The derivation for this step is pretty similar as for step 1, except for the directions of the magnetic field and the initial conditions. As described in section 6 we have the stationary states at the end of the free-fall[52]. Therefore we have that the separation distance of the superimposed states during the acceleration period towards each other becomes: $|x_{|\uparrow\rangle_k}-x_{|\downarrow\rangle_k}|=-at^2+\Delta x=-at^2+2a\left(\frac{\tau}{2}\right)^2$. Using the similar approach as for step 1 we obtain:

$$\int(x_{|\uparrow\rangle_k}-x_{|\downarrow\rangle_k})^2\mathrm{d}t=\int_0^{\tau/2}\left(-at^2+2a\left(\frac{\tau}{2}\right)^2\right)^2\mathrm{d}t=-\frac{a^2}{5}\left(\frac{\tau}{2}\right)^5+\frac{46}{15}a^2\left(\frac{\tau}{2}\right)^5 \tag{183}$$

This is to no surprise the same as Eq.(180) as it is the reverse action.

For the deceleration period we get using the initial velocity and position of the last velocity and position of the superposition of the acceleration period that $|x_{|\uparrow\rangle_k}-x_{|\downarrow\rangle_k}|=at^2-2a\frac{\tau}{2}t+a\left(\frac{\tau}{2}\right)^2$. This will give that the integral for this step becomes:

$$\int(x_{|\uparrow\rangle_k}-x_{|\downarrow\rangle_k})^2\mathrm{d}t=\int_0^{\tau/2}\left(at^2-2a\frac{\tau}{2}t+a\left(\frac{\tau}{2}\right)^2\right)^2\mathrm{d}t=\frac{a^2}{5}\left(\frac{\tau}{2}\right)^5 \tag{184}$$

This is to no surprise the same as Eq.(179) as it is again the reverse action. Hence we will get just as for step 1 that the second term of Eq.(122) becomes:

$$\sum_{i=1}^{3}\Lambda_i\int(x_{|\uparrow\rangle_k}-x_{|\downarrow\rangle_k})^2\mathrm{d}t=\sum_{i=1}^{3}\Lambda_i\frac{46}{15}a^2\left(\frac{\tau}{2}\right)^5 \tag{185}$$

Now that we have the analytic expression for the second term of Eq.(122) for all steps of the experiment we can substitute the obtained expressions, Eq.(181),Eq.(182), and Eq.(185), in Eq.(122) to obtain:

$$\int\gamma_k\mathrm{d}t=\Gamma_{\text{air}}(t_{\text{int}}+2\tau)+2a^2\left(\frac{\tau}{2}\right)^4\sum_{i=1}^{3}\Lambda_i(\frac{46}{15}\frac{\tau}{2}+2t_{int}) \tag{186}$$

Then by substituting this expression in Eq.(38) one will obtain that the decoherence factor of superposition is given by:

$$\exp[-\int\gamma_k\mathrm{d}t]=\exp[-[\Gamma_{\text{air}}(t_{\text{int}}+2\tau)+2a^2\left(\frac{\tau}{2}\right)^4\sum_{i=1}^{3}\Lambda_i(\frac{46}{15}\frac{\tau}{2}+2t_{int})]] \tag{187}$$

B.3.2 Changing superposition size

In the case of the modified setup, for the lower magnetic field gradients, step 1 is still the same giving the same expression as Eq.(181), however, for step 2 we have no longer the constant distance Δx. As we can see from figure 3 and the analysis done in Sec.(10.2) we have for the modified setup that the superposition distance, during the free-fall, changes by a factor of s_n as the inner states, for the relevant masses, travel

[52]For the modified setup the inner states are not stationary as we have the acceleration towards the conductive plate, however for the high magnetic field gradient it will take around a millisecond extra to turn the states around and bring the superposition back and can be considered to be negligible compared to the acceleration period.

a distance s_n and the acceleration of the outer states can be neglected,see Sec.(10.3). As s_n was obtained numerically the integral of Eq.(122) should be replaced by a summation with an infinitesimal limit of Δt to obtain the second term of Eq.(122) for this step:

$$\sum_{i=1}^{3}\Lambda_i\sum_k(x_{|\uparrow\rangle_k}-x_{|\downarrow\rangle_k})^2\Delta t=\sum_{i=1}^{3}\Lambda_i\sum_k(\Delta x+s_k)^2\Delta t=\sum_{i=1}^{3}\Lambda_i[4a^2\left(\frac{\tau}{2}\right)^4 t_{int}+\sum_k(4a\left(\frac{\tau}{2}\right)^2 s_k+s_k^2)\Delta t] \tag{188}$$

Here use has been made of Eq.(182) and the definition of Δx.

For the third step we have that a larger time then $\tau = 500$ ms is needed to bring the superposition back as the superposition size at the end of the free fall is now $\Delta x + s_{k_{\max}}$. The assumption will be made that the inner state will instantly "turn around" when the magnetic field is turned back on. This assumption is discussed in Sec.(13). With this assumption we have that the when the magnetic field is switched back on the superposition size that needs to be brought back is $\Delta x + s_{k_{\max}}$. At the end of the acceleration period this distance should be half that and with the constant acceleration of the magnetic field this becomes:

$$\frac{\Delta x+s_{k_{\max}}}{2}=at^2\rightarrow t=\sqrt{\left(\frac{\tau}{2}\right)^2+\frac{s_{k_{\max}}}{2a}} \tag{189}$$

This is the acceleration time, and because the deceleration time is the same we have that τ becomes:

$$\tau\rightarrow 2\sqrt{\left(\frac{\tau}{2}\right)^2+\frac{s_{k_{\max}}}{2a}}=\tau_1 \tag{190}$$

We see that this reduces back to τ when $s_{k_{\max}}=0$. With this expression we can just substitute this new value for τ in Eq.(185) to obtain:

$$\sum_{i=1}^{3}\Lambda_i\sum_k(x_{|\uparrow\rangle_k}-x_{|\downarrow\rangle_k})^2\Delta t=\sum_{i=1}^{3}\Lambda_i\frac{46}{15}a^2\left(\frac{\tau_1}{2}\right)^5 \tag{191}$$

The last observation to be made is that the time of τ_1 also changes the whole time of the experiment to $t_{\text{int}}+\tau+\tau_1$. This last observation together with Eq.(181), Eq.(188) and Eq.(191), will give a total decoherence factor of:

$$\exp[-\sum_k\gamma_k\Delta t]=\exp\Bigg[-\Bigg[\Gamma_{\text{air}}(t_{\text{int}}+\tau+\tau_1)+\sum_{i=1}^{3}\Lambda_i\left(\frac{46}{15}a^2\{\left(\frac{\tau}{2}\right)^5+\left(\frac{\tau_1}{2}\right)^5\}+4a^2\left(\frac{\tau}{2}\right)^4 t_{int}+\sum_k(4a\left(\frac{\tau}{2}\right)^2 s_k+s_k^2)\Delta t\right)\Bigg]\Bigg] \tag{192}$$

From this expression, one can see that with $s_{k_{\max}}=0$ we retrieve Eq.(187).

B.4 Accumulated phases step 1 and step 3 of the QGEM-protocol

For generalization I will stick to the notation that d is the initial separation of both setups as depicted in figures 1 and 3. During the acceleration period of step 1 the superposition is split up due to the acceleration created by the magnetic field gradient, for both setups, as the acceleration due to the plate is negligible in this step for the modified setup. This has the consequence that the phase evolution of Eq.(63) during this acceleration period of $\tau/2$ reduced to:

$$\begin{aligned}\Phi_{\text{eff}}=&\frac{Gm^2}{\hbar}\int_0^{\frac{\tau}{2}}\left(\frac{1}{d-at^2}+\frac{1}{d+at^2}-\frac{2}{d}\right)\mathrm{d}t\\=&\frac{Gm^2}{\hbar}\left(-\frac{\ln\left(\frac{\left|\frac{a\tau}{2}-\sqrt{ad}\right|}{\frac{a\tau}{2}+\sqrt{ad}}\right)}{2\sqrt{ad}}+\frac{\arctan\left(\frac{a\tau}{2\sqrt{ad}}\right)}{\sqrt{ad}}-\frac{\tau}{d}\right)\end{aligned} \tag{193}$$

During the deceleration period, we get with the initial conditions determined by the acceleration period then the equation given by:

$$\Phi_{\text{eff}} = \frac{Gm^2}{\hbar}\int_0^{\frac{\tau}{2}}\left(\frac{1}{d+at^2-a\tau t-a\left(\frac{\tau}{2}\right)^2}+\right.$$
$$\left.\frac{1}{d-at^2+a\tau t+a\left(\frac{\tau}{2}\right)^2}-\frac{2}{d}\right)\mathrm{d}t \tag{194}$$

Now by defining $d_1 = d - a\left(\frac{\tau}{2}\right)^2$ and $d_2 = d + a\left(\frac{\tau}{2}\right)^2$, one arrives at effective phase accumulated during the deceleration period:

$$\Phi_{\text{eff}} = \frac{Gm^2}{\hbar}\left(\frac{2}{\sqrt{4d_1a-(a\tau)^2}}\arctan\left(\frac{a\tau}{\sqrt{4d_1a-(a\tau)^2}}\right)\right.$$
$$\left.-\frac{1}{\sqrt{(a\tau)^2+4ad_2}}\ln\left(\frac{-a\tau+\sqrt{(a\tau)^2+4ad_2}}{a\tau+\sqrt{(a\tau)^2+4ad_2}}\right)-\frac{\tau}{d}\right) \tag{195}$$

Where the assumptions are made that $4d_1a > (a\tau)^2$ and $(a\tau)^2 < 4ad_2$. These assumptions are valid for the current setup as well as for the parameters of the modified setup used for the calculations in Sec.(10.6). Therefore, Eq.(193) and Eq.(195) describe the total phase evolution during step 1 of the experiment.

In step 3 of the experiment, we have to distinguish between the current and modified setup. For the current setup as we have no significant forces acting on the states and as step 3 is the inverse of step 1, the phase evolution will have the same outcome as the total phase evolution of step 1 and is, therefore, represented by the sum of Eq.(193) and Eq.(195), just as is the case for step 1.

For the modified setup, on the other hand, we have that the superposition size is slightly enhanced, towards $\Delta x + s_{\max}$, but as Δx is an order of magnitude larger it is fairly reasonable to make the assumption that the phase evolution of step 3 is the same as step 1 with $\tau \to \tau_1$ and $d \to d - s_{\max} = d'$ as step 3 is the inverse mechanism as step 1. With τ_1 and d' the assumptions $4d_1'a > (a\tau_1)^2$ and $(a\tau_1)^2 < 4ad_2'$ still hold. Therefore the total phase evolution during step 1 and step 3 for the alternatiive setup are given by Eq.(193) and Eq.(195) for step 1 and the same equations with $\tau \to \tau_1$ and $d \to d - s_{\max} = d'$ for step 3.

C Python codes

C.1 Python code Sec.(10.2) and Sec.(10.3)

Below is the python code used for the results of the modified setup obtained in Sec.(10.2) and Sec.(10.3):

```
import numpy as np
import math
import matplotlib.pyplot as plt
import numpy as np
def heatmap3(density,m1,m2,N,t_int,t_acc,grad_B,W):
    def potential2(m,grad_B,density,t_int,N,t_acc,W):
        bohr=9.274*10**-24
        g=2.00231930436256
        epsilon=5.7
        c=2.998*10**8
        delta_x=2*g*bohr*grad_B*(t_acc/2)**2/m
        R=(3*m/(4*np.pi*density*10**3))**(1/3)
```

```
    d=delta_x+N*R
    hbar=1.054571800*10**-34
    G=6.67408*10**-11
    x0=(d-delta_x)/2
    initial = [x0-W/2, x0-W/2]
    initial2=[delta_x+x0-W/2,delta_x+x0-W/2]
    acc_magnetic=bohr*g/m*grad_B
    A=-9/(8*density*10**3*np.pi**2)*(epsilon-1)/(epsilon+2)*hbar*c
    time=0.001
    dt=time
    ts = [time]
    vals = [0]
    vals2=[1/(2*x0)]
    vals3=[1/(d)]
    vals4=[1/(d+delta_x)]
    tmax=t_int
    while time < tmax:
        n2, n1 = initial
        n5,n4=initial2
        n3=A/n2**5*dt**2+2*n2-n1
        n6=A/n5**5*dt**2+2*n5-n4
        acc=A/n3**5
        D=d+delta_x
        initial=(n3,n2)
        initial2=(n6,n5)
        if abs(acc)>acc_magnetic/10:
            break
        vals.append(x0-W/2-initial[0])
        vals2.append(1/(2*x0-2*(x0-W/2-initial[0])))
        vals3.append(1/(d-(delta_x+x0-W/2-initial2[0])-(x0-W/2-initial[0])))
        vals4.append(1/(D-2*(delta_x+x0-W/2-initial2[0])))
        ts.append(time)
        time += dt
    times=np.array(ts)
    phasefactor=G*m**2/hbar
    phase_RL=phasefactor*dt*sum(np.array(vals2))
    phase_LR=phasefactor*dt*sum(np.array(vals4))
    phase_LL=phasefactor*dt*sum(np.array(vals3))
    if len(times)<t_int/dt:
        phase=-0.01
    else:
        phase=abs(phase_RL+phase_LR-2*phase_LL)
    return phase
M=np.linspace(m1,m2,100)
T=len(M)
it=0
S=[]
h=[]
while it<T:
    data1=potential2(M[it],grad_B,density,t_int,N,t_acc,W)
    S.append(data1)
    it+=1
    h.append(S)
    S=[]
```

```
    data1=np.array(h)
    data1=data1[data1>0]
    M=M[len(M)-len(data1):]
    return data1,M
```

It should be noted that this code corresponds to the data of the graph around the given phase requirements and not for the maximum phase of Fig.(9). For this a slight altercation in the code is used and can be given upon request.

C.2 Python code Sec.(13.3)

Below is the python code used for the results obtained in Sec.(13.3):

```
import numpy as np
def backtrack(m,grad_B,density,t_int,N,t_acc,W):
    bohr=9.274*10**-24
    g=2.00231930436256
    epsilon=5.7
    c=2.998*10**8
    K=8.98755*10**9
    delta_x=2*g*bohr*grad_B*(t_acc/2)**2/m
    R=(3*m/(4*np.pi*density*10**3))**(1/3)
    d=delta_x+N*R
    hbar=1.054571800*10**-34
    G=6.67408*10**-11
    def potential289(m,grad_B,density,t_int,N,t_acc,W):
            x0=(d-delta_x)/2
            initial = [x0-W/2, x0-W/2]
            initial2=[delta_x+x0-W/2,delta_x+x0-W/2]
            acc_magnetic=bohr*g/m*grad_B
            A=-9/(8*density*10**3*np.pi**2)*(epsilon-1)/(epsilon+2)*hbar*c
            time=0.001
            dt=time
            ts = [time]
            vals = [0]
            vals2=[1/(2*x0)]
            vals3=[delta_x/2]
            vals4=[1/(d+delta_x)]
            vals5=[0]
            tmax=t_int
            while time < tmax:
                n2, n1 = initial
                n5,n4=initial2
                n3=A/n2**5*dt**2+2*n2-n1
                n6=A/n5**5*dt**2+2*n5-n4
                acc=A/n3**5
                velocity=(n3-n2)/dt
                D=d+delta_x
                initial=(n3,n2)
                initial2=(n6,n5)
                vals.append(initial[0])
                vals3.append(delta_x/2+x0-W/2-initial[0])
                vals5.append(velocity)
                ts.append(time)
                time += dt
```

```
        times=np.array(time)
        distance=np.array(vals)
        supsize=np.array(vals3)
        velo=np.array(vals5)
        return distance[-1],velo[-1],supsize[-1]

x0,v0,sup=potential289(m,grad_B,density,t_int,N,t_acc,W)
acc_magnetic=g*bohr*grad_B/m
time=0.001
dt=time
initial=[v0*dt+x0,x0]
vals7=[x0,v0*dt+x0]
vals8=[v0]
vals9=[sup,sup+v0*dt]
tmax=0.05
times=[time,time+dt]
A=-9/(8*density*10**3*np.pi**2)*(epsilon-1)/(epsilon+2)*hbar*c
while time<tmax:
    n2,n1=initial
    n3=A/n2**5*dt**2+2*n2-n1+acc_magnetic*dt**2
    vel=(n3-n2)/dt
    initial=(n3,n2)
    vals7.append(initial[0])
    vals8.append(vel)
    vals9.append(sup+x0-initial[0])
    time+=dt
    times.append(time+dt)
times2=np.array(times)
tijd=np.linspace(0,0.25,5000)
distances=np.array(vals7)
distances2=np.array(vals9)
velocity=np.array(vals8)
mymin = np.min(distances)
min_positions = [i for i, x in enumerate(distances) if x == mymin]
turnpointtime=times2[min_positions]
no_casimir=acc_magnetic*tijd**2/2+np.amin(distances)
n0_casimir_vel=acc_magnetic*tijd
return turnpointtime
```